Adipose tissue mesenchymal stromal cells as therapeutic vehicles against glioblastoma

Maria Alieva Krasheninnikova

Universidad de Barcelona

Facultad de Medicina

Adipose tissue mesenchymal stromal cells as therapeutic vehicles against glioblastoma.

Maria Alieva Krasheninnikova

2012

Universidad de Barcelona

Doctorado de Biomedicina

Titulo:

Adipose tissue mesenchymal stromal cells as therapeutic vehicles against glioblastoma.

Memoria presentada por la Licenciada en Biología Maria Alieva Krasheninnikova, para optar al grado de Doctor por la Universidad de Barcelona, por el programa de Doctorado en Biomedicina.

La presente Tesis doctoral: "Adipose tissue mesenchymal stromal cells as therapeutic vehicles against glioblastoma", ha sido realizada en el Centro de Investigación Cardiovascular (Instituto Catalán de Ciencias Cardiovasculares-Consejo Superior de Investigaciones Científicas, Hospital de la Santa Cruz y San Pau) y el Centro de Investigación Biomédica en Red en Bioingeniería, Biomateriales y Nanomedicina (CIBER-BBN) bajo la dirección del Dr. Jerónimo Blanco Fernández.

Doctoranda: Maria Alieva Krasheninnikova

Director de Tesis: Jeronimo Blanco Fernández

Barcelona, 2012

INDEX

ABBREVIATIONS

- AMSC: adipose-tissue mesenchymal stromal cells
- BLI: bioluminescence imaging
- BMSC: bone-marrow derived mesenchymal stem cells
- CCD: charge coupled device
- CD-UPRT: cytosine deaminase::uracil phosphoribosyltransferase
- CMV: cytomegalovirus promoter
- CSC: cancer stem cell
- CT: computed tomography
- DMEM: Dulbecco's modified eagle media-high glucose
- EPC: endothelial progenitor stem cell
- FBS: fetal bovine serum
- FITC: fluorescein-conjugated high MW dextran
- FMT: fluorescence-mediated tomography
- GBM: glioblastoma multiforme
- GCV: monophosphorylating ganciclovir
- GCV-MP: ganciclovir monophosphate
- GCV-TP: ganciclovir ttriphosphate
- GSC: glioma stem cell
- hAMSC: human AMSC
- HSV-TK: thymidine kinase from herpes simplex virus
- iPSC: induced pluripotent stem cell
- ISCT: International Society for Cell Therapy
- mRFP: monomeric red fluorescent protein
- MRI: magnetic resonance imaging
- MSC: mesenchymal stem or stromal cell
- non-GSC: non-stem glioma cell
- NSC: neural stem cell
- PET: positron-emission tomography
- PHCs: photon counts
- PLuc: *Photinus pyralis* luciferase
- RLuc: *Renilla reniformis* luciferase
- SPECT: single-photon-emission computed tomography
- TEM: Tie2-expressing monocyte
- TRAIL: tumor necrosis factor-related apoptosis-inducing ligand
- tTK: truncated SR39 thymidine kinase
- WHO: World Health Organization

INTRODUCTION

1 GLIOMA

One of the ten most common causes of cancer deaths is due to primary brain tumors. High mortality rates are mainly found in patients with gliomas accounting for 30% to 40% of all intracranial tumors[1]. It is estimated that in the US the incidence of primary brain tumors of 10 per 100 000 persons per year, with a male-female ratio of 6:4 and that they are usually developed in middle age, with peak frequency between the ages of 40 and 65 years[2]. Though glioma incidence is not as frequent as colon, breast or lung cancers, they are a major goal of scientific research because the affected patients have a very poor clinical outcome.

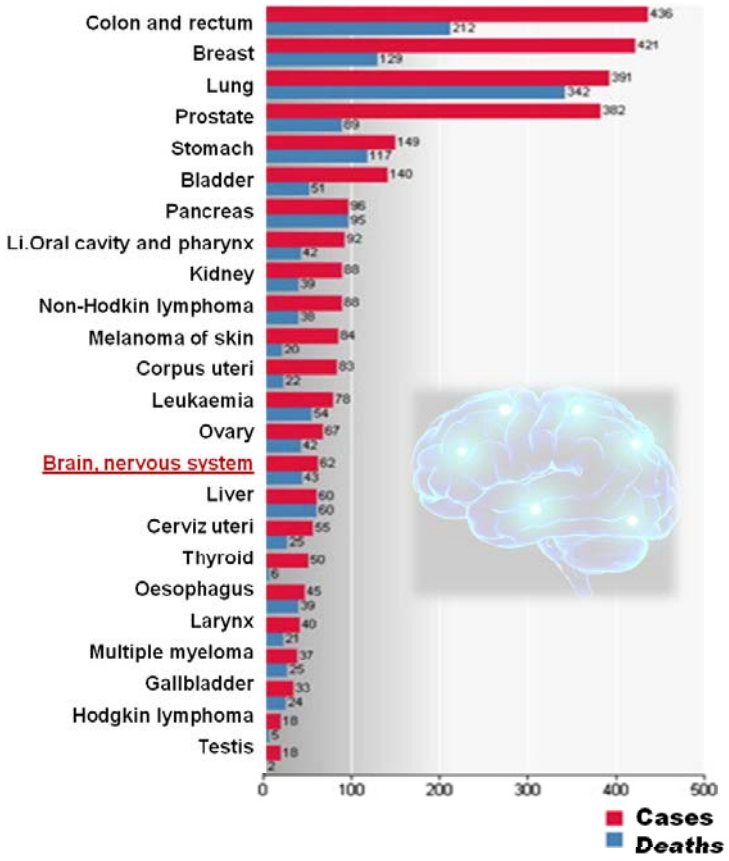

Figure 1 Estimated numbers of cancer cases and cancer deaths in the 40 European countries in 2008 (in thousands) (Adapted from Ferlay J.et al [1])

1.1 Definition and neuropathology

The medical definition of a glioma is a primary brain tumor that originates from a glial cell, in the brain or spinal cord. From a neuropathological point of view gliomas have been described as tumors that grow by diffuse infiltration into the white matter of the brain, normally located in the cerebral hemispheres and thus are rarely visible on the brain surface[2]. The most aggressive types of glioma present massively dilated vessels in the periphery of the tumor, and thrombosed vessels in the center. Gliomas often infiltrate across the corpus callosum into both hemispheres producing the so-called "butterfly gliomas". The ability of glioma cells to infiltrate away from the primary tumor mass is the pathological feature that makes glial tumor so aggressive. Thus, 5% to 10% of patient diagnosed with glioma already present multifocal tumors that cannot be totally removed by surgery or any form of local treatment[2].

1.2 Classification

Gliomas are a family of tumors with almost a continuous range of histology and malignancy that are not easy to separate into distinct categories. The World Health Organization (WHO), a international public health agency of the United Nations classifies gliomas depending on the presumed cell origin, distinguishing astrocytic, oligodendrocytic and mixed gliomas. The WHO classification is a commonly accepted grading system that is based on the presence of the following criteria: increased cellular density, nuclear atypias, mitosis, vascular proliferation and necrosis[3 4]:

- WHO grade I are benign tumors, termed pilocytic astrocytomas.
- WHO grade II are the more slowly growing tumors, named astrocytomas, oligodendrogliomas, or mixed gliomas.
- WHO grade III are tumors similarly termed but with the word anaplastic preceding the names, i.e., anaplastic astrocytomas, anaplastic oligodendrogliomas or mixed anaplastic gliomas.
- WHO grade IV: the most malignant form of gliomas, referred to as glioblastoma or glioblastoma multiforme (GBM).

WHO grade	Astrocytic Tumor		Oligodendrocitic Tumor	
II	Astrocytoma	(46,82%)	Oligondendroglioma	(79,25%)
III	Anaplastic Astrocytoma	(27%)	Anaplastic Oligodendroglioma	(48,42%)
IV	Glioblastoma Multiforme	(4,7%)	Not applicable	

Table 1 The World Health Organization gliomas classification based on cellular origin and histologic appearance; and five year survival relative rate (www.cbtrus.org).

1.2.1 Glioblastoma multiforme

GBM, the most common type of gliomas, accounts for a very poor prognosis with a median survival of 12 to 18 months post-diagnosis (Figure 2)[5]. Average age of GBM cases is 55 years, though this tumor can appear at any age, including childhood. Statistics indicate a small prevalence in men compared with women.

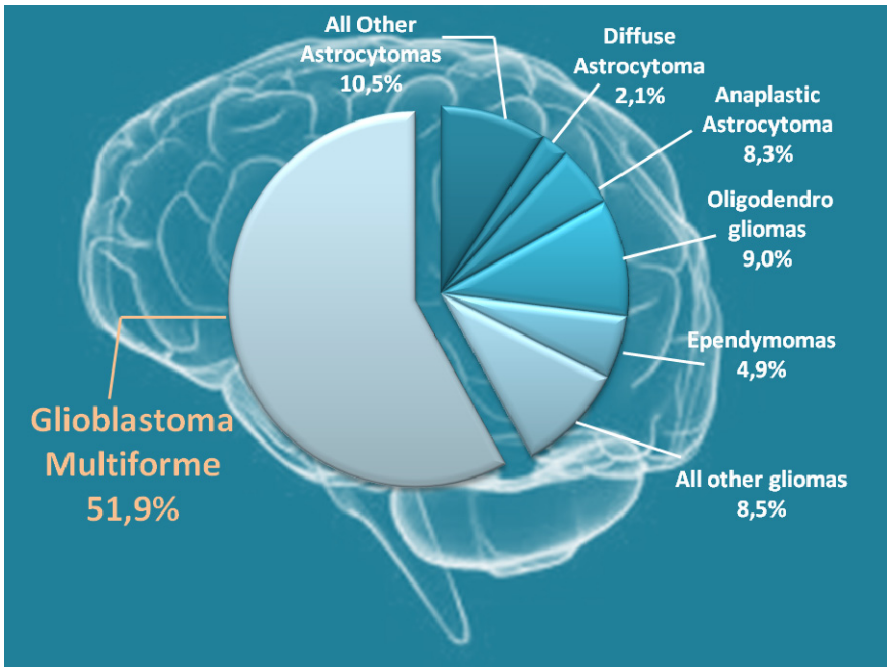

Figure 2 The higher-grade tumors account for the majority of primary brain tumors, and GBM accounts for the majority of malignant **t**umors (Adapted from Prados M. et al)

GBM occurence results in a variety of neurological and pathological symptoms. Neurological signs may include seizures, motor or sensory abnormalities, vision problems, or speech and language difficulties. Depending of the region of the brain

that is affected it can generate an alteration in neurocognitive function and changes in behavior[6]. Pathological features of gliomas include increased cellularity with clear nuclear pleomorphism (variable size and shape), frequent mitoses, endothelial proliferation and necrotic areas. Epidermal growth factor receptor amplification and mutation and loss of the PTEN tumor suppressor gene are characteristic genetic alterations in these tumors.

1.2.2 GBM classification

The above mentioned genetic alterations in addition to others identify the molecular signature of 3 subtypes of GBM that are termed proneural, proliferative, and mesenchymal [7]. Table 2 summarizes the characteristic of each GBM subtype.

	Proneural	Proliferative	Mesenchymal
Histological grade	WHO grade III or WHO grade IV with or without necrosis	WHO grade IV with necrosis	WHO grade IV with necrosis
Cellular morphology	Astocytic or Oligodendroglial	Astocytic	Astocytic
Evolution of signature	Arises in 1º tumor, may persist or convert to *Mes*	Arises in 1º tumor, may persist or convert to *Mes*	Arises in 1º tumor or by conversion from ther subtype
Histological Markers	Olig2, DLL3, BCAN	PCNA, TOP2A	CHI3L1/YKL40, CD44, VEGF
Patient age	Younger (~40yrs)	Older (~50yrs)	Older (~50yrs)
Prognosis	Longer survival	Short survival	Short survival
Chemotherapy/ radiation response	Non-responder to chemotherapy	Clinical outcome improved	Clinical outcome improved
Chromosome gain/loss	None	Gain of 7&Loss of 10 or 10q	Gain of 7&Loss of 10 or 10q
PTEN locus	PTEN intact	PTEN loss	PTEN loss
EGFR locus	EGFR normal	EGFR amplified or normal	EGFR amplified or normal
Signaling	Notch activation	Akt activation	Akt activation

Table 2 GBM classification into subtypes relating prognostic value, activation of signaling pathways, and changes in gene expression (Adapted Phillips H. et al)

1.3 Glioma etiology

Several studies have shown that the risk of glioma is elevated 2-fold in first-degree relatives of patients with glioma and other primary brain tumors[8]. Thus it seems that

genetic influences play a role in the etiology of gliomas, however it is unlikely that the disease susceptibility is based exclusively on high-risk mutations. As described in other cancers, it seems more probable that the inherited risk is a consequence of the coinheritance of multiple low-risk variants, some of which are very common. Most cases of glioma cannot be explained by endogenous or exogenous causes; however there exist some accepted risk factors and inherited susceptibility.

1.3.1 Ionizing radiation

The strongest risk factor for brain tumors is therapeutic ionizing radiation. Studies have reported that there is a high prevalence of prior therapeutic irradiation among patients with GBM (17%) [9], and an increased risk of glioma in patients who have been treated with irradiation for acute lymphoblastic leukemia as children [10]. Another study realized with the survivors of the atomic bombing of Hiroshima showed a high incidence of meningioma, that is directly proportional to the dose of radiation to the brain and the distance to the hypocenter [11].

1.3.2 Hereditary syndromes

Convincing evidence for the existence of an inherited component strongly associated with the development of primary brain tumors has been provided. However these components account for rare genetic syndromes that represent the minority of cases, including Li-Fraumeni syndrome, neurofibromatosis type 1 and type 2, tuberous sclerosis, von Hippel-Lindau disease, Turcot's syndrome and familial polyposis [12].

1.3.3 Novel susceptibility genes

It has been reported that familial clustering of gliomas may occur in families that are not affected by any of the previously mentioned syndromes. Scans of single-nucleotide polymorphisms have proved to be a powerful strategy for identifying low-penetrance genes associated to glioma. Current studies provide evidence that risk of glioma increases with increasing numbers of variant alleles for 5 loci [13] (Figure 3).

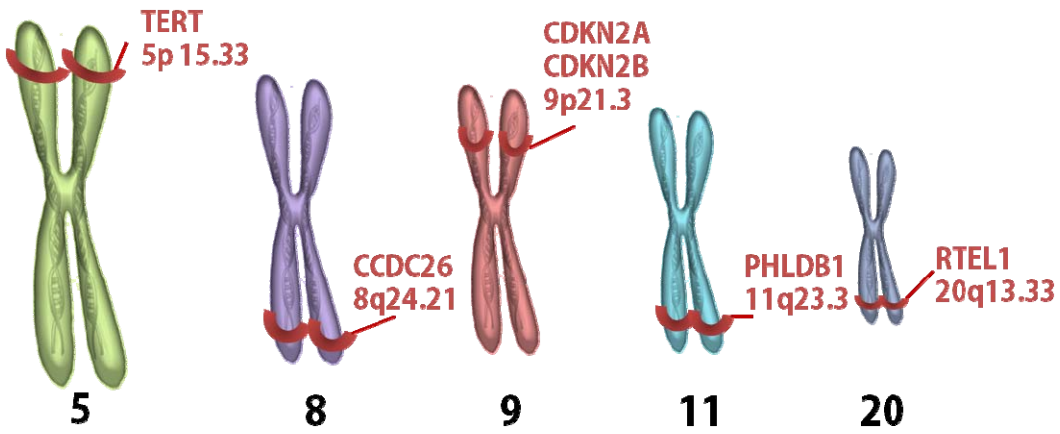

Figure 3 Chromosome location of the 5 risk loci identified from the glioma genome-wide association study (GWAS).

Although the risk of glioma associated with each of these 5 risk variants is low, the incidence of these alleles within the population is high and they play a major role in disease predisposition. Individuals with 8 or more risk alleles have a greater than 3-fold increase in glioma risk compared with those carrying a median number of risk alleles.

There is also some evidence indicating an association between adult gliomas onset and season of birth and also exposure to specific occupational or industrial chemicals[6,14,15]. However, the only widely accepted risk factors (high doses of ionizing radiation and rare genetic syndromes) can only explain a small percentage of all glioma cases. Without considering few rare mendelian cancer predisposition syndromes the genetic basis of inherited susceptibility to glioma is currently undefined.

2 GLIOMA TREATMENT

2.1 Diagnosis

Patients affected by glioma present several symptoms related to mass effect, parenchymal infiltration, and tissue destruction (Table 3). Headache is the most common presenting symptom, related to mass effect, it appears in approximately 35% of patients. Usually the headaches are more severe in the morning and are associated with nausea, vomiting, seizures or focal neurologic deficits[16].

Presenting Signs and Symptoms in Patients with Primary Brain Tumors

Sign or symptom	Percentage with the sign or symptom
Headache	56
Memory loss	35
Cognitive changes	34
Motor deficit	33
Language deficit	32
Seizures	32
Personality change	23
Visual problems	22
Changes in consciousness	16
Nausea and vomiting	13
Sensory deficit	13
Papilledema	5

Table 3 Presenting signs and symptoms in patients with primary brain tumors (Adapted from Sreenivasa R. et al)

To confirm a glioma diagnosis the patient is subject to appropriate brain imaging, followed by histopathology analysis. To reveal the tumor localization computed tomography (CT) and magnetic resonance imaging (MRI) are normally used; thought MRI is more sensitive than CT. Recent advances in structural and functional brain imaging techniques allow the determination of not only tumor location but also of tumor biologic activity, the effects of treatment, differentiation between tumor recurrence and radiation necrosis, and the evaluation of tumor progression (Table 4)[17].

Imaging modalities for the management of Primary Brain Tumors

Modality	Uses
Computed tomography	Localizing the tumor and defining its dimensions, morphology
Magnetic resonance imaging	Localizing the tumor and surrounding structures with high-resolution image, diagnosis of supra- and subtentorial tumors, diagnosis of extra- and intra-axial tumors, presurgical planning with three-dimensional imaging stereotactic biopsy, radiotherpay
Diffusion tensor imaging	Establishing spatial relationships between tumor border and white matter, assessing the progression and regression of white matter tracks caused by tumor growth or resection
Functional magnetic resonance	Neurosurgical planning and neurologic risk assessment by localizing the cortical regions that control language, motor and memory functions
Magnetic resonance angiography	Understanding tumor vascularity and identifying the anatomic relationship between the tumor and blood vessels
Magnetic rsonance spectroscopy	Obtaining biochemical and metabolic information about the tumor, determining tumor type and grade by assessing the cellular contents, differentiating tumor from radiation necrosis
Positron emission tomograpy	Metabolic assessment of tumor aggressiveness (grade), assessing the highly metabolic areas within the tumor, differentiating between tumor recurrence and radiation necrosis, functional localization of cortical regions, predicting patients survival and prognosis

Table 4 Several imaging modalities are used when performing the initial diagnosis, evaluation and treatment of brain tumors (Adapted from Sreenivasa R. et al)

2.2 Surgery

Surgery remains the initial therapy for nearly all patients with brain tumors but it can be curative merely for benign tumors. For patients with gliomas the main goal of surgery is to reduce mass effects while preserving neurologic function, promote cytoreduction of the tumor, treat hydrocephalus (abnormal accumulation of cerebrospinal fluid) if present, and obtain tissue for histological diagnosis and analysis of molecular markers [16]. Most gliomas are very infiltrative and it is almost impossible to remove all the tumor cells with surgical resection. However, it still results in symptomatic improvement and gives some time for the safe administration of subsequent treatment. Radiotherapy and chemotherapy are usual complementary treatments after surgery as indicated on Table 5[18].

	Newly diagnosed	Recurrence or progression
Anaplastic astrocytoma WHO grade III	Resection (or biopsy) and radiotherapy or temozolomide (or radiotherapy plus temozolomide)	(Re-resection and) temozolomide or radiotherapy (or re-irradiation) or bevacizumab
Anaplastic oligodendroglioma and anaplastic oligoastrocytoma WHO grade III	Resection or biopsy and radiotherapy or temozolomide (or radiotherapy plus temozolomide)	(Re-resection and) temozolomide or radiotherapy (or re-irradiation) or bevacizumab
Glioblastoma WHO grade IV	Resection (or biopsy) and radiotherapy and chemotherapy (temozolomide)	(Re-resection an) chemotherapy (dose-intense temozolomide or nitrosourea) (or re-irradiation) or bevacizumab

Table 5 Current treatment options for malignant glioma patients (Adapted from Weller et al).

2.3 Radiotherapy

Radiotherapy is based on the use of ionizing radiation (X or γ rays) to destroy cancer cells and thus reduce the tumor. Radiation is directed the tumor area and leads to cell death by inducing irreparable DNA damage either directly or by free radicals. The main problem associated to radiotherapy is that normal cells present in the irradiated area are also affected by the treatment, though most of the differentiated cells are able to repair their DNA and function correctly after irradiation. Almost no side-effects arise in low-dose palliative treatments. However treatment with higher doses can produce different side effects during or after treatment. The nature, severity, and duration of side effects depends the treatment itself (type of radiation, dose, fractionation, concurrent chemotherapy), and the patient [16].

There are different types of radiotherapy used in glioma patients. Standard of treatment includes *involved-field radiation* using multiple field techniques. The advantage of this procedure is that it reduces the dose of radiation to normal brain tissue, greatly reducing radiation-related damage. *Fractionated radiotherapy* allows improvement of the therapeutic ratio by taking advantage of different radiosensitivities of normal tissues and tumors [16]. A high precision modality of radiosurgery is *stereotactic radiosurgery*, that delivers a single high dose of radiation in a one-day session, but it can also be administered in several doses. This procedure is

used to palliate small, well defined volumes of recurrent GBM and as an addition to conventional external radiotherapy. *Internal radiotherapy* (brachytherapy) is based on surgical implantation of radioactive material directly in the tumor [16,17]. The major disadvantage of radiotherapy is the toxicity to normal brain tissue that can lead to additional brain damage.

2.4 Chemotherapy

Chemotherapy is based on the use of chemical agents, antineoplastics, that target fast-proliferating cells. Most chemotherapy agents affect cell replication and division or induce cell apoptosis. Unfortunately, the most common antineoplastics also affect the normal fast-dividing cells, such as blood cells and the cells forming the epithelium of the mouth, stomach, and intestines, resulting in the most frequent side effects of chemotherapy: myelosuppression, mucositis, and alopecia[16].

In glioma patients, chemotherapy provides only modest benefits, but it plays an important role in palliation and can have an adjuvant effect in combination with surgery and radiotherapy. The standard chemotherapy for gliomas is temozolamide, an alkylating agent. Temozolamide taken orally has rare side-effects facilitating its extended use[19]. Several studies have shown that combining temozolamide with radiatherapy improves survival in patients with high-grade gliomas. A phase III trial of newly diagnosed GBM patients showed that daily, low-dose temozolomide plus standard radiation followed by standard-dose temozolomide (75mg/m^2) improves patients survival compared with radiation alone. However the median survival increase was only of two months (14.6 versus 12.1 months) [20,21].

2.5 Targeted molecular therapy

Drug	Target
Gefitinib	EGFR
Erlotinib	
AEE788	
TP-38	
Imatinib mesylate	PDGFR
SU6668	
MLN518/608	
PTK787/ZK222584	VEGFR
SU5416	
Tipifarnib	Ras
Lonafarnib	
Rapamycin	mTOR
CCI-779	
RAD001	
AP23573	
Tamoxifen	PKC
LY317615	
13-cis-retinoic acid	HDAC
LAQ824	
SAHA	
IL13 PE38QQR	IL-13

Targeted therapies are based on the use of specific molecules that block specific proteins in cancer cells. As in the majority of tumors, gliomas have abnormalities in signal transduction pathways, such as intracellular growth signaling and angiogenesis. A list of inhibitors of specific signaling pathways is shown in Table 6 [22].

Table 6 Targeted agents for malignant gliomas patients (Adapted from Rich et al.).

2.5.1 Targeting of intracellular growth signaling

Over the past 30 years genetic studies have exposed the major mutational targets in the human genome that are associated with the development of brain tumors. Several mutated genes that are implicated in the intracellular growth signaling have been described such as EGFR and mTOR. EGFR is widely used as one of the most attractive therapeutic targets in GBM and other cancers. Small-molecule EGFR inhibitors such as gefitinib and erlotinib have shown to be well tolerated in patients with malignant gliomas, but responses are sporadic and survival is not prolonged[23].

The PI3K/Akt/mTOR pathway is a critical regulator of tumor cell metabolism, growth, proliferation, and survival, and its signaling is frequently amplified in malignant

gliomas. Several mTOR inhibitors for GBM are being tested, such as sirolimus (rapamycin), temsirolimus (CCI-779), everolimus (RAD001), and ridaforolimus (AP23573). However, to date, they have demonstrated reduced single agent activity against these tumors. [24]

2.5.2 Inhibition of angiogenesis

New vessel growth is critical for the development of tumors. Treatment directed toward inhibition of angiogenesis in malignant gliomas has proven to be one of the most promising areas of targeted molecular therapy. A commonly used angiogenesis inhibitor in different types of tumors is Bevacizumab, a humanized monoclonal antibody against VEGF that was approved in US for treatment of recurrent gliomas. Bevacizumab has shown to improve clinical symptoms and reduce tumor edema in patients with glioma. Unfortunately, this agent didn't prolong survival significantly and induced the shift of the glioblastoma phenotype to more invasive with a rapid tumor expansion, which resulted in the withdrawal of the treatment[25].

In conclusion the first molecular targeted trials for malignant gliomas have shown disappointing results: with relatively rare radiographic responses and no significant prolongation of progression-free survival reported. Some factors that may be responsible for the minimal efficacy of targeted molecular drugs in malignant gliomas are deficient penetration into the tumor tissue due to a partially intact blood-brain barrier or an active efflux transporter that secretes the drug. Due to the difficulty of obtaining tumor tissue from these patients very few clinical trials have successfully measured drug levels in tumor tissue[23].

2.6 Resistance of GBM to current treatments

The therapeutic advances mentioned above, have so far shown very modest results and compared to the progress attained in the treatment of other types of tumors, the prognosis for GBM patients has improved only minimally over decades. The main difficulty of GBM therapy is that it is highly infiltrative into the brain and spinal cord

preventing surgical removal even with the most accurate resections. Additionally invading tumor cells are particularly resistant to cytotoxic therapy [26].

As the name indicates, glioblastoma multiforme, presents remarkable intratumoral heterogeneity at the cellular and the molecular levels. The diversity of cell populations and responses to antitumor effects interfere in the treatments.

2.6.1 Cancer stem cells

In the last decade subpopulations of cancer cells with greater potential for tumor initiation, maintenance and propagation have been identified in a variety of tumors including blood, breast, brain, and colon[27]. This cell fraction has been termed cancer stem cells (CSC), stem cell-like cancer cells, tumor initiating cells, or tumor propagating cells. CSCs have revealed to be resistant to many current therapies including radiation and chemotherapy due to highly efficient DNA repair capacity [28]. In addition, CSCs appear to exhibit unique regulatory pathways that promote their maintenance, some of which, such as self-renewal, differentiation, and maintained proliferation capacities are shared by stem cells during development and adult homeostasis[29].

The CSC hypothesis is widely accepted by researchers, although their identification is still a controversial subject. CSCs present in a GBM tumor are termed glioma stem cells (GSC). This cells present some characteristics of normal neural stem cells (NSCs), including the expression of NSC markers (Sox2, Nestin and CD133); the capacity for self-renewal and long-term proliferation; and the ability to differentiate into neurons, astrocytes, and oligodendrocytes. GSCs are implicated in several malignant behaviors, such as tumor repopulation, angiogenesis, invasion and therapeutic resistance (Figure 4) [30]. These particular features make GSCs population the ideal target for anti-glioma therapies.

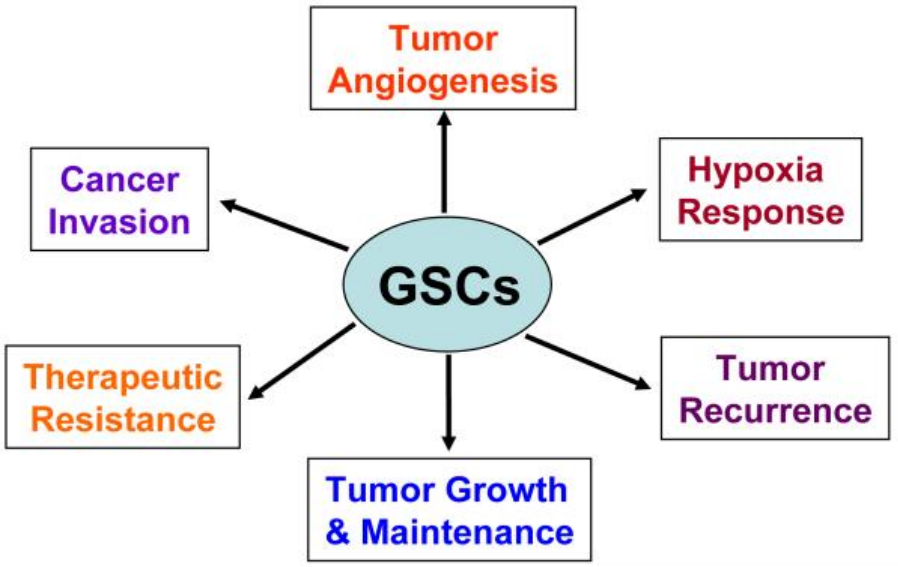

Figure 4 A summary of roles of GSCs in glioblastoma tumor progression and therapeutic resistance. (Cheng L. et al)

Nevertheless, elimination of both, GSCs and non-stem glioma cells (non-GSCs), populations seem to be necessary for a successful therapy, since the non-GSC may be able to reprogram into GSCs under certain conditions [31,32] (Figure 5). Recent studies have shown that some signaling pathways are differentially present or regulated in GSCs and non-GSCs. Identification and targeting of this signaling pathways or specific gene promotors that differentially control the phenotypes and tumorigenic potential of GSCs will offer new targets for the development of novel therapeutics against GSCs. As mentioned above progression is limited by availability of functional vasculature to feed the tumor and remove waste products. The degree of GBM vascularization is significantly correlated with the tumor malignancy, aggressiveness, and clinical prognosis. Importantly, it has been reported that GSCs locate next to capillaries in brain tumors constituting a niche that is critical for their maintenance[33,34] and play an important role in neovascularization through elevated secretion of VEGF [35]. Targeting of GSC in their vascular niche may be another therapeutic approach in GBM treatment.

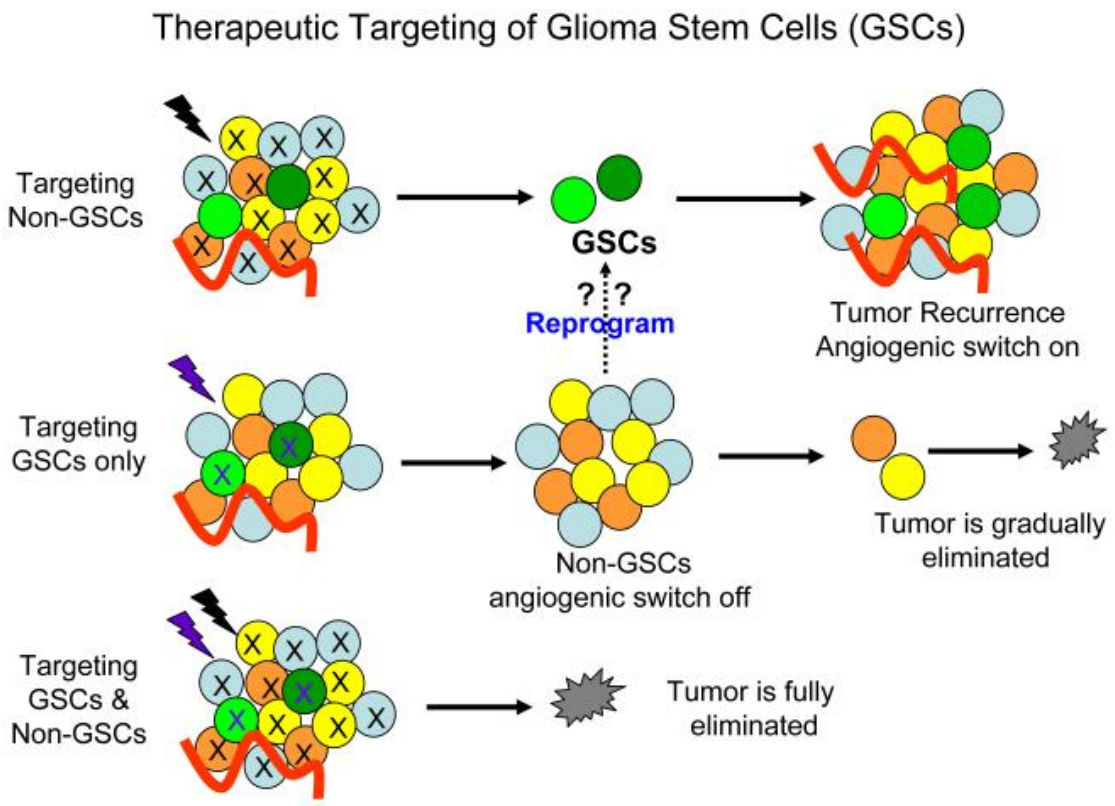

Figure 5 Therapeutic targeting of GSCs and Non-GSCs is necessary for complete tumor elimination. (Cheng L. et al)

2.7 Alternative therapies, post surgical resection

It is now evident that the major challenge for complete glioma eradication is to target GSCs and non-GSC that have deeply infiltrated into the normal brain parenchyma. New experimental therapies to follow surgical resection and radio/chemotherapy are currently under study, amongst them oncolytic virotherapy, immunotherapy and gene therapy (delivered by vector or cellular vehicle).

2.7.1 Immunotherapy

Cancer immunotherapy is based on the use of the immune system to reject the tumor. There are two categories of immunotherapy. In “active immunotherapy” immune cells activated *in vitro* are administrated to the patient to stimulate the immune system and induce it to attack cancer cells. Endogenous immune cells may be activated by cellular or non-cellular vaccines (such as tumor protein lysates, tumour-derived mRNA, peptides eluded from tumor MHC class I molecules and synthetic peptides). Antigens

can be used alone and injected in the presence of different adjuvants. Alternatively antigens can be presented to dendrityc cells which in turn play a key role of educating the immune reaction [36]. In "passive immunotherapy" immune cells or specific molecules are activated *in vitro* and injected in the patient to directly target tumor cells. Several types of effector cells have been tested: cytotoxic T lymphocytes, that are sensitized to glioma associated antigens and exhibit human leukocyte antigen restriction; natural killers or lymphokine-activated killer cells [4]. Also monoclonal antibodies have been used to target specific tumor antigens: cell adhesion molecules, matrix proteins, growth factor receptors, wild-type EGFR, or their glioma-associated variant, EGFR variant III [37].

2.7.2 Gene therapy

Gene therapy is based on the use of DNA vectors to transfer a therapeutic gene for mutation compensation, immunopotentiation, or prodrug activation in neoplastic cells. In cancer gene therapy different strategies have been used including suicide gene therapy, immune gene therapy, oncolytic viral therapy, tumor suppressor gene therapy, and antisense therapy. The main requirements for vectors are safety, efficiency and specificity. Various viral and non-viral vectors have been engineered and used for gene transfer: retrovirus [38], adenovirus, herpes simplex virus[39] and lipofectants [40,41].

2.7.3 Adenovirus

Adenovirus is the most widely used vector in glioma gene therapy because of its capacity for large gene transfer, high transduction efficiency and stable, long-term transgene expression (up to 1 year)[42]. Another advantage of adenoviruses is that they do not integrate into the host cell genome, therefore minimizing the possibility of insertional inactivation of host genes[43]. The first studies with adenoviral vectors showed promising results [42,44], but exhibited several disadvantages, such as inefficient *in vivo* transduction, high immunogenicity and lack of targeting capacity. To solve these problems a variety of strategies have been developed, including reconstructing the adenovirus to target and kill tumors; modifying of the viral fiber and surface proteins.

Despite the recent progress in experimental animal models, human clinical trials fail to show a significant therapeutic effect [45].

2.7.4 Oncolytic virotherapy

The first gene therapy attempts for the treatment of cancer included viral vectors that were modified to delete the function of self-replication to ensure a safe gene transfer without inducing lysis of normal cells and tissues. However the therapeutic effect of non-replicative viruses was very limited in clinical trials. In order to improve treatment efficiency, conditional tumor replicating "oncolytic viruses" were developed[46]. This strategy is based on replication-competent viruses that selectively infect and kill cancer cells but not normal un-transformed cells. For effective oncolytic activity, the vector must have the following features: selectivity for the tumor cells, minimal brain and systemic toxicities, capacity to penetrate and diffuse throughout the brain to reach all cancer cells residing beyond the resection border of the tumor, and survive despite the immune response [47]**.** Currently four oncolitical viruses have been used in clinical trials against glioma: Herpes Simplex Virus [48], Newcastle Disease Virus [49], Adenovirus [50], and Reovirus [51]. In general, it was found that these viruses were safe, and some anti-glioma activity was found in a small number of patients. However some limitations of virotherapy must be improved for a significant effectiveness (Figure 6). The patient's immune response to the virus must be altered so that either anti-tumor immunity is induced or oncolytic activity protected. Viral delivery must be optimized in order to overcome the barriers to the glioma microenvironment.

Among all the emerging therapeutic options for GBM, virotherapy targeting GSC, the renewal source of cancer cells, may allow overcoming recurrence [52]. Targetting may be based on the use of specific tissue promoters that allow transcriptional control of viral gene expression. Fueyo et al, using Delta-24-RGD, an oncolytic adenovirus with enhanced tropism for glioma cells and selective replication in cells with abnormal p16INK4/Rb pathway to target GSCs showed that GSCs are susceptible to adenovirus mediated cell death via autophagy [53,54]. Identification of GSC specific promoters and design of vectors that drive transgene expression under these promoters will further improve the efficiency of oncolytic virotherapy. Additionally the creation of selective-

adenovirus by the use of specific promoters provides safety to oncolytic virotherapy and has already shown positive results in other types of cancers[55].

Different strategies in gene therapy have been approached; however problems of efficient gene delivery and transfer have slowed progress in this promising field [56].

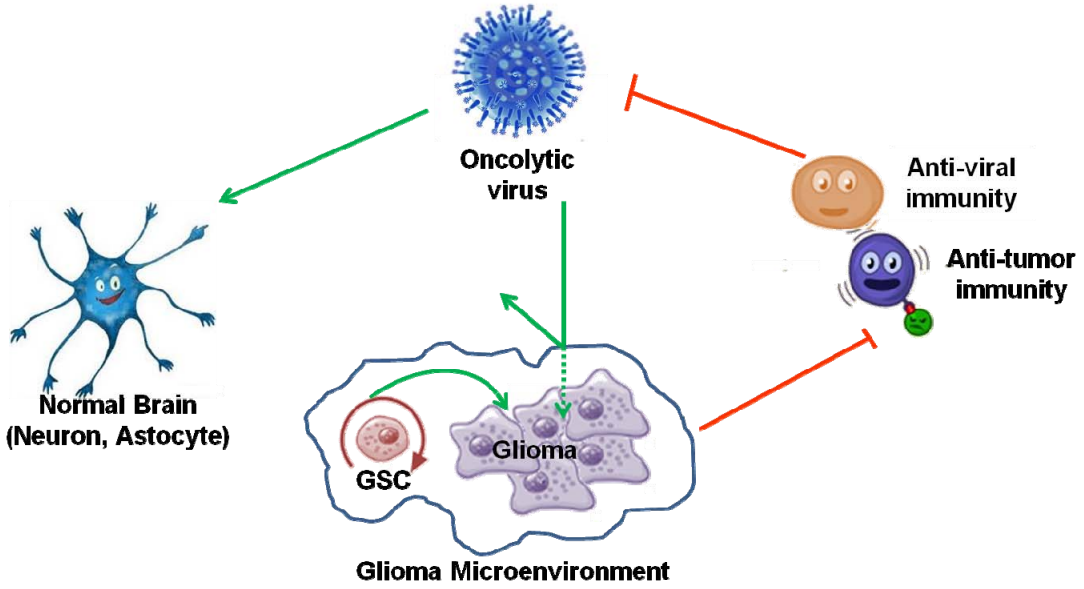

Figure 6 Oncolitic virotherapy limitations for malignant gliomas include overcoming/recruiting the antiviral/antitumor immune response, overcoming the glioma microenvironment, avoiding neurovirulence, and targeting GSCs. (Adapted from Zemp F. et al)

2.7.5 Cellular gene therapy

A more recent approach to deliver a therapeutic effect is to transduce cellular vehicles for the expression of therapeutic gene/products in the vicinity of tumors [57].

3 STEM CELL-MEDIATED GENE THERAPY

It is now evident that the key challenge of glioma treatment is how to target glioma cells that have deeply infiltrated into the normal brain parenchyma. Stem cell mediated gene therapy uses cell vehicles genetically modified *ex vivo* to express therapeutic molecules and implant them in GBM patients. The capacity of stem cells to

migrate towards the tumors may facilitate the delivery of a therapeutic molecule to tumor cells that have dispersed from the main tumor mass [58].

The first cellular carriers for cancer treatment were murine fibroblasts[59] and human embryonic kidney 293 producer cells[60]. However, they are probably not the most appropriate cell vehicle since they are not motile and therefore the delivery of therapeutic agents to deeply infiltrating cells is restricted. The ideal cell vehicle for cancer treatment should display the following features: it should have tumor-selective homing capacity, it should be susceptible of genetic manipulation *in vitro* for the expression of a variety of therapeutic genes, and it should be able to carry the therapeutic molecules to the tumor while protecting it from the host immune system[61]. A variety of adult stem cells exhibit many of these characteristics and in the last decade have become attractive candidates for therapy delivery.

Cell Type	Therapeutic load
EPC	Oncolytic measles virus
HPC	IFN alpha
MSC	Oncolytic adenovirus
	IL-7
	IL-12
	IL-18
	IFN beta
	TRAIL
	HSV-1 TK expressing retrovirusvirus
	PEX
NSC	Cytosine deaminase
	HSV-1 TK
	Replication conditional HSV-1 vector
	Oncolytic adenovirus
	IL-4
	IL-12
	IL-23
	TRAIL
	PEX
	TSP-1

EPC, epithelial progenitr cells; HPC, Hematopoietic progenitor cells; MSC, Mesenchymal stem cells, NSC, neural stem cells, IFN, interferon, IL, interleukin, HSV-TK, herpes simplex virus thymidine kinase; TRAIL, tumor necrosis factor-related apoptosis inducing ligand; PEX, hemopoxin-like protein; TSP-1, thromospondin

Table 7 Stem cell-mediated therapies for experimental gliomas (Adapted from Ghazaleh T. et al)

One of the advantages of using stem cells as gene carriers for clinical application is their self-renewing capacity thus reducing or eliminating the necessity for repeated administrations of the therapeutic cells. By contrast to viral vectors used in gene therapy, autologous stem cells are usually not detected and destroyed by the immune system and high doses of cells exhibit no toxicity. In addition, stem cells are able to transverse physiological barriers and display a homing capacity towards tumors[62-64]. This tropism allows stem cells to reach organs and

tissues that are not accessible by surgery or other gene transfer systems.

Neural stem cells [65,66], hematopoietic progenitor cells[67], bone-marrow mesenchymal stem cells [68], adipose tissue mesenchymal stem cells[62], endothelial progenitor cells[69] have been proposed as possible candidate carriers with therapeutic potential against glioblastomas (Table 7). All these stem cell types exhibit homing capacity to gliomas, arrive at sites of hypoxia and invasive borders which are usually not reached by other therapeutic approaches[58]. Therefore the use of these cells as therapeutic vehicles could overcome some of the limitations of radiotherapy and chemotherapy while also avoiding toxicity to normal brain cells.

3.1 Neural stem cells

Neural stem cells (NSC) have been widely used as delivery vehicles for anticancer gene therapy in the past decade. The majority of studies on NSC-based anticancer therapy have used an enzyme-prodrug suicide gene therapy system (See page 43)[70], Immunomodulatory cytokines[66] or proteins with anti-angiogenic activity[71]. Additionally NSCs have been used as cell vehicles to deliver oncolytic viruses or other viral vectors, thus protecting the viruses from host immunosurveillance and allowing selective delivery of the therapeutic agent to the tumor cells[72].

NSC have shown to posses tumor tropism in a variety of brain tumor models thus can be clinically useful in the targeted delivery of therapeutic agents to widely dispersed tumors[73]. However, the optimal NSC type and therapeutic molecule must still be identified [61]. The main limitation of this system is that that autologous NSC are not available, and the use of allogeneic NSCs is limited by their immunogenicity and low availability of donors[58].

3.2 Hematopoietic progenitor cells

Some hematopoietic progenitor cells (HPC) such as, tumor associated macrophages, neutrophils, dendritic cell precursors and Tie2-expressing monocytes (TEM) have been recently implicated in the promotion of tumor angiogenesis[74]. TEMs are a small subpopulation of monocytes that circulate in the mouse and human peripheral blood

and seem to be recruited to tumors and other sites of angiogenesis. This tumor-homing capacity of TEMs has been exploited to deliver IFN-alpha to tumors, resulting in tumor angiogenesis inhibition and activation of innate and adaptive immune cells. However wound healing ability of TEMs was not impaired, despite the fact that these cells are also recruited to angiogenic tissues other than tumors[67]. For clinical application in cancer therapy genetically modified cord blood stem cells can be injected alone after mild immune suppression, or combined with non-modified autologous cells, following a high-dose of chemotherapy[75].

3.3 Endothelial progenitor stem cells

Endothelial progenitor stem cells (EPC) obtained from peripheral blood are also implicated in tumor angiogenesis[69], suggesting their use as tumor-homing vehicles. Intratumoral injection of EPC that contained oncolytic measles virus resulted in significant prolongation of survival in U87MG-bearing animals[76].

3.4 Induced pluripotent stem cells (iPSC)

In 2006, Takahashi and Yamanaka first induced "pluripotency" in adult somatic cells (iPSC) by the incorporation of four transgenes – Oct3/4, Sox2, c-Myc and Klf4 – in fibroblasts[77]. While iPSCs pluripotency is very similar to that of embryonic stem cells (ESCs), the latter cannot be used in therapy due to histo-incompatibility and ethical issues. iPSCs have a great potential as an unlimited cell source for different purposes: generating disease models, drug screening and cell replacement therapy for various conditions. Due to their novelty, to our knowledge, no studies have so far used iPSCs for gliomas treatment[78,79]. However, due to their characteristics of unlimited self-renewal and high proliferation rate, the use of these cells would be accompanied by a risk of tumor formation that must be taken into account[80].

3.5 Mesenchymal stromal cells

Mesenchymal stromal cells (MSCs) are a group of heterogeneous multipotent cells that can be found in many adult and fetal tissues throughout the body, including bone marrow, amniotic fluid, heart, skeletal muscle, adipose tissue, synovial tissue, pancreas, placenta, cord blood and circulating blood. MSCs are detected in almost all

organs that contain connective tissue [81]. MSCs originate from the mesodermal germ layer and can differentiate into cells of the mesodermal lineage, such as bone, fat and cartilage cells. However, recently it has been shown that they also have endodermic and neuroectodermic differentiation potential, though still controversial[82,83]. These cells are hypoimmunogenic and immunomodulatory, can migrate to damaged tissues and participate in repair processes by secretion of bioactive molecules [84 85].

MSC have acquired biologic and clinical interest over the last two decades, however the characteristics defining MSC are still under discussion among investigators. To solve this problem, the Mesenchymal and Tissue Stem Cell Committee of the International Society for Cell Therapy (ISCT) has proposed a set of standard characteristics to define human MSC for experimental studies: MSC must be adherent to plastic when maintained in standard culture conditions; ≥95% of the MSC population must express CD105, CD73 and CD90, as measured by flow cytometry; cells must lack expression (≤2% positive) of CD45, CD34, CD14 or CD11b, CD79α or CD19 and HLA class II; cells must be able to differentiate to osteoblasts, adipocytes and chondroblasts under standard *in vitro* differentiating conditions[86] (Table 8).

1 Adherence to plastic in standard culture conditions		
2 Phenotype:	Positive (>95%+)	Negative(<2%+)
	CD105	CD45
	CD73	CD34
	CD90	CD14 or CD11b
		CD79α or CD19
		HLA-DR
3 *In vitro* differentiation: osteoblasts, adipocytes, chondroblasts		

Table 8 Summary of criteria to define MSC (Dominici M. et al)

Although the details of MSCs proliferation and differentiation are still under investigation, these cells have acquired particular interest for several clinical applications, including cancer treatment (Figure 7). MSCs derived from bone marrow and adipose tissue are the most studied.

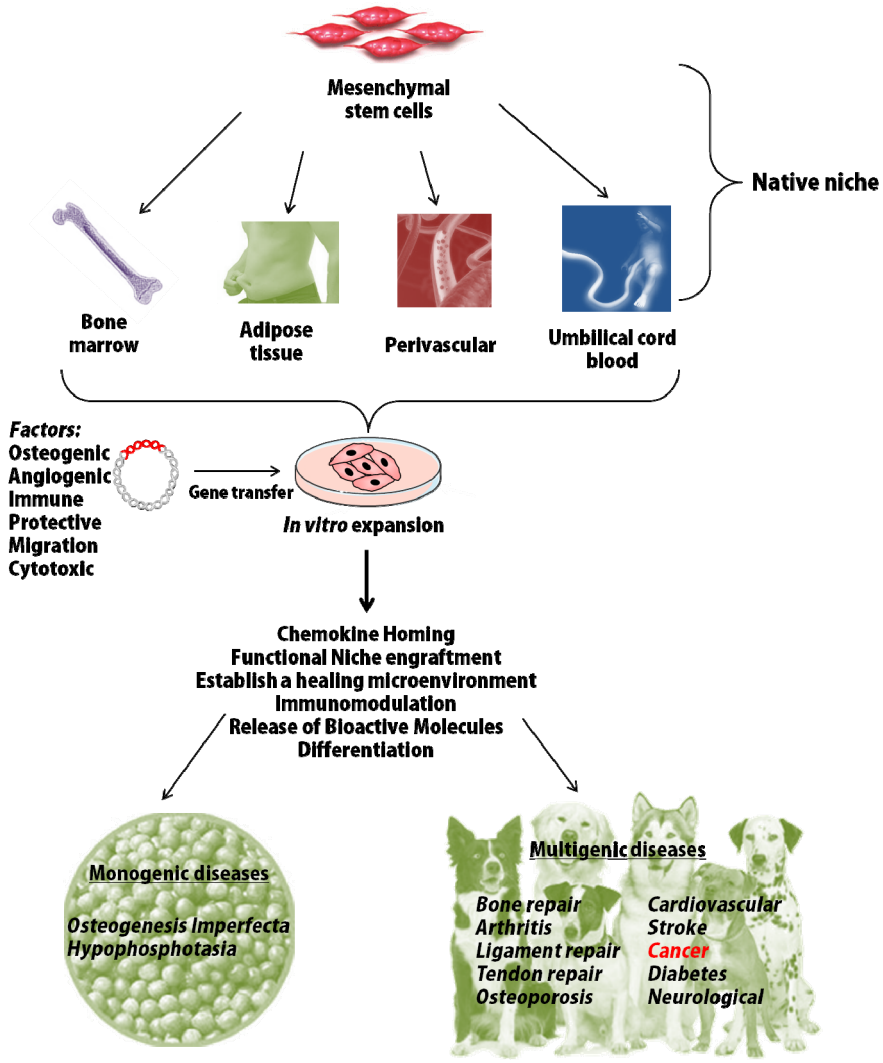

Figure 7 MSCs natural niches and potential of MSC-based therapeutics

(Adapted from Myers T.et al)

3.5.1 Bone-marrow derived mesenchymal stem cells (BMSC)

Bone marrow is the main site of hematopoiesis and plays an important role in the immune system. This organ contains two populations of stem cells: HSCs which produce all blood cell lineages, and BMSCs that are able to originate various differentiated cell types including muscle, blood, vascular, and bone cells, among others [87,88]. BMSC also present transdifferentiation capacity, the genetic reprogramming induced switching between different developmental commitments [89].

BMSC have shown capacity for migration and tumor tropism to gliomas which makes them promising candidates as therapy delivery vehicles. An orthotopic animal model of glioma has shown that human BMSCs migrate toward gliomas after local delivery and are capable of localizing in gliomas after regional intra-carotid delivery and contralateral injection [63,90].

BMSCs have been used as delivery agents for several molecules that can inhibit tumor growth. IFN-α delivery by BMSCs, which leads to accumulation of cells in S phase and increase apoptosis, was described as an effective treatment in several cancer models, including gliomas[91]. BMSCs were used to carry Delta24 replicative oncolytic adenovirus to human experimental glioma showing inhibition of glioma growth and increase of median survival[92]. Another study successfully treated an established C6 brain tumor using BMSCs transduced with the herpes simplex virus-thymidine kinase gene and ganciclovir in the rat[93]. BMSCs have also been effectively used to deliver S-TRAIL [68], IL-2 [90] and IFN-beta [63].

Thought BMSC have demonstrated to be effective delivery vehicles, the painful procedure required for their harvest and the small yield of stromal cells constitute a significative limitation for their use. Alternative sources of MSC such as the adipose tissue appear more convenient for clinical applications.

3.5.2 Adipose-tissue mesenchymal stromal cells (AMSC)

Unlike BMSC, AMSCs are easily harvested with little patient discomfort and morbidity. Abundant stem cells can be extracted from adipose tissue and enough quantity for therapeutic treatment can be obtained in a short culture period. The notion of using AMSC as another source of autologous pluripotent stem cells is relatively recent[94]. AMSC obtained from bone marrow and adipose tissue are very similar showing no differences in fibroblast-like morphology, immune phenotype, success rate of isolation MSCs, colony frequency, and differentiation capacity [95,96].

The possible uses of AMSC in tissue repair/regeneration and cancer treatment are very extensive including ischemia revascularization, cardiovascular tissue regeneration,

bone/cartilage repair, and urinary tract reconstruction, peripheral nerve repair, liver injury repair[97]. Nevertheless, for medical applications AMSCs should fulfill the following criteria (Figure 8)[98]:

Figure 8 Criteria for ideal stem cell for medical applications (Adapted from Gimble J. et al)

As well as with BMSCs the characteristics defining AMSCs are subject to debate. However the ISCT has provided guidelines for the definition of MSCs based on their plastic adherent properties, immunophenotype (CD73+ CD90+ CD105+ CD11b/14− CD19/CD73b− CD34− CD45− HLA-DR−), and multipotent differentiation potential (adipogenic, chondrogenic, and osteogenic)[86]. Still these criteria do not exactly suit all AMSC populations and while some studies indicate that early passages AMSCs are usually CD34+ [99,100], others report that AMSCs become a CD34- population after culturing over a several-day period [101,102].

Interestingly, some studies indicate that AMSC function as pericytes that maintain vascular integrity[101]. It was described that pericytes around microvessels express alpha-smooth muscle actin as well as certain MSC markers, but not endothelial or hematopoietic cell markers[103]. Although it has been proposed that pericytes are the precursors of AMSCs, this does not imply that all AMSCs are descendants of pericytes or that all pericytes are necessarily stem cells [104].

The vascular origin of AMSCs could be related to the tumor homing capacity of these cells. Tumor growth is dependent on blood vessel formation, and mature and progenitor cells are recruited from remote organs for neovascularization [105]. In normal conditions MSCs are rarely found in the peripheral circulation; though, hypoxia or

inflammation signals can lead to MSC mobilization, migration and tumor homing [106]. Recent evidence indicates that AMSC also home to tumors, where they contribute to the formation of tumor-associated stroma[62,107-109]. It is still unclear how AMSC are recruited to the tumor site thought some studies support that they could locally migrate to the sites of inflammation from the surrounding solid tissues, arrive through the systemic circulation, or both [110].

AMSCs have also shown homing capacity to GBM. Both ipsilateral as well as contralateral injection of these cells in brains of glioma-bearing mice, led to extensive accumulation in the tumor[109,111].

The therapeutic effect of AMSCs genetically engineered to deliver therapy to gliomas has been evaluated only in a few studies. Human AMSCs (hAMSCs) encoding TRAIL induced potent apoptotic activity on experimental gliomas and a significant survival prolongation[112]. Additionally hAMSCs expressing the suicide gene cytosine deaminase::uracil phosphoribosyltransferase (CD-UPRT) were directly administrated to treat intracranial rat C6 glioblastoma with improved survival in a therapeutic stem cell dose-dependent manner and induction of complete tumor regression in a significant number of animals [113].

4 THERAPEUTIC GENE SYSTEMS

Cellular gene therapy involves the use of cell vehicles to transfer foreign genetic material into a patient in an effort to treat a disease (Figure 9). Various systems concerning the therapeutic molecules have been developed for cancer gene therapy [114]:

- Transfer of tumor suppressor genes
- Suicide enzyme/pro-drug approach
- Expression of cytokines, co-stimulatory molecules, tumor specific antigens
- Expression of molecules that affect angiogenesis, cell adhesion and metastasis
- Chemosensitization and radiosensitization approaches
- Chemoprotection of stem cells

- Expression of antisense, ribozymes or siRNAs for dominant oncogenes
- Expression of cell surface receptors/ligands to target cancer cells
- Tumor-specific promoter driven transgene expression
- Oncolytic vector

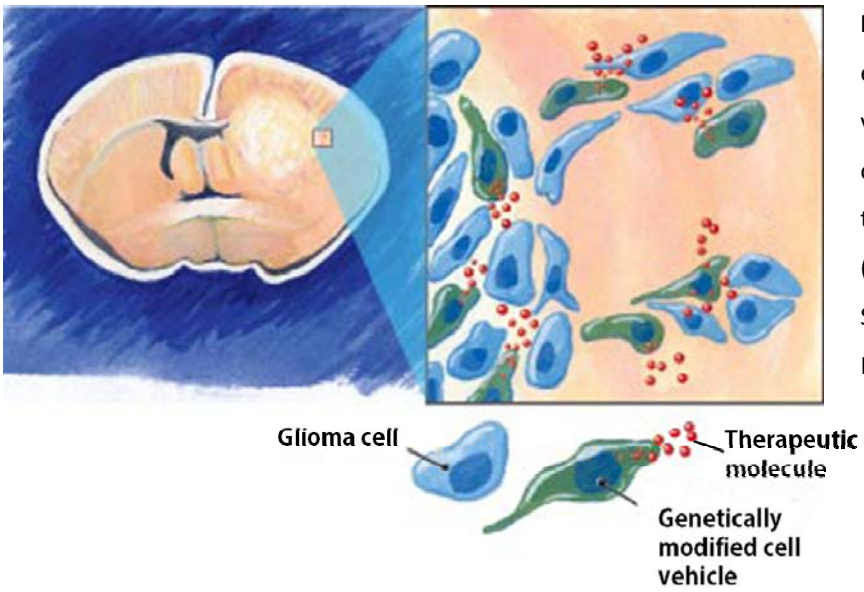

Figure 9 Genetically engineered cellular vehicles track gliomas cells and deliver the therapeutic molecule. (Adapted from R&D Systems Cytokine Bulletin)

4.1 Cytotoxic gene therapy

Cytotoxic gene therapy approach is directed to initiate tumor self-destruction, that can be achieved by two strategies: by "toxic genes", that encode proteins which cause cell death directly or by the expression of "suicide genes" [115]. The suicide gene based approach consists in the delivery of an enzyme that converts a nontoxic prodrug into a lethal compound resulting in the killing of local cancer cells. For the cytotoxic cell therapy perspective, genetically modified cellular vehicles that express a toxic or suicide gene are placed near the tumor site in the patient, where they liberate the toxic product in the tumor environment or transfer it directly to cancer cells.

4.1.1 Suicide cytotoxic gene therapy advantages

Suicide cytotoxic gene therapy hold several advantages respect classical chemotherapy, mostly related to the reduction of systemic toxicity[114]: non toxic prodrugs with no intrinsic activity in unmodified human cells can be used; concentrations of the toxic agent in the tumor can be much higher than in rest of

organs since the prodrug is activated only in the target cells or in cells in close proximity; different suicide gene/prodrug combinations can be designed to confer tumor specificity on the treatment regime (by the use of tumor-specific promotors to drive expression of the therapeutic gene [116], or by the use of prodrugs which are preferentially active in, e.g., hypoxic cells [117]). An important aim of suicide gene therapy is that intercellular transport of the activated prodrug generates a "bystander killing effect", which allows the eradication of tumor cells even if not all of the target cells have been transduced with the suicide gene.

For clinical application in cancer treatment the suicide gene/prodrug combination should exhibit the following properties [114]:

Suicide gene ideal proprieties

- be absent in the human genome to minimize toxicity
- exhibit high catalytic activity upon expression in tumors at low prodrug concentration
- be both necessary and sufficient for full activation of the prodrug
- be monomeric, allowing easier expression

Prodrug ideal proprieties

- have high affinity for the enzyme encoded by the suicide gene and low affinity for endogenous enzymes
- be able to penetrate into the solid tumor and into the cancer cells
- exhibit no toxicity prior to activation
- active drug should be capable of intercellular diffusion to allow killing via the bystander effect
- active drug should have a half life long enough to maximize the bystander effect within the tumor

4.1.2 Bystander effect

Bystander effect refers to the induction of tumor cell death by neighboring transgenic cell vehicles capable of converting a non-toxic prodrug into a toxic agent (Figure 10). A

major aim of this therapy is to deliver the gene toxic product to a sufficient number of tumor cells and induce tumor regression. As clinical trial have shown gene transfer efficiencies reach less than 10% of the target tissue[118].

Bystander effect can take place by several molecular, cellular and systemic mechanisms. It can rely on the free diffusion of toxic metabolites or intercellular communication via gap junctions [119]. The potency of the bystander effect usually correlates with the efficiency of gap junction intercellular communication[120]. Free diffusion on toxic metabolites is useful to treat tumors that do not have functional gap junctions, but may also carry the risk of systemic diffusion and toxicity[121].

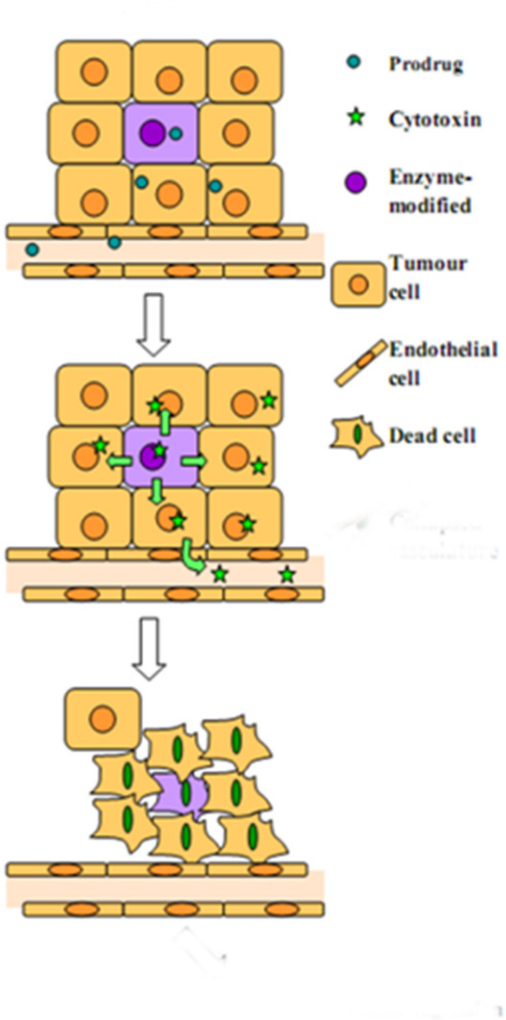

Figure 10 Diagram representing bystander effect. The therapeutic gene encodes an enzyme that converts the prodrug to a cytotoxin, leading to cell death. Surrounding cells may also be killed due to the local bystander effect. (Adapted from Dachs et al)

The bystander effect can be even further potentiated by the immune system. Tumor cells death caused in first instance by toxic metabolites can stimulate recognition of tumor antigens leading to local inflammation and additional death of other tumor cells mediated by the immune system. This effect can occur even when cells are separated

either spatially ("distant bystander effect") or temporally ("vaccination effect") from the suicide gene expressing cells[122,123]. Opportunely, it could even lead to the destruction of metastases originated from a primary tumor. To some extent the role of the immune system may be modulated by the choice of the suicide gene/prodrug combination, depending on whether cell killing is mediated predominantly by apoptosis or necrosis.

It has also been proposed that in certain cases the bystander effect is induced by intercellular transfer of hydrolases, lytic enzymes and apoptotic vesicles containing toxic drugs released from the dying cells which are phagocytosed by tumor cells [124].

4.1.3 Types of suicide genes

Although a large variety of enzyme-prodrug combinations has been designed for use as cytotoxic systems for therapy, only a few have been applied in human clinical trials, as indicated in Table 9.

Enzyme	Prodrug	Cytotoxin	Bystander
Carboxylesterase	Irinotectan	SN-38	High
	Capecitabine	5-FU	
	Paclitaxel-2-ethylcarbonate	Paclitaxel	
	Dp VP-16	VP16	
Cytochrome P450	CPA and IFO	Alkylating agents	High
	Acetaminophen	N-acetyl benzoquinone imine	Low
Cytosine deaminase (±UPRT)	5-FC	5-FU	High
NADPH-cytochrome P450 reductase	Tirapazamine, EO9, misonidazole	Reduced metabolites	Medium
Nitroreductase	CB1954	Alkylating agents	High to very high
	Self-immolative prodrugs	Alkylating agents, pyrazolidines, enedines	
	Metronidazole	Alkylating agent	
Pyrimidine nucleoside phosphorylase	5'-deoxy-5-fluorouridine	5-FU	High
Thymidine kinase	GCV, ACV, Valacyclovir, araM, BVDU	Monophosphorylated nucleotide analogues	High, dependent on gap junctions

Table 9 Selected enzyme prodrug systems used in gene therapy (Adapted from Dachs et al)

4.1.4 Thymidine kinase

Thymidine kinase from herpes simplex virus (HSV-TK) was used for the first proof-of-principle of suicide gene therapy [125], and the combination and variations of this system still remain one of the most widely used systems in both clinical and experimental gene therapy applications.

HSV-TK is needed by the virus for reactivation from ganglionic neurons during the latent stage of its life-cycle, since these cells express very low levels of endogenous mammalian TK (the enzyme responsible for initiating the phosphorylation of deoxythymidine to deoxythymidine triphosphate for incorporation into nascent DNA) [126].

The benefit of this system for cancer gene therapy is based on the 1000-fold lower efficiency of endogenous TK to monophosphorylate ganciclovir (GCV) compared to that of HSV-TK. Following the monophosphorylation of GCV to GCV-monophosphate (GCV-MP), GCV-MP is further phosphorylated to its diphosphate (GCV-DP) and triphosphate (GCV-TP) forms by endogenous guanylate kinase and several other enzymes such as phosphoglycerate kinase [127]. GCV-TP is incorporated into DNA during replication, causing inhibition of DNA polymerases, rapid chain termination and the formation of single strand breaks, leading to cell death (Figure 11)[128]. This process affects mainly fast proliferating cancer cells.

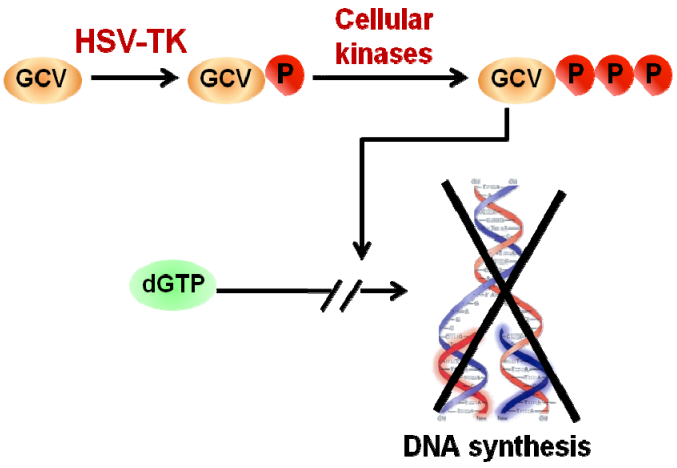

Figure 11 Diagram representing GCV phospohorylation and incorporation of GCV-TP during DNA replication

The exact mechanism of HSVtk/GCV mediated cell death is still not completely understood. While in general it seems that apoptosis plays a major role, in some specific cell types non-apoptotic mechanisms may also be involved[127].

This system exerts the potent bystander effect by transfer of GCV-TP across gap junctions. However, one of the main limitations on HSV-TK/GCV system is that although the prodrug can passively diffuse into target cells, the cytotoxic GCV-TP is highly charged and therefore insoluble in lipid membranes, and cannot freely diffuse into neighboring cells to exert its toxic effects. The fact that HSV-TK/GCV expressed by MSCs is effective for GBM treatment poses the interesting question of whether there

are gap junctions between both cell types or other mechanisms are also involved. Although, HSV-TK/GCV seems to be suitable for GBM treatment, since primary cultures of malignant gliomas showed evidence of efficient gap junction communication[129].

In attempts to potentiate the bystander effect mutant HSV-TKs and alternative prodrugs have been studied. New HSV-TK mutants with increased specificity for substrate have been discovered and characterized. The most extensively evaluated of these is mutant SR39, which is 43-fold more sensitive to GCV than the parental HSV-TK[130-132]. SR39 provides a significant advantage over the wild-type TK for suicide gene therapy applications by enhancing prodrug-mediated cell killing and by reducing the required GCV dose. A truncated version of SR39 mutant (tTK) was generated by deletion of the nuclear localization signal and a cryptic testis-specific transcriptional start point leading to a more cytoplasmic localization of the TK enzyme, access to higher substrate concentrations and enhanced TK effectiveness[133].

5 *IN VIVO* AND *IN VITRO* CELL MONITORIZATION

Cell based gene therapies appear to be promising treatments for GBM remnants post surgical removal. To better understand the behavior cell vehicles in the brain and their interaction with tumor cells *in vivo* monitorization system have been developed. Ideally, a non-invasive tracking platform should be sensitive, allow monitorization of cells in real time and economically accessible.

The following list contains some of the characteristics desirable in a system to monitor tumor behavior[134]:

- biocompatibility, safety, and nontoxicity
- single-cell detection capability
- quantification of cell number
- no dilution with cell proliferation
- non-invasive imaging in living subjects

In the past decades, a number of imaging technologies to analyze the *in vivo* behavior of tumors has emerged. Currently, these procedures have become valuable tools for

cancer research, monitoring clinical trials and medical diagnosis (Figure 12)[135]. Modern molecular imaging systems enable clinicians to determine tumor location, though in future advances it would be desirable to visualize the expression and activity of particular molecules, cells and biological processes that characterize the behavior of tumors and response to therapy[136].

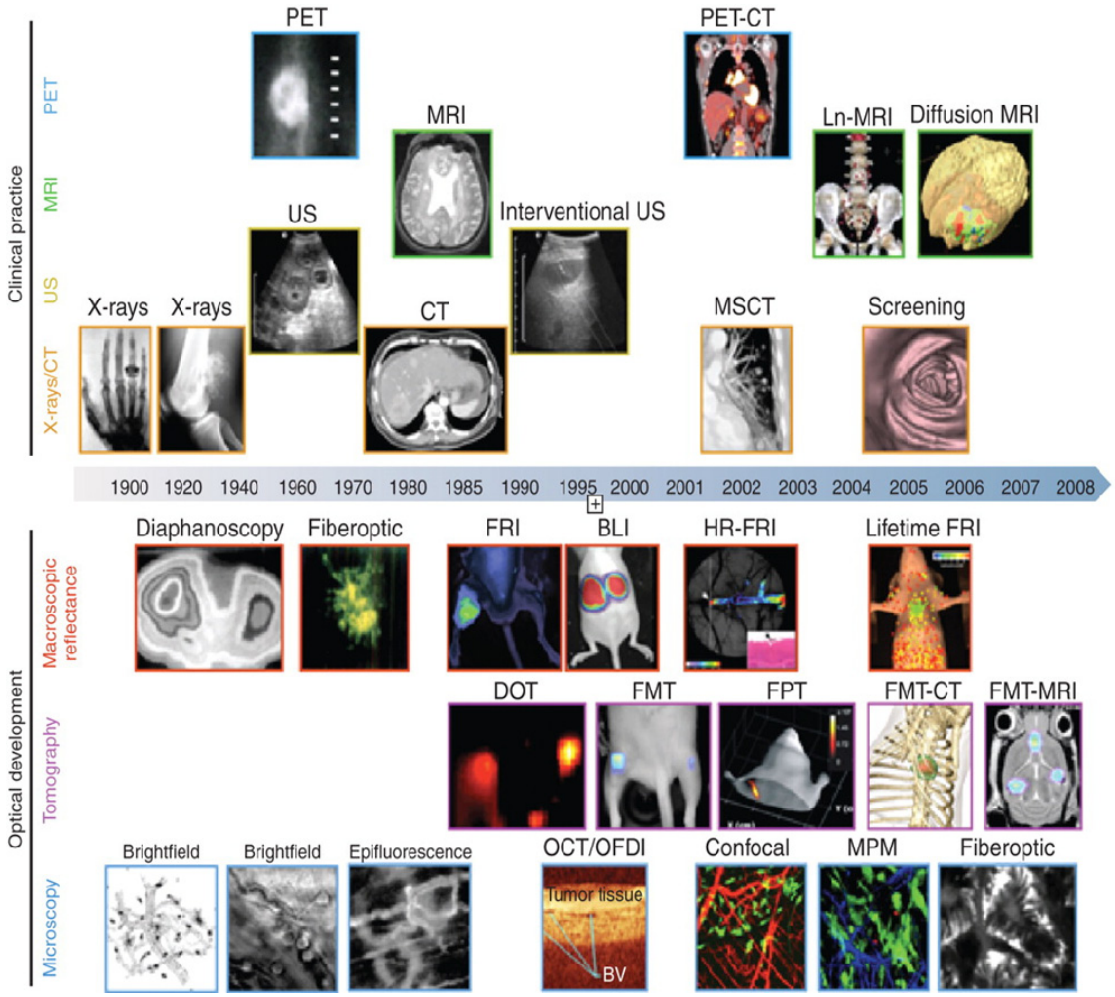

Figure 12 Imaging technologies used in oncology (Condeelis J. et al 2010)

5.1 Overview of actual imaging systems

Imaging systems can be classified by a variety of criteria; the energy used to obtain information (X-rays, positrons, photons or sound waves), the spatial resolution that is attained (macroscopic, mesoscopic or microscopic) or the type of information that is acquire (anatomical, physiological, cellular or molecular). Different features of imaging platforms are more valuable for clinical or research applications. Clinicians use macroscopic imaging systems that provide anatomical and physiological information including CT, MRI and ultrasonography. On the other hand, platforms that provide molecular information are often shared by researchers and clinicians: positron-emission tomography (PET), single-photon-emission CT (SPECT), fluorescence reflectance imaging, fluorescence-mediated tomography (FMT), fibre-optic microscopy, optical frequency-domain imaging, bioluminescence imaging (BLI), laser-scanning confocal microscopy and multiphoton microscopy (Table 10) [136].

It is important that acquired data would be quantitative, allow high resolution and repetition over time, provide molecular information whenever possible[136]. Quantification is absolute in systems where signals are independent of sample position and quantifiable information is provided intrinsically (CT, FMT, MRI and PET). Other techniques such as BLI, fluorescence reflectance imaging and multiphoton microscopy provide only relative quantitative information, since signal intensity depends on the depth of samples in tissues the type of intervening tissues.

Each imaging platform presents advantages and limitations, thus new “multi-modal” systems that combine different platforms and improve visualization are emerging: PET-CT, FMT-CT, FMT-MRI, PET-MRI and PET-BLI and fluorescence [137].

Technique	Resolution	Depth	Time	Quantitation	Multi channel imaging	Imaging agents	Target	Cost	Primary small animal use	Clinical use
MR imaging	10–100 μm	No limit	Min–hours	Absolute	No[1]	Paramagnetic chelates, magnetic particles	A, P, M	$$$	Versatile imaging modality with high soft tissue contrast	Yes
CT imaging	50 μm	No limit	Min	Absolute	No	Iodine	A, P, M[2]	$$	Primarily for vascular, lung, and bone imaging	Yes
Ultrasound imaging	50 μm	Cm	Sec–min	Absolute	No	Microbubbles	A, P, M[2]	$$	Vascular and interventional imaging	Yes
PET imaging	1–2 mm	No limit	Min–hours	Absolute	No	F-18, Cu-64, C-11 and Ga-68 labeled compounds	P, M	$$$	Versatile imaging modality with many different tracers	Yes
SPECT imaging	1–2 mm	No limit	Min–hours	Absolute	Two	Tc-99m, In-111, I-131-labeled compounds, Ga-67, Tl-201	P, M	$$	Commonly used to image labeled antibodies, peptides, or perfusion, etc.	Yes
Fluorescence reflectance imaging (FRI)	1 mm	<1 cm	Sec–min	Relative	Multiple	Photoproteins, fluorochromes	P, M	$	Rapid screening of molecular events in surface-based disease	Yes
Fluorescence mediated tomography (FMT)	1 mm	2–3 cm	Mins	Absolute	Multiple	Near infrared, fluorochromes	P, M	$$	Quantitative imaging of targeted or "smart" fluorochrome reporters	In development
Bioluminescence imaging	Several mm–cm	cm	Sec–min	Relative	Multiple	Luciferins, coelenterazines, luminol	M	$$	Gene expression, cell and bacterial tracking, protein processing, and MPO activity	Potentially in development
Intravital microscopy (e.g., confocal, multiphoton)	1 μm	<400–800 μm	Sec–hours	Relative	Multiple	Photoproteins, fluorochromes	A, P, M	$$$	All of the above at higher resolutions but at limited depths and coverage	In development (endoscopy, skin)

Table 10 Overview of actual imaging systems (Adapted from Condeelis J. et al. 2010)

5.2 Bioluminescence imaging

For this thesis work we took advantage of a BLI platform that allowed us to monitor and fine tune models of GBM therapy in real time.

Bioluminescence is the enzyme catalized conversion of chemical energy into visible light. The substrate molecule that emits light in such a reaction is called luciferin. The enzymes that catalyse the oxidation of luciferins to give rise to non-reactive oxyluciferins and release photons of light are termed luciferases[138].

Bioluminescence imaging strategies are generally used to non-invasively monitor in real time the behavior, distribution, proliferation or differentiation of cells, whether in culture or implanted in live animals. Thus, imaging strategies are based on the modification of cells for the expression of bioluminescent reporters. Genetic reporters are ideal in the sense that their integration on the target cell genome not only guaranties they won't undergo loss due to dilution with cell replication, but also their use to quantify cell number. Light generated by luciferase expressing cells can be detected and quantified using imaging equipment comprising either photo tubes or charge couple devices (CCD) as photon detectors. The extraordinary sensitivity of such detectors together with their capacity of lineal response through 6 orders of magnitude results in extraordinary useful measuring instruments [139].

Depending on the particular type of information to be gather, BLI strategies require taking into consideration multiple variables: animal model, capabilities of imaging equipment, target cells, procedures for reporter generation and genetic manipulation of cells, appropriate luciferase reporter/substrate system, imaging equipment, design of the appropriate vector system for the genetic manipulation of target cells, procedure for the transfection/transduction of target cells.

Luciferase coding sequences, combined with adequate promoter sequences can be engineered in a variety of DNA based constructs as vectors that can be introduced in cells by multiple procedures such as lipofection, electroporation, or infection using viral vectors for their expression in eukaryotic cells. Promoter sequences expressed in the mayority of cell types can be used to produce reporters to gain information on cell

distribution and number. Alternatively, the use of promoter sequences only active in specific cell types allows the generation of luciferase reporters useful to image changes in gene expression or response to environmental agents, eg., during cell differentiation, hypoxia, infectious agents[140-142].

Frequently used luciferases include bacterial luciferases from (*Photobacterium* and *Vibrio)*, Firefly luciferase (*Photinus*), aequorin (from jellyfish *Aequorea*), vargulin (marine ostracod *Vargula*), oplophoran luciferase (deep-sea shrimp *Oplophorus*) and Renilla luciferase (anthozoan sea pansy, *Renilla reniformis*) [143](Figure 13).

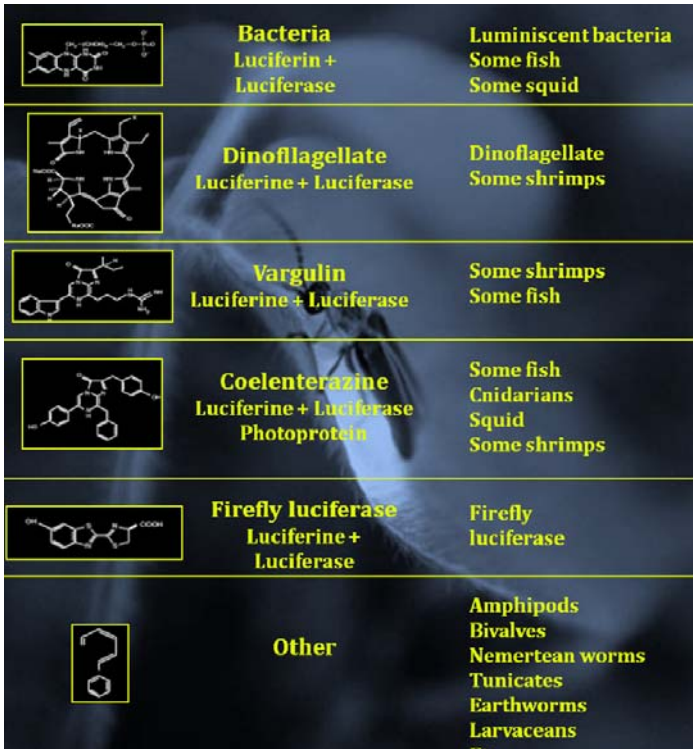

Figure 13 Basic luciferin-luciferase systems found across many phyla.

5.2.1 Firefly luciferase-luciferin system

The luciferase from the firefly *Photinus Photinus pyralis* (Pluc), a Photinus luciferin:oxygen 4-oxidoreductase, was purified and characterized in 1985[144]. PLuc differs from other luciferases in its requirement of ATP as a co-factor to convert its substrate, the luciferin. For this reason firefly luciferin-luciferase system is also used to determine the presence of ATP in the medium. A part from ATP, also O_2 is necessary for light emission of the luciferin oxidation reaction catalized by Pluc takes place in two steps:

- luciferin + **ATP** → luciferyl adenylate + PPi
- luciferyl adenylate + **O2** → oxyluciferin + AMP + **light**

Light photons are emitted when electronically excited oxyluciferin returns to the ground state.

The typical emission spectrum for luciferase is in the yellow-green region (550–570 nm). While in free medium or isolated cells the reaction duration is only a few minutes, luciferase peak activity lasts between 15 and 25 minutes after luciferin ip injection in mice, and can be detected even several hours later. There is a linear relationship between light emission and substrate concentration, as well as acquisition time during peak emission of photons. Due to the sensitivity of luminometers as little as several femtomol of luciferase can be detected in cell preparations[145].

5.2.2 Sea pansy luciferase-coelenterazine system

The Renilla luciferase (RLuc) is an enzyme found in the sea pansy (*Renilla reniformis*) and among other coelenterates, fishes, squids, and shrimps [146]. Rluc has been cloned and sequenced by Lorenz et al. in 1991 and commonly used as a reporter of gene expression in bacteria, yeast, plant, and mammalian cells[147].

RLuc activity is reliant on the concentration of Ca^{2+} for the oxidation of its substrate coelenterazine, an imidazolopyrazine, for the release of light photons. Rluc catalized oxidation of coelenterazine results in the generation of 418-475 nm blue light. RLuc kinetics are fast peaking within 10s after substrate addition, followed by a rapid decline during a 10 min period[148]. Light production reaction is simpler than that of PLuc, as no ATP is required, what results in less damaged cells. This luciferase is of great use in experiments were persistent light emission is not required, due to its fast kinetics.

One of the limitations of the RLuc is its emission of light in the blue region of the spectrum. Blue light is strongly absorbed by biological tissues. To address this problem, variants of RLuc that exhibit red shifted emission spectrum (547 nm peak) and posses greater stability and higher quantum yields have been generated [149].

Due to the lack of crossreactivity between RLuc and PLuc for their respective substrates both luciferases can be used simultaneously in the same cell or animal.

5.3 BLI applications

BLI has been used as a sensitive tool for monitoring gene expression, protein localization, and protein-protein interactions, monitoring of cell death and apoptosis, tumor growth and metastasis in whole animals[150,151].

Luciferase activity is used in standard assays to determine ATP and Ca^{2+} concentration in the medium and detect contamination in the environment or food. Labelling of different bacterial strains with luciferase genes permits to screen their proliferation, metabolism and distribution in the hosts[142].

BLI can be used to study time and space dynamics of physiological processes. Since tissues are translucent, BLI can be used to noninvasive visualize behavior of cells implanted in live animals in real time. In oncology BLI has been used to determine location and quantify growth of xenografted tumors constitutively expressing a luciferase gene, a powerful approach to monitor effectiveness of anti-tumor therapy and metastatic dispersion *in vivo*[152,153]. Additionally, the use of tissue-specific promoters permits the study of changes in gene expression during cell differentiation in real time[154,155]. To this aim cells can be doubly labeled for expression of: a bioluminescent reporter (e.g., RLuc) under constitutive promoter transcriptional control and a different reporter (e.g., PLuc) under control of a differentiation state specific promoter. Measurement of the ratio of light produced by both luciferases allows to the evaluation of changes in gene expression independently of cell number (Figure 14).

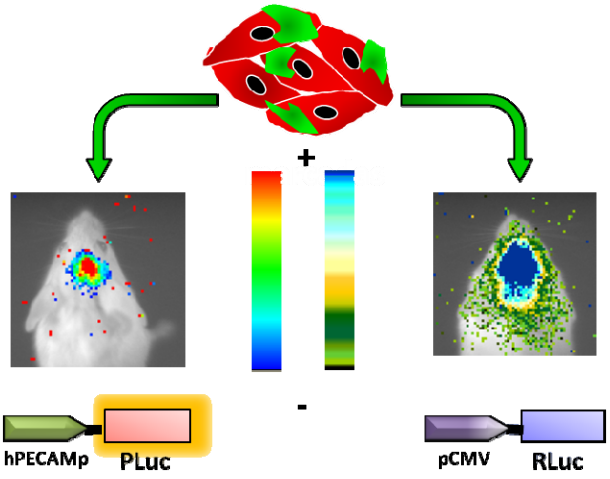

Figure 14 *In vivo* monitorization of cells injected in mouse brain: cells express RLuc under CMV constitutive control and PLuc under PECAM1 promotor transcriptional control. The analysis of the ratio of both luciferases expression permits to determine transcriptional state of PECAM1 gene *in vivo*.

5.4 BLI advantages and disadvantages

Due to the capacity of light photons to transverse many tissues, BLI allows non invasive detection of cells implanted in live small animals[156]. Additionally, since there are no endogene light emitting reactions in mammals, interference by background photons are minimal and measurements can be made with high signal to noise ratios. This allows high sensitivity measurements detecting from single cells *in vitro,* to as little as 500 cells implanted in live animals. Some of the more recent BLI instruments permit imaging of 150 to 200 mice in a single day, since several animals can be imaged at the same time. The time for data acquisition ranges between a few seconds to 10 minutes or hours. The cost of BLI systems is significantly lower than other imaging technologies such as SPECT, PET, or MRI, which only allow imaging one animal at a time and may require 30 to 60 minutes for data acquisition. In addition, data analysis is more complex, requires more time and in some cases injection of radiolabeled molecules is needed (PET, SPECT) [157].

BLI generates 2D images of relatively low resolution, although new imaging algorithms allow some instruments to generate 3D reconstructions[158]. Additional limitations include the need of genetically encoded luciferase in the target cells, the requirement of injecting the substrate to enable light emission, and the dependence of light signal on tissue depth. Light transmission through tissues is rather inefficient and tissue type dependent. In general terms, the bioluminescence signal undergoes a net reduction of approximately 10-fold for every centimeter of tissue depth, restricting the maximal depth to 2-3 cm[159]. Hemoglobin is the main cause for light absortion. Thus, organs with the highest transmission are skin and muscle, while those with the lowest transmission include oxy/deoxyhemoglobin rich liver and spleen. This constitutes the major disadvantage of BLI; the impossibility of its application in large animals including humans. However, these handicaps are not limiting for research using small animals.

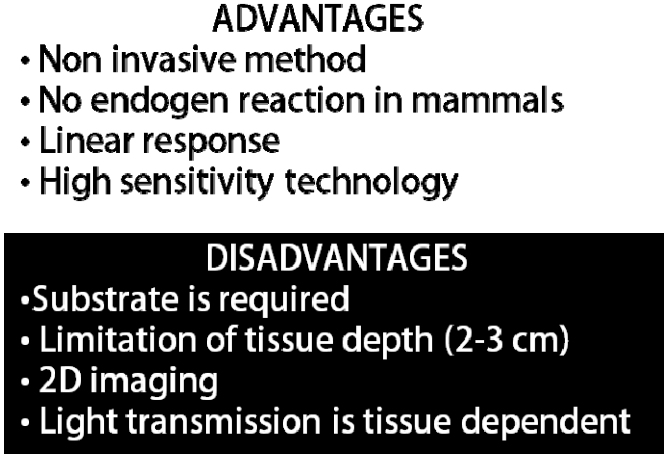

Table 12 Advantages and disadvantages of bioluminescence imaging platform.

OBJECTIVES

The main objective of this thesis was to develop an in vivo model of glioblastoma cell therapy based on the delivery of tumor cytotoxicity deliverd by hAMSCs

To attain the main goal the following sub-objectives were devised:

Develop a system to evaluate tumor growth and therapy efficacy in live animals

I. Generate tumor and cytotoxic hAMSCs (therapeutic cells) expressing bioluminescent and fluorescent reporters for non invasive imaging of tumor and therapeutic cell behavior in live animals.
II. Development of a glioma therapy model based on stereotactic intracerebral implantation of tumoral and cytotoxic therapeutic cells in SCID mice brain.

Optimize the therapy model

III. Optimize a bioluminescence imaging system to non-invasively monitor cell responses.
IV. Optimize delivery of the cytotoxic agent.

Gain insight on the therapeutic mechanism

V. Analyze the differentiation behavior of therapeutic cells in the tumor microenvironment.
VI. Study the interaction of therapeutic hAMSCs with tumor cells.
VII. Evaluate the homing capacity of tumor and therapeutic cells.

MATERIALS AND METHODS

1 CELL CULTURE

1.1 Cell types

1.1.1 293T

Human cell line 293T, originally derived from human embryonic kidney, was obtained from American Type Culture Collection (ATCC, Rockville, EUA). This cell line is a highly transfectable derivative of the 293 cell line into which the temperature sensitive gene for SV40 T-antigen was inserted. In this thesis, 293T were used as a virus packaging cell line, by transient transfections.

293T were cultured at 37ºC with 5% CO_2 in the following medium:

- Dulbecco's modified eagle media-high glucose (DMEM) 4500 glucose (Sigma, Steinheim, Germany)
- 2mM L-glutamine (Sigma)
- 50 µ/ml peniciline/streptomicine (P/S) (Sigma)
- 10% fetal bovine serum (FBS) (Sigma)
- 25mM Hepes (Sigma)

For virus production, and after transient transfection, the same culture medium lacking FBS was used.

1.1.2 hAMSC

hAMSC were isolated from adipose tissue derived from cosmetic subdermal liposuctions, with patient consent. After rinsing with PBS 1X, lipoaspirates were suspended in one volume of 1X collagenase I (Invitrogen, Carlsbad, CA) solution and incubated 30 min at 37ºC with gentle agitation. Digestion was terminated by inactivation of the collagenase I by addition of one volume of DMEM + 10% FBS. Cells were seeded at 5000 cl/cm^2 density at 37ºC with 5% CO_2 in the following medium:

- DMEM 4500 glucose
- 2 mM L-glutamine

- 50 µ/ml P/S
- 10% FBS

1.1.3 U87 MG

U87 MG (ATCC) is a glioblastoma multiforme, astrocytoma cell line obtained from a human malignant glioma. The karyotype of these cells is hypodiploid female, usual chromosome number of 44 in 48% of cells and 5.9% present a higher ploidy rate. Cells were cultured at 37ºC with 5% CO_2 in the following medium:

- 1:1 mixture DMEM 4500 glucose and HAM's F-12
- 2 mM L-glutamine
- 50 µ/ml P/S
- 10% FBS

1.2 Cell storage

Freezing medium contained:

- 90% FBS
- 10% dimethil sulfoxide (DMSO)

Before resuspending cell pellets, freezing medium was maintained at 4ºC for 15 minutes. Cell concentration was of 1-5 x 10^6 cells/ml, aliquots were prepared in criotubes and hold in feezing containers at -80ºC. After 48 hours, cells were conserved in liquid nitrogen for a long-term conservation.

1.3 Flow cytometry analysis

- hAMSC were suspended in PBS + 1% bovine serum albumin (BSA)
- Cells were incubated with following antibodies: mouse anti-human cd90-PE (BD Bioscience); mouse anti-human cd34-PE (Abcam, Cambridge, UK); mouse anti-human cd105-PE (BD Bioscience); mouse anti human cd 106-PE (BD, Bioscience); mouse anti-human cd73-PE (BD, Bioscience); mouse anti-human cd29 (BD, Bioscience); mouse anti-human cd45-FITC (BD, Bioscience); mouse

anti-human cd44-PE(BD, Bioscience).Unspecific binding was assessed by isotype control mouse IgG2α-PE (BD, Biosciences), mouse IgG1κ-PE (BD, Bioscience) and mouse IgG1κ-FITC (BD, Bioscience).

- Antibody-FITC and PE binding was analyzed by fluorescence-activated cell sorting (FACS) in an EPICS XLTM Flow Cytometer.

1.4 *In vitro* tube formation assay

- 50 µl of Matrigel TM (BD Bioscience Inc, Franklin Lakes, New Jersey, EUA) solution manipulated at 4ºC were added per well in a 96-well plate and incubated for 30 minutes at 37ºC.
- $1x10^4$ cells in 100 µl of EGM-2 (Lonza Walkersville, Inc.; ref. CC-3162) were seeded on Matrigel coated wells.
- Formation of tube-like structures was monitorized for 7 hours by phase contrast microscopy.

1.5 Cell proliferation assay

CellTiter 96 Aqueous One Solution Cell Proliferation Assay (Promega) was used for cell doubling time determination, ganciclovir toxicity and cytotoxic bystander effect *in vitro*:

- Quadruplicates of $3x10^3$ hAMSC and $5x10^3$ U87 cells were plated into 96-well plates and incubated overnight at 37ºC.
- Culture medium was replaced 24 h later (T=0).
- 20µl of CellTiter 96® AQueous One Solution Reagent was added into each well of the 96-well assay plate containing the samples in 100µl of culture medium.
- The plate was incubated at 37°C for 2 hours in a humidified, 5% CO_2 atmosphere.
- Proliferation was evaluated spectrophotometrically at 490 nm at days 0, 5 and 9.
- Results were expressed as the percentage of proliferation, where the proliferation of cells in culture medium at day 0 was set to 100%.

1.6 Cell invasion assay

To analyze *in vitro* homing capacity of hAMSCs and U87 we used a 2D invasion assay with µ-Dish35mm, low Culture-Insert (Ibidi, Martinsried, Germany).

- Cell suspensions containing 10^3 of hAMSCs or $2x10^3$ U87 in 70 µl of medium were prepared.
- Different suspensions were seeded in each well of the culture-insert and incubated at 37 °C and 5 % CO2 as usual.
- After appropriate cell attachment (24 hours) the culture-insert was gently removed by using sterile tweezers and the dish was washed and filled with medium.
- Cell invasion was monitorized for 24 hours by phase contrast microscopy.

1.7 BLI determination of luciferase activity *in vitro*

Mixed cell cultures containing 10^4 U87 with several proportions of hAMSC were seeded on 48-well plates and analyzed by BLI at days 0, 5 and 9, with changes of medium every 3 days:

- Medium was removed from the wells.
- Wells were rinsed twice with PBS 1x.
- 100 µl of Pluc or Rluc substrate stock reagent (Caliper, Hopkinton, MA, US and Prolume, Pinetop, AZ, US) was added.
- For imaging, plates were placed in the detection chamber of a high-efficiency ORCA-2BT Imaging System (Hamamtsu Photonics, Hamamatsu City, Japan) provided with a C4742-98-LWG-MOD camera fitted with a 512 x 512 pixel charge couple device cooled at -80ºC.
- Immediately following substrate addition images were acquired during 1 min using 1x1 array (binning 1x1), and in order to register the position of the light signal, an additional image was obtained using a white light from a lamp in the detection chamber.

- Light events were calculated using the Hokawo2.1 image analysis software and expressed as PHC after discounting the background of wells without cells. The net number of PHCs in the area of interest was calculated using the formula: PHCs = (total number of PHCs in the area of interest)-[(number of pixels in the area of interest)x(average background PHCs per pixel)].
- Pseudo color images were generated using arbitrary color bars representing standard light intensity levels for Pluc (blue: lowest; red: highest) and for Rluc (black: lowest; blue: highest).

Viral vectors were used for cell labelling for stable expression of bioluminescent and fluorescent proteins. Lentivirus system was employed since hAMSC have low division rate.

2.1.1 pRRL-Luc-IRES-EGFP vector

The construction pRRL-Luc-IRES-EGFP was kindly provided by Dr. Alvarez-Vallina [160]. The vector contained the PLuc under control of the cytomegalovirus (CMV) promoter followed by and IRES to express an eGFP.

2.1.2 hrl-mrfp-tk vector

hrl-mrfp-tk vector, kindly donated by Dr. S. Gambhir[133] (Standford University, US), contains a chimeric trifunctional reporter comprising Rluc, monomeric red fluorescent protein (mRFP1) and a truncated version of the herpes simplex virus thymidine kinase coding sequences (sr39tk) regulated by the CMV.

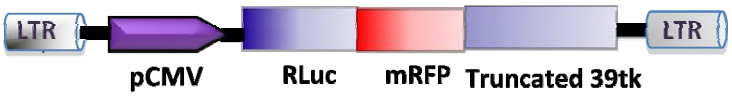

2.1.3 PLox:hPECAMp:PLuc:eGFP

This vector that expresses chimeric Pluc and eGFP regulated by the endothelial specific promoter PECAM was constructed in our group [155]. First, a pLox:PLuc:eGFP lentiviral vector containing a fusion reporter comprising PLuc and eGFP, was obtained by polymerase chain reaction amplification and standard cloning procedures using the PLuc and eGFP genes from plasmid pGL4.10:PLuc (Promega Corporation, Madison, WI, USA) and pEGFP-N1 plasmid (Clontech Lab., Palo Alto, CA, USA). In a second step the HPECAM-1p, kindly provided by Dr. Carmelo Bernabéu (Centro de Investigaciones Biologicas, CSIC, Madrid), was cloned into pLox:PLuc:eGFP using XbaI/SpeI and SpeI enzymes respectively.

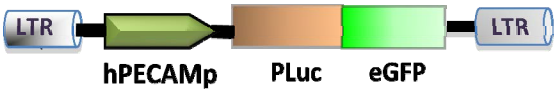

2.1.4 Notch homolog 1 MISSION® shRNA Lentiviral Transduction Particle

This vector that expresses a shRNA anti-Notch1 in a PLKO.1-puro backbone vector was purchased from Sigma-Aldrich (NM_017617). The following clones were tested: TRCN0000003358, TRCN0000003359, TRCN0000003360, TRCN0000003361, TRCN0000003362. The clone TRCN0000003360 showed the most effective inhibition and was used in the experiments.

2.1.5 MISSION® pLKO.1-puro Empty Vector Control Plasmid

The MISSION pLKO.1-puro Control Vector is a lentivirus plasmid vector purchased from Sigma-Aldrich (SHC001). The vector does not contain any shRNA insert and was used as a negative control in experiments using the MISSION shRNA library clones.

2.2 Lentiviral particle production

The day before transfection, 3 x 10^6 trypsinized 293T cells were seeded on 10 cm^2 poly-D-lysine treated plates (Sigma), allowing cell adherence. 24 hours later, and 2 hours before transfection, cell medium is changed and 9 ml of fresh mendium were added.

For each transfection 6 µg of lentiviral transfer vector (pRRL-Luc-IRES-EGFP, hrl-mrfp-tk, pLox:Pecam-Luc:eGFP), were mixed with 2 µg of viral envelope plasmid (pMD-G-VSV-G) and 4 µg of packaging construct (pCMV DR8.2) in 250 µl of 150 mM NaCl. Then DNA mix was supplied with 48 µl of 1 mg/ml polyethylene amine (Polyscience, Warrington, PA, US) in 250 µl of 150 mM NaCl, and incubated at room temperature (RT) for 20 min. This DNA solution was then added drop wise to the plate containing the 293T cells in growth medium, swirled gently and then incubated for 16 hours at 37º C with 5% CO2. The following day, the transfection solution was removed, the cells were rinsed with PBS 1X and medium without FBS was added to the cells. After 48 hour incubation, the supernatant was collected, centrifuged at 400g to remove cell debris, and filtered through a 0.45 µm low protein binding filter (Corning, Bath, UK). The filtered supernatant was then kept at -80ºC for storage.

2.3 Virus titration

Viral titers were determined using the HIV-1 p24 antigen EiA 96 test kit(Beckman Coulter).

- Test and blank aliquots were placed in 96-well plate and incubated with lysis buffer for 1 hour at 37ºC. Medium was removed and wells were washed with washing buffer 6 times during 30 seconds.

- 200 µL of reconstituted Biotin Reagent was added to all testing wells, except the substrate blank well and incubated for 1 hour at 37ºC. Subsequently medium was removed and well were washed with wash buffer 6 times during 30 seconds.
- 200 µL of SA-HRPO Working Dilution was added to all testing wells, except the substrate blank well and incubated for 30 minutes at 37ºC. Wells were washed as described above.
- Finally, 200 µL of TMB-Substrate Solution (containing Streptavidin conjugated to horseradish peroxidase) were added to all wells and dark incubated for 30 minutes at RT.
- 50 µL of CSR-1 was added to all wells to stop the reaction.
- Absorbance was read at 450/470 nm. Results were obtained in pg/ml of HIV-1 p24 quantity. With the used transfection conditions we obtained that 10ng of p24 matched with 10^6 transecting units (TU).

2.4 Cell transduction

- hAMSC were seeded at 5000 cells/cm^2 and U87MG at 1000 cells/cm^2 in 12-well plates.
- Cell medium, containing polybrene (hexadimethrine bromide) (Sigma) at a final concentration of 10 µg/ml and 500 µl of concentrated virus at 21 MOI ($2x10^6$ TU/ml Multiplicity of Infection) was supplied to the cells.
- Cells were incubated in transduction medium for 48 hours and were washed with PBS 1x. Fresh medium was added and cells were cultivated for several passes.
- Viral transduction efficiency was determined by fluorescent protein detection by fluorescent microscopy or by flow cytometry.

2.5 Transduced cell selection

Fluorescent cells were selected by fluorescence-activated cell sorting (FACS), for cells labeled with Plox-G-Luc (green fluorescence) and for cells labeled with hrl-mrfp-ttk

(red fluorescence). Depending on the cell type and proliferation capacity, selection was performed between 5% and 30% of the maximal labeling.

2.6 Bioluminescent and fluorescent cell lines

Table 13: shows a list of reporter expressing cell lines generated:

- PL-G-U87
- RL-R-tTK-hAMSC
- RL-R-tTK: PECAM-PL-G-hAMSC
- RL-R-tTK: αNotch1-hAMSC
- RL-R-tTK: PECAM-PL-G: αNotch1-hAMSC
- Sh:RL-R-tTK-hAMSC
- Sh:RL-R-tTK: PECAM-PL-G-hAMSC

	Cell line	Constitutive bioluminiscent marker	Constitutive fluorescent marker	PECAM 1 induced bioluminiscent marker	PECAM 1 induced fluorescent marker	shRNA	Cytotoxic gene
PL-G-U87	U87	*Photynus* luciferase	eGFP				
RL-R-tTK-hAMSC	hAMSC	*Renilla* luciferase	RFP				Thymidine kinase
RL-R-tTK: PECAM-PL-G-hAMSC	hAMSC	*Renilla* luciferase	RFP	*Photynus* luciferase	eGFP		Thymidine kinase
RL-R-tTK: αNotch1-hAMSC	hAMSC	*Renilla* luciferase	RFP			Anti-Notch1	Thymidine kinase
RL-R-tTK: PECAM-PL-G: αNotch1-hAMSC	hAMSC	*Renilla* luciferase	RFP	*Photynus* luciferase	eGFP	Anti-Notch1	Thymidine kinase
Sh:RL-R-tTK-hAMSC	hAMSC	*Renilla* luciferase	RFP			Empty	Thymidine kinase
Sh:RL-R-tTK: PECAM-PL-G-hAMSC	hAMSC	*Renilla* luciferase	RFP	*Photynus* luciferase	eGFP	Empty	Thymidine kinase

Table 13 Compilation of genes expressed by the cell lines used during the thesis

3 *IN VIVO* ANIMAL MODEL

3.1 SCID mice

Severe Combined Immunodeficiency (SCID) mice used during these studies were purchased from (Charles Rivers, Wilmington, MA, USA) and kept under pathogen-free conditions in laminar flow boxes. Animal maintenance and experiments were performed in accordance with established institutional guidelines and approved protocols.

3.2 Stereotactic implantation in SCID mice brain

All *in vivo* experiments used an orthotopic U87 tumor model with or without hAMSCs implanted in the brain of 6 weeks old SCID mice:

- Animals were anesthetized by i.p. injections of xylazine (Henry Schein, Melville, NY,USA) 3.3 mg/kg and ketamine (Merial, Duluth, GA, USA) 100 mg/kg.
- Subsequently mice were mounted in a stereotactic frame (Stoelting, Wood Dale, IL, U.S.A.) and their heads were secured using a nose clamp and two ear bars, and a skin flap was lifted to expose the skull surface and further anesthetized, by injection of fentanil (Kernpharma, Barcelona, Spain).
- For stereotactic cell implantation, a burr hole was drilled at the following coordinates (0,6 mm posterior, 2 mm lateral and 2,75 mm depth respect Bregma). The injections were delivered at a rate of 0.25 µl/min in volume of 4 µl, using a Hamilton syringe series 700 and the needle was slowly withdrawn after additional 5 minutes (Figure **15**).
- The scalp was closed by suture and the animals were placed in individual recovery cages and supplied with buprenorfine (Buprex, Schering Plough SA, Madrid, Spain) in the drinking water when needed.

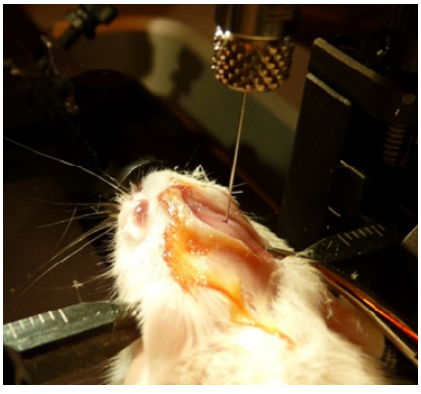

Figure 15 Stereotactic cell injection

3.2.1 Implantation of tumor and hAMSC mixtures

Tumor and hAMSC mixes in different proportions were implanted in a 6 µl volume.

3.2.2 hAMSCs injection

In some studies hAMSCs were implanted into an established tumor or in the contralateral hemisphere. The same protocol described in previous sections was used, except for contralateral injection where cells were injected at coordinates 0,6 mm posterior, -2 mm lateral and 2,75 mm depth respect Bregma (Figure 16). For studies involving frontal migration, hAMSCs were injected 1mm anterior, -2 mm lateral and 2,75 mm depth respect Bregma.

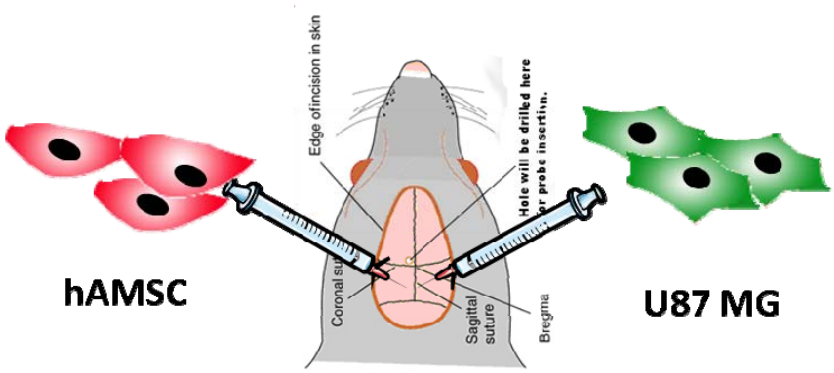

Figure 16 Diagram of contralateral hAMSC injection

4 NON INVASIVE BIOLUMINESCENCE IMAGING

- Mice were anesthetized by i.p. injection with 3.3 mg/kg of xylazine (Henry Schein) and 100 mg/kg of ketamine (Merial).
- Mice were then injected i.p. with 150 µl of luciferin (Caliper) (16.7 mg/ml in saline) or through tail vein with 25 µl of benzyl coelenterazine (1 mg/ml in 50/50 propilenglycol/ethanol) (Prolume) diluted in 125 µl of water.
- Animals were placed on a black methacrylate plate in the detection chamber of the high efficiency ORCA-2BT Imaging System at a determined distance (255cm). This distance permitted to acquire an image of the whole head of the animal at the maximal aperture of the camera objective (HFP-Schneider Xenon 0,95/25 mm).

- Images were acquired from the dorsal direction during different time periods depending of the emitted light. During the analysis emmited photons are correlated to the time of acquisition. In general time of acquisition was 5 minutes. In cases of detection of hAMSCs after a long period post-injection time of acquisition was 10-15 minutes. For tumors in advanced phase the time of acquisition was of 5-30 seconds. To increase detection sensitivity, the readout noise of the recorded signal was reduced by adding together the light events registered by arrays of 8 x 8 adjacent pixels that are read simultaneously (binning 8 x 8) of the camera CCD.
- A second image of the animal was obtained using a white-light source inside the detection chamber, to register the position of the luminescence signal, during 125 milliseconds at 1x1 binning.
- Mice were imaged weekly during experiments.
- Quantification and analysis of photons recorded in images was done using the Wasabi image analysis software (Hamamatsu Photonics) as described above.

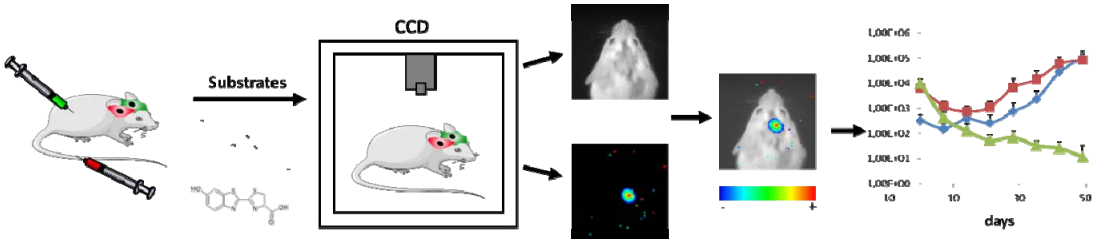

Figure 17 General diagram of BLI protocol

4.1 Quantification and analysis of photons recorded in the images

Quantification and analysis of photons recorded in images was done using the Wasabi image analysis software (Hamamatsu Photonics). Light events were expressed as Photon counts (PHCs) and determined by the following scheme:

- Using the Hokawo image analysis software the area of interest was selected and the total number of recorded PHCs was extracted.

- Background was determined extracting PHCs from an area with no detectable signal from the same image.
- The net number of PHCs for the study was calculated using the formula: (**total number of PHCs in the area of interest**)-[(**number of pixels in the area of interest**)x(**average background PHCs per pixel**)].
- When required for the study the PHC values were correlated to the initial number of PHCs.

4.2 Assessment of the cell number from the light measurements

Predetermined numbers of PL-G-U87 ($1x10^4$, $2,5x10^4$, $5x10^4$ and $1x10^5$) and RL-R-tTK-hAMSC ($1x10^4$, $3x10^4$, $5x10^4$ and $1.5x10^5$) were implanted in the brain of live mice at the previously indicated coordinates (the same as used for the experiments) and immediately after implantation imaged by BLI after administration of the corresponding luciferase substrate, luciferin or coelenterazine.

Light measurements were expressed as PHCs following subtraction of background as previously described. Data were represented as a standard curve with the number of PHCs versus number of grafted cells.

Pseudo color images were generated using arbitrary color bars representing standard light intensity levels for Pluc (blue: lowest; red: highest) and for Rluc (black: lowest; blue: highest).

5 MICROSCOPIC ANALYSES

Brain from sacrificed mice were harvested, washed with physiological serum, fixed with paraformaldehyde during 48 hours and placed in 30% sucrose for 48 hours in order to cryoprotect the tissue. Brains were then washed with PBS 1x, embedded in OCT, sliced in 10-20 µm sections and mounted on glass slides.

Hoechst staining was performed for detection of cell nuclei. For macroscopic view analysis 20 µm brain sections were stained with Hematoxylin and Eosin (HE).

5.1 Fluorescence angiography

For tumor microvessel imaging, mice were anesthetized and injected trough the lateral tail vein with 200 µl (10 mg/ml) of a high molecular weight (2,000,000 MW) FITC-conjugated dextran Sigma (St Louis, MO, US). Ten minutes after the injection mice were sacrificed and brains were retrieved and fixed in paraformaldehyde during 24 hours. The fixed brains were sliced 10-20 µm sections and analyzed for microvessel formation and presence of fluorescent hAMSCs and U87 using confocal laser scanning microscopy (Leica TS1 SP2).

5.2 Immunofluorescence histology

Fluorescent immunodetection was performed on 10 µm thick section as follows:

- The slides were washed 2 x 5 minutes in TBS.
- The slides were washed 3 x 10 minutes in TBS + 0, 5% Tritó-X100 (0, 5% TBS-T).
- Blocked in 1% BSA + 5% NDS en TBS-T for 1 hour at room temperature.
- Primary antibody diluted in blocking solution was applied and incubated overnight at 4ºC with gentle agitation (Table 14).
- Slides were tempered and rinsed 3 x 5min with 0, 5% TBS-T.
- Secondary antibody diluted in TBS with 1% BSA was incubated for 1 hour at room temperature and darkness.
- Slides were washed 3 X 5 min in TBS.
- Slides were incubated with Bisbenzimide (Hoechst, Sigma) (1 µg/ml) for 15 min
- Slides were washed 2 X 5 min in TBS.
- Slides were mounted in FluoromountTM (Sigma).

Antigen	Primary antibody host	Primary antibody dilution	Primary antibody comercial house	Specie recognized by secondary antibody	Secundary antibody dilution	Secondary antibody labelling	Secondary antibody comercial house
PECAM 1	Mouse	1:50	Abcam	Mouse	1:200	Cy5	Jackson ImmunoResearch
αSm22	Mouse	1:50	Abcam	Mouse	1:200	Cy5	Jackson ImmunoResearch
CD133	Mouse	1:50	R&D Systems	Mouse	1:200	Cy5	Jackson ImmunoResearch
RFP	Rabbit	1:50	Abcam	Rabbit	1:200	Alexa 549	Jackson ImmunoResearch
GFP	Chicken	1:200	Abcam	Chicken	1:200	DyLight 488	Jackson ImmunoResearch

Table 14 Compilation of different primary and secondary antibodies used for immunofluorescence

6 REAL-TIME PCR

- Total RNA from the sample was obtained with RNeasy Plus Micro Kit (QIAGEN) following the indicated procedure (http://www1.qiagen.com/HB/RNeasyPlusMicroKit_EN).
- RNA was quantified by Nanodrop spectrophotometer (Thermo Scientific, Waltham, Massachusetts, EUA).
- cDNA was synthesized from 2 µg of RNA following the kit Script One-Step RT_PCR kit (Bio-Rad, Hercules, CA, EUA) protocol:
    - 25 µl 2X RT-PCR reaction
    - (21,5-X) µl nuclease free H_2O (adjusted to 50 µl final volume of reaction)
    - X µl RNA (~2 µg)
    - 2,5 µl (≈250 nM) Random hexamers (50 µM)(Qiagen)
    - 1 µl iScript Reverse Transcriptase (50X)
    - Thermal cycler (Bio-Rad) was programed to run the following protocol:
    - 10 min a 25ºC (hexamers annealing)
    - 10 min a 50ºC (cDNA synthesis)
    - 5 min a 95ºC (reverse transcriptase inactivation)
- Real-time PCR was performed with 2 µl of cDNA in a final volume of 20 µl containing:
    - 7 µl nuclease free H_2O

- 10 µl TaqMan 2X Universal PCR Master Mix (Applied Biosystems, Carlsbad, CA, EUA)
- 1 µl primers from Applied Biosystems EGR-3 (Hs00231780_m1); CD31 (Hs00169777_m1); ILK (Hs00177914_m1); SDF-1 (Hs00930455_m1); VEGFa1 (Hs00173626_m1); Notch1 (Hs01062014_m1); Osteocalcin BGLAP (Hs01587813_g1), GADPH (Hs99999905_ml).

- Data were analyzed using ABI Prism 7000 Sequence Detection System program.

Relative quantification with standard curve method was used to determine the changes in steady-state mRNA levels of the genes across multiple samples and express them relative to the levels of an internal control RNA (GAPDH). The classic comparative 2-ΔΔCt method [161] was used to calculate the expression level of the gene of interest relative the reference sample.

RESULTS

1 *IN VIVO* RL-R-TTK-HAMSC MEDIATED BYSTANDER GLIOBLASTOMA THERAPY

Current treatment protocols for GBM are ineffective due to its invasiveness, which prevents complete surgical removal and promotes persistence of radiation and chemotherapy resistant cells after therapy. A promising approach has emerged based on the use of cellular vehicles to deliver localized treatment targeting the primary tumor mass[57]. In the current thesis, an efficient therapeutic strategy model using hAMSCs was developed against glioblastoma. Fine tune and evaluation of the therapeutic process in real time was possible by taking advantage of BLI to noninvasively monitor tumor and therapeutic cells.

Therefore the first objective of this thesis to achieve was:

I. Generate tumor and cytotoxic hAMSCs (therapeutic cells) expressing bioluminescent and fluorescent reporters for non invasive imaging of tumor and therapeutic cell behavior in live animals.

1.1 Transgene expression in hAMSC and U87 cells.

To noninvasively monitor the behavior of tumor and therapeutic cells during therapy lentiviral vectors were used to introduce the genes of interest. Lentiviral vectors can transduce with high-efficiency dividing and quiescent cells and incorporate their genome into the host genome, allowing stable gene expression. In addition, lentiviral vectors do not seem to induce a strong immune response and are less disposed to transcriptional silencing than onco-retroviral vectors[162].

Human glioblastoma U87 MG tumor cells were transduced with lentiviral construct pRRL-Luc-IRES-EGFP, kindly provided by Dr. Alvarez-Vallina[160]. Transduction with this vector resulted in the stable expression of the chimeric reporter with Pluc and eGFP activities, to generate “PL-G-U87” tumor cells.

hAMSCs were genetically modified with a lentiviral vector to express a tri-functional reporter hrl-mrfp-tk, kindly donated by Dr. S. Gambhir[133] comprising Rluc, RFP and a truncated version of HSV-TK (tTK) to generate RL-R-tTK-hAMSC “therapeutic vehicles”.

One of the advantages of this system is that bioluminescent and fluorescent reporters as well as suicide gene expression are under the same constitutive promoter control. Thus expression of all gene activities is always proportional to each other.

This use of two different luciferase systems allowed independent imaging of therapeutic and tumor cells using non-cross-reacting luciferase substrates, coelenterazine and luciferin, respectively (see page 53). In addition, the inclusion of two different fluorescent protein reporters, allowed selection of labeled cells by FACS, and detection of therapeutic and tumor cells by fluorescence confocal microscopy of tissue sections.

1.1.1 RL-R-tTK-hAMSCs characterization.

Sometimes viral transfection can bring undesirable consequences such as changes in gene expression or extreme proliferation. To determine whether lentiviral transduction and consequent gene expression had modified hAMSC growth characteristics we compared RL-R-tTK-hAMSCs and untransduced hAMSC doubling time and immunophenotype.

Flow cytometry analysis of following hAMSC markers was performed: CD105, CD44, CD29, CD90, CD73, CD106, CD34, CD45. As represented on Figure 18 hAMSCs and RL-R-tTK-hAMSCs presented the same immunophenotype that defines hAMSC (see page 40).

Proliferation rate of RL-R-tTK-hAMSCs and untransduced hAMSCs was evaluated spectrophotometrically by CellTiter 96 Aqueous One Solution Cell Proliferation Assay. As represented on Figure 19 no significative difference was detected in different cell populations doubling time.

Thus we assumed that lentiviral transduction did not have a detectable effect on these hAMSCs features.

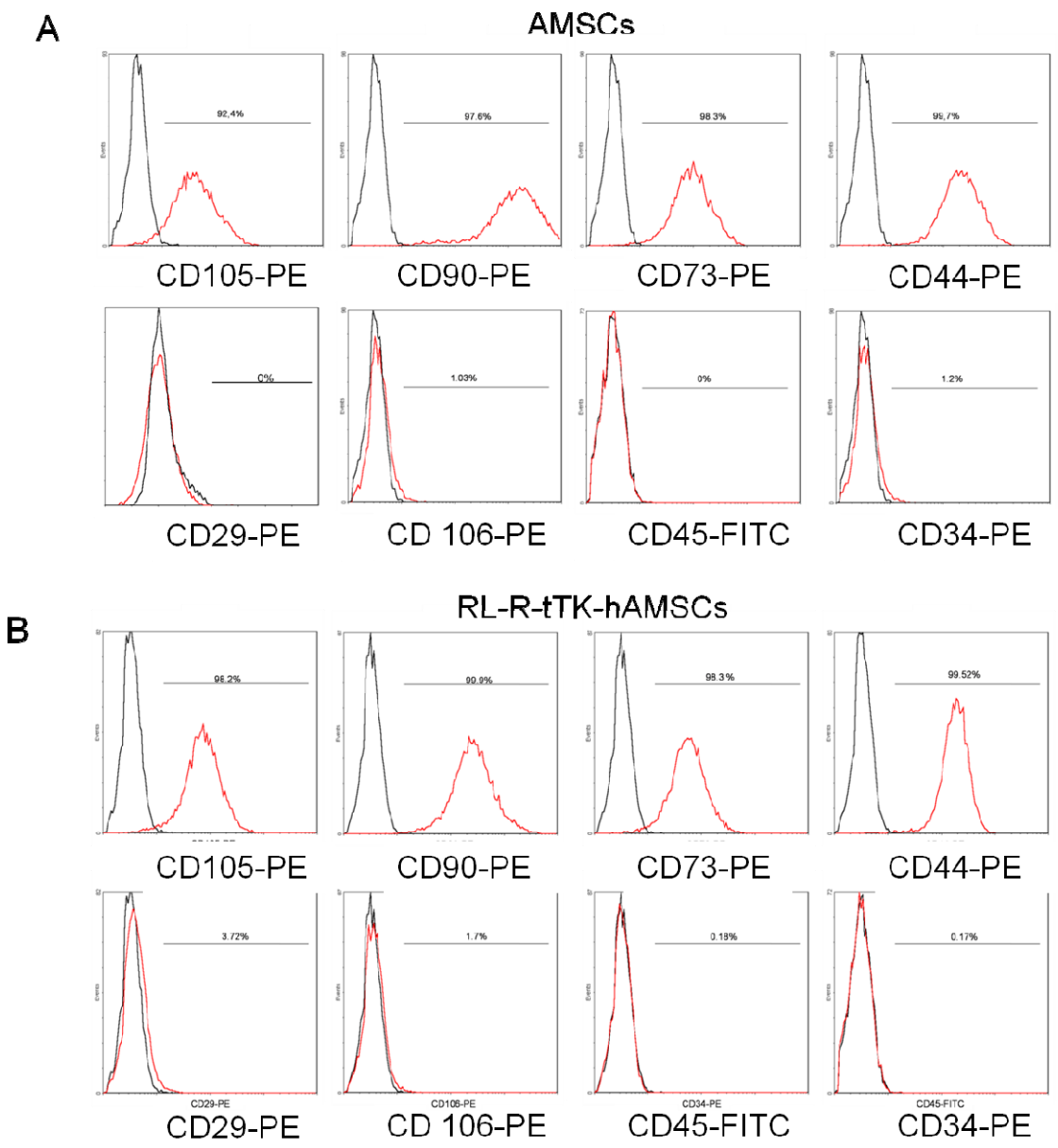

Figure 18 Characterisation of transduced and untransduced hAMSC. Flow cytometric analysis of hAMSCs (A) and RL-R-tTK-hAMSCs (B) using antibodies against CD105, CD44, CD29, CD90, CD73, CD106, CD34, CD45 showed no difference in marker expression.

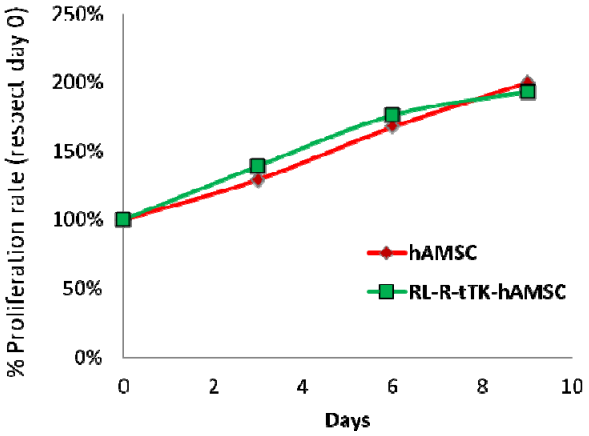

Figure 19 Proliferation rate of transduced and untransduced hAMSCs was evaluated spectrophotometrically by standard MTS assay and expressed as percentage of cell proliferation (respect day 0).

1.1.2 Cells sensitivity to GCV

Before beginning bystander killing experiments we needed to demonstrate that tTK gene was functional in the genetically modified therapeutic vehicles and to determine GCV effect on tumoral and therapeutic cells.

Replicate cultures of PL-G-U87, hAMSCs and RL-R-tTK-hAMSCs were seeded in tissue culture plates and were treated with GCV (4µg/ml) or normal medium. Cell survival or proliferation was assessed using the CellTiter 96 Aqueous One Solution Cell Proliferation Assay.

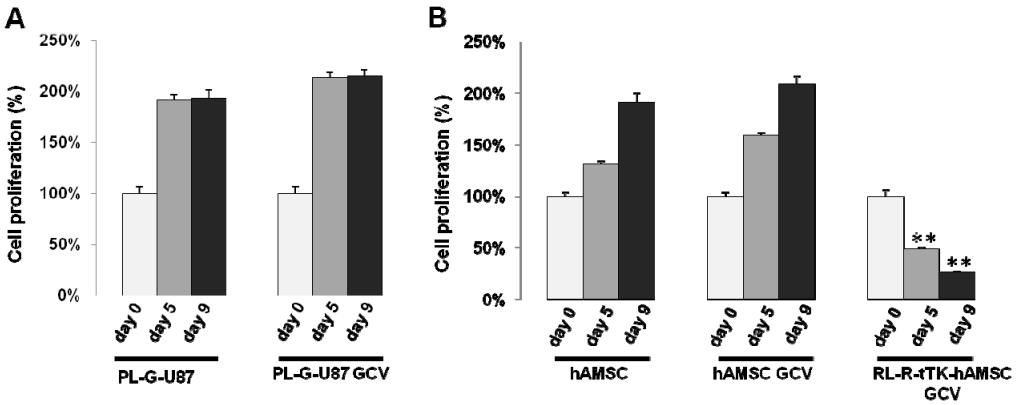

Figure 20 Sensitivity of PL-G-U87 cells (A), RL-R-tTK-hAMSC and hAMSC (B) to GCV. Cells were grown during the indicated times and treated with GCV (4 µg/ml) or not, as indicated. Number of viable cells was evaluated spectrophotometrically by MTS assay and expressed as percentage increase relative to cell number at day 0. Histograms show mean ± SEM, **p<0.01 respect untreated cells, n=4 for each group.

As shown on Figure 20 A treatment with GCV had no effect on survival of PL-G-U87. Proliferation rate was the same whether treated with GCV or not. GCV treatment had no effect on growth pattern of unmodified hAMSCs, lacking the tTK gene, either on PL-G-U87 (Figure 20 B). However, as expected, GCV treatment did exert a strong cytotoxic effect on tTK expressing hAMSCs, that increased in time (Figure 20 B). What is more, hAMSCs and RL-R-tTK-hAMSCs where grown in increasing concentrations of GCV (0 µg/ml, 2 µg/ml, 4 µg/ml and 8 µg/ml) and it was determined that cytotoxic effect of tTK was proportional to GCV concentration (Figure 21). However untransduced hAMSCs would proliferate without significant change even in the presence of high concentrations of GCV, confirming its low toxicity.

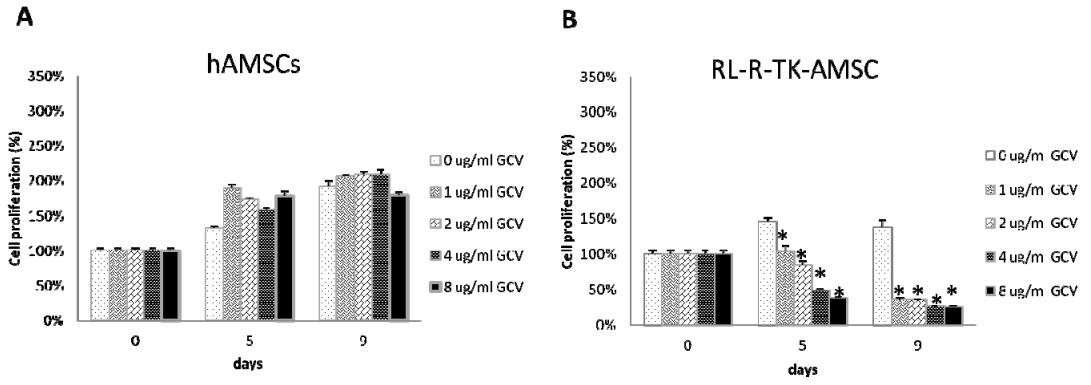

Figure 21 Cell sensitivity to increasing dose of GCV. hAMSC and RL-R-tTK-hAMSC were cultured in medium containing GCV at indicated concentrations (0 µg/ml, 2 µg/ml, 4 µg/ml and 8 µg/ml). Cell viability was evaluated spectrophotometrically by standard MTS assay and expressed as percentage of cell proliferation (respect day 0) * P<0,01, respect same day and same concentration of hAMSC, n=4 for each group. (**A**) RL-R-tTK-hAMSC proliferation rate is sensitive to GCV dose. At day 5 there is a linear correlation between GCV concentration and cell death. (**B**) hAMSCs and U87 proliferate without significant change even in the presence of high concentrations of GCV confirming its low toxicity.

1.1.3 Bystander killing of PL-G-U87 glioblastoma cells by RL-R-tTK-hAMSC *in vitro*

Once demonstrated functionality of tTK gene expressed by RL-R-tTK-hAMSC, we studied the bystander effect of these cells on tumoral cells. To assess this purpose we used BLI that allowed us to monitorize proliferation of different cell populations separately in the same well. Cocultures of luciferase expressing RL-R-tTK-hAMSC and PL-G-U87 were plated in different proportions (1:20, 2:20, 4:20). Cells were treated

with GCV (4 μg/ml) or PBS. Survival of PL-G-U87 cells was determined by BLI at days 0, 4 and 8.

As shown in Figure 22, viability of PL-G-U87 cells in the presence of GCV was inversely proportional to the ratio of therapeutic to tumor cells (88%, 93%, 94% killing for 1:20, 2:20, 4:20 RL-R-tTK-hAMSC:PL-G-U87), but was not affected by treatment with PBS. Thus bystander killing effect produced by RL-R-tTK-hAMSC is directly reliant on therapeutic cell number.

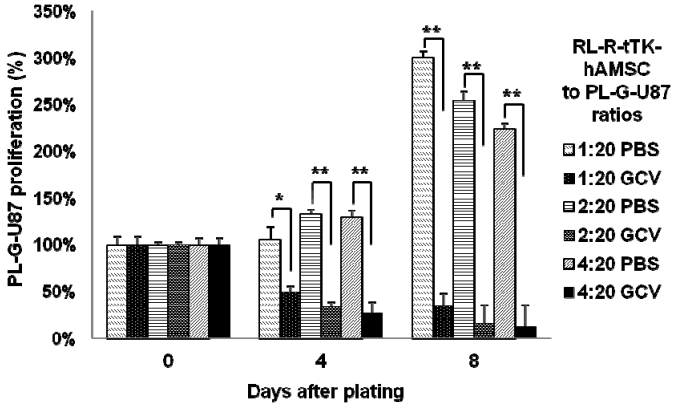

Figure 22 Bystander effect in co-cultures comprising different proportions of RL-R-tTK-hAMSCs and PL-G-U87 cells to GCV. Cells were grown during the indicated times and treated with either GCV (4 μg/ml) or PBS, as indicated. Number of viable PL-G-U87 was evaluated by BLI, and expressed as percentage increase relative to cell number at day 0. Histograms show mean ± SEM, *p<0.05, **p<0.01 n=4 for each group.

1.1.4 Detection sensitivity of PL-G-U87 and RL-R-tTK hAMSC *in vivo*

Before performing experiments *in vivo* with luciferase expressing PL-G-U87 and RL-R-tTK hAMSC we needed to determine the detection sensitivity of these cells. Skull bone and intervening brain tissue in live animals reduce the efficiency with which light photons reach the video camera detector used for BLI. Establishing a correlation between light measurements and cell number was essential.

We implanted predetermined numbers of PL-G-U87 and RL-R-tTK-hAMSC in the brain of live mice at specific coordinates (0,6 mm posterior, 2 mm lateral and 2,75 mm depth respect Bregma) later used for experiments. Immediately after implantation, mice

were imaged by BLI after administration of the corresponding luciferase substrate, luciferin or coelenterazine (PL-G-U87 and RL-R-tTK-hAMSC). The number of recorded photon events (PHCs) was extracted from recorded images and plotted, after background subtraction, versus the number of inoculated cells. As shown in Figure 23, detection sensitivity (slope of the correlation curve) was similar for both cell types and there was a good linear correlation between the amount of light produced and the number of cells implanted, 34,2 PHCs /cell, R^2 = 0,994 and 20,64 PHCs /cell, R^2 = 0,974 for PL-G-U87 and RL-R-tTK-hAMSC, respectively.

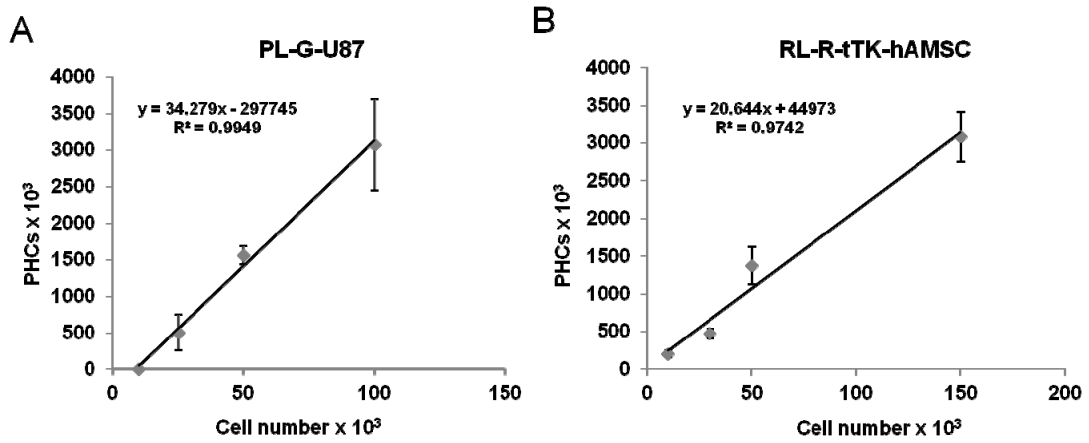

Figure 23 *In vivo* BLI sensitivity. The indicated numbers of PL-G-U87 (A) and RL-R-tTK-hAMSC (B) were stereotactically implanted, at the same coordinates later used for experiments in the brain of immunosupressed mice and imaged after luciferin or coelenterazine substrate administration, respectively. The number of light events (PHCs) recorded from the mice brains was plotted, after background subtraction, versus the number of implanted cells. R^2 correlation coefficient. Data are presented as mean ±SEM, n=4 in each group.

Once we determined that modified tumoral and therapeutic cells correctly expressed the corresponding transgenes in vitro and in vivo we proceeded to accomplish the following objectives:

II. Development of a glioma therapy model based on stereotactic intracerebral implantation of tumoral and cytotoxic therapeutic cells in SCID mice brain.

III. Optimize a bioluminescence imaging system to non-invasively monitor cell responses.

IV. Optimize delivery of the cytotoxic agent.

1.2 Optimal RL-R-tTK-hAMSC dose for *in vivo* bystander effect

As previously shown *in vitro* bystander killing effect produced by RL-R-tTK-hAMSC is directly dependent on therapeutic cell number. We wanted to observe if this correlation persisted *in vivo* and determine the optimal dose of tTK expressing hAMSCs for an efficient therapy.

To establish the best proportion of therapeutic to tumor cells we injected mixed cell populations comprising PL-G-U87 cells ($4x10^4$) and different proportions of RL-R-tTK-hAMSCs, (1:1, 1:2, 1:4) respectively in the brain of SCID mice at the previously indicated coordinates (see page 71) (n=15). Two control groups (n=10), were also included, one of them consisting of mice injected with $4x10^4$ PL-G-U87 cells only, that was treated with GCV; and the other consisting of mice injected with the same number of PL-G-U87 cells in a 1:1 proportion with RL-R-tTK-hAMSCs, that was treated with PBS. Beginning six days after the cell implantation (T=0), and during a 35 day period, the inoculated mice were treated daily by i.p. administration of GCV or PBS, as indicated. Light emission by tumoral cells expressing Pluc luciferase was monitored by BLI from the beginning of GCV treatment and every week thereafter. Image sequences of tumors were used to monitor tumor growth during the experiment.

Figure 24 shows statistical evaluation and analysis of photons captured in all images. Mixed cell tumors (1:1) treated with PBS grew at a similar rate than control tumors treated with GCV but without therapeutic cells ($p > 0,05$). However, treatment with GCV of tumors bearing therapeutic cells inhibited tumor growth relative to controls. Although a trend in tumor growth inhibition appears from the start of the GCV treatment, a clear inhibition of tumor growth was apparent by day 21 and was evident by day 35 of GCV treatment in all the therapeutic cell proportions tested. The therapeutic effect directly correlated with the proportion of therapeutic cells used, being 1:4 the most effective cell dose (Figure 24 B).

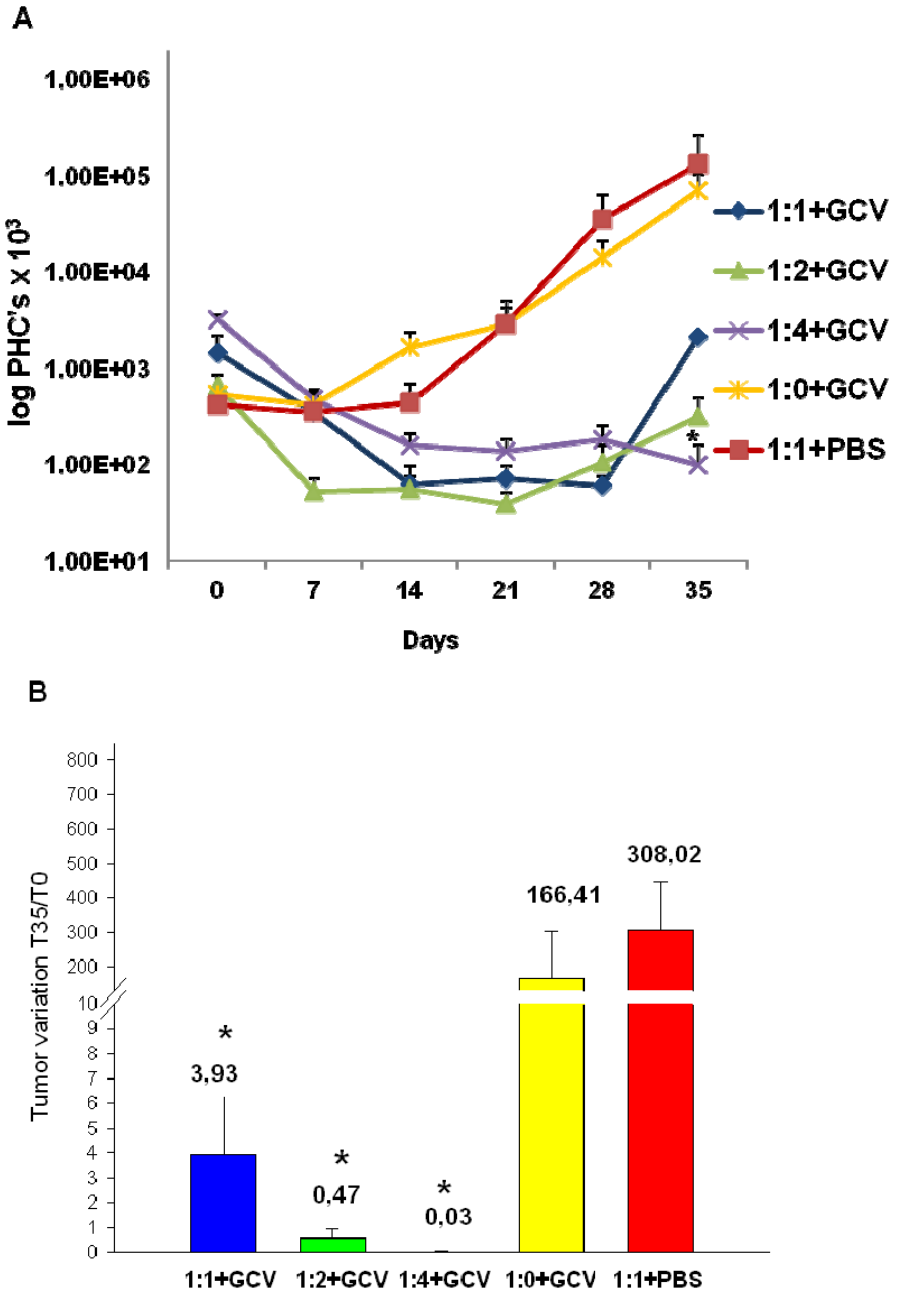

Figure 24 *In vivo* optimization of tumor to therapeutic cell ratio. Tumor and therapeutic cells mixed in proportions 1:0, 1:1, 1:2 and 1:4 (PL-G-U87:RL-R-tTK-hAMSC) were implanted in the brain of SCID mice and treated at day 6 i.p. with either GCV or PBS as indicated and monitored by BLI at weekly intervals. (**A**) The graph shows *in vivo* changes in light production by Pluc expressing tumor cells resulting from GCV treatment. (**B**) Histogram showing PHC values at the end of the experiment (T=35). Values were normalized relative to those at T=0 according to the formula [(T35/T0) x 100 = tumor variation (%)]. Data are shown as mean ± SEM, *P<0.05, compared to the 1:0+GCV group, n=5 for each group.

In this group of mice, by the end of the experiment (T=35) the amount of light produced by the tumors was 0,14% of the light produced by those in the control group (PL-G-U87 only) ($p<0,05$). Analysis comparing tumor size at the start (T= 0) and end (T= 35) of treatments shows a significant size reduction ($p< 0,05$) for all the tumors treated with therapeutic cells plus GCV, but not for controls where either GCV or therapeutic cells were omitted. In the 1:4 + GCV group, only 3% of light produced by tumor cells at T=0 persisted at the inoculation sites following GCV treatment (Figure 24 B).

1.3 *In vivo* RL-R-tTK-hAMSC mediated bystander glioblastoma therapy

The following experimental protocol was applied: a group of 24, 6 week old SCID mice was stereotactically inoculated at the previously indicated coordinates with either a mixture of $4x10^4$ PL-G-U87 cells and $1.6x10^5$ RL-R-tTK-hAMSCs (n=16) or with $4x10^4$ PL-G-U87 tumor cells only (n=8). Six days post implantation (T= 0), the mice were imaged by BLI to monitor Pluc activity from the PL-G-U87 tumors and Rluc activity from RL-R-tTK-hAMSC cells, and a treatment regime was initiated as described in the diagram of Figure 25. In brief, one half of the mice implanted with PL-G-U87 and RL-R-tTK-hAMSC cells received GCV, while the other half received the same volume of PBS. Mice implanted with only PL-G-U87 cells also received GCV. Treatment was administered during two 3 week periods, separated by a one week rest period. At day 49 all the control mice were sacrificed, as required by the animal welfare protocol.

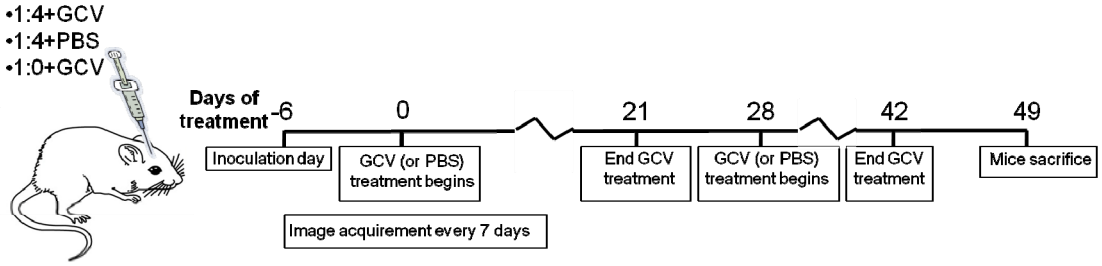

Figure 25 Diagram illustrating experimental procedure.

BLI was used to monitor tumor development during the experiment. Figure 26 A shows representative images from single animals in each of the experimental groups. Treatment of mixed cell tumors with PBS, or of control tumors (lacking therapeutic

cells) with GCV had no inhibitory effect on tumor growth, and light production by PL-G-U87 cells progressively increased up to the end of the experiment. However, treatment of mixed cell tumors with GCV resulted in the progressive reduction of light produced by PL-G-U87 cells up to the end of the experiment, when light from PL-G-U87 cells reached background level.

Quantitative evaluation of therapeutic effect is shown by plots of total light events recorded in images from the tumor areas vs. time (Figure 26 C). This analysis shows that the amount of light produced by tumors containing therapeutic cells that were treated with GCV, by the end of the experiment, was 10^4 times lower than that produced by control tumors treated with GCV or by tumors with therapeutic cells treated with PBS ($p< 0,05$). Moreover, by the end of the experiment, light produced by tumors treated with therapeutic cells plus GCV was only 0,12% the amount of light produced by the same tumors at T=0 (6 days after cell implantation) (n=8).

Cell killing detected by BLI could also be verified at the macroscopic level by visual comparison of brain sections from control mice and those treated with therapeutic cells plus GCV (Figure 26 B), and while sections from control mice brains showed a clear tumor mass, those from mice inoculated with tumor plus therapeutic cells and treated with GCV had a normal macroscopic appearance and showed no signs of tumors.

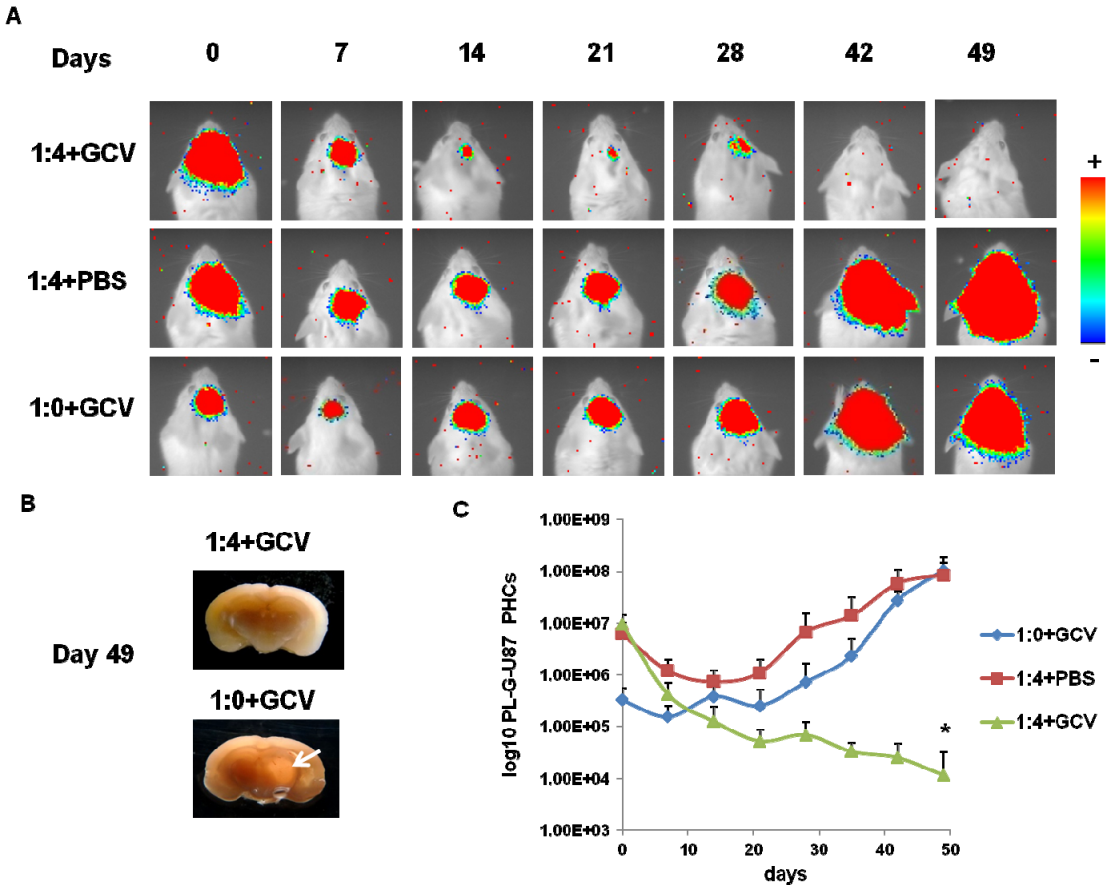

Figure 26 *In vivo* BLI of hAMSC mediated tumor therapy. (A) Composite pseudo-color BLI images from mice implanted with $4x10^4$ PL-G-U87 plus $1.6x10^5$ RL-R-tTK-hAMSCs and treated with GCV (1:4+GCV); $4x10^4$ PL-G-U87 plus $1.6x10^5$ RL-R-tTK-hAMSC and treated with PBS (1:0+GCV); and with $4x10^4$ PL-G-U87 only and treated with GCV. Images were acquired once per week. Arbitrary color bars illustrate relative light intensities from PLuc luciferase, lowest: blue; highest: red. (B) Representative images of brain sections at day 49. Top: brain of a 1:4+GCV treated mouse. Bottom: brain of a 1:0+GCV mouse, arrow points to tumor area. (C) *In vivo* changes in light production by U87 tumors expressing Pluc, resulting from GCV treatment and tumor cell death. Light values, calculated from the recorded images, are represented as log10 mean ± SEM; n=8; * p< 0.05, compared to the 1:0+GCV.

Validation of BLI analysis was also provided by fluorescence confocal microscope observation of mouse brain sections that showed the presence of red fluorescent RL-R-tTK-hAMSCs evenly distributed throughout the tumor implantation site mixed with green fluorescent tumor cells, at T= 0 before starting GCV treatment (Figure 27 A).

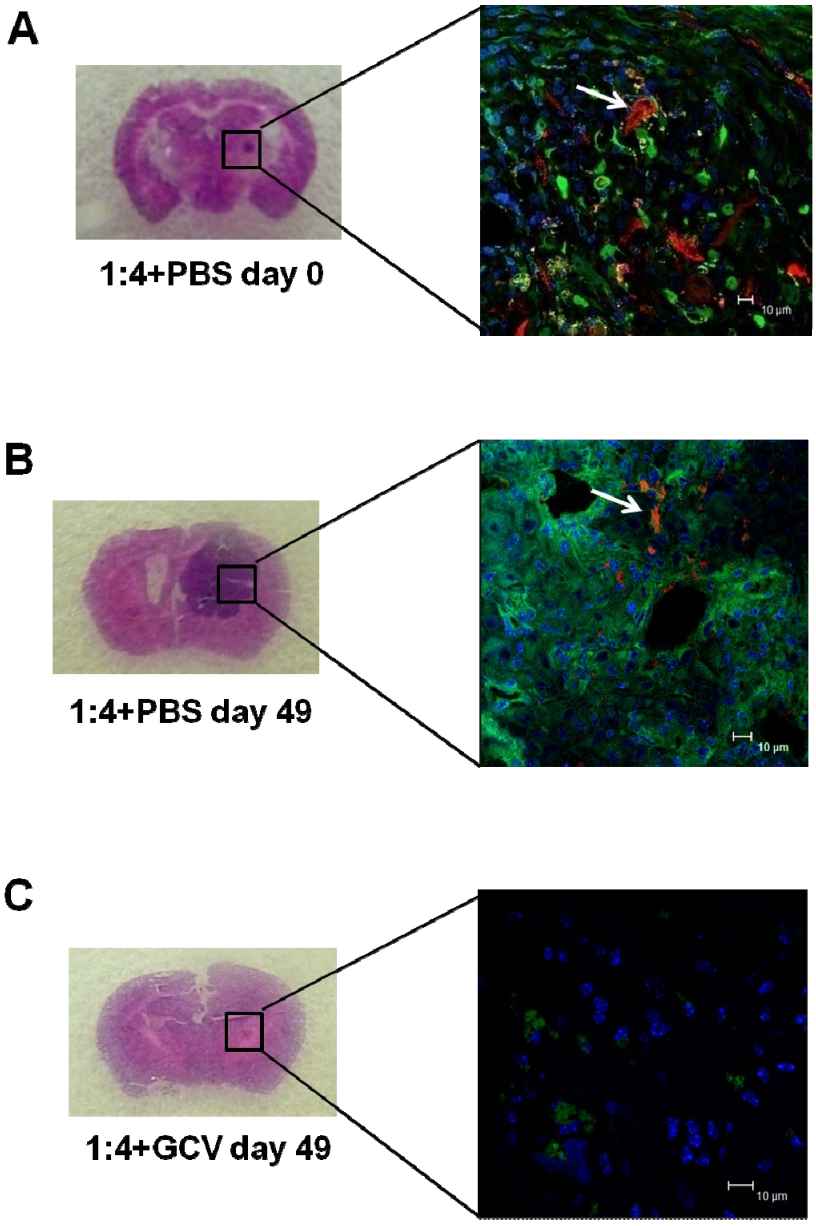

Figure 27 Effect of GCV on fluorescent RL-R-tTK-hAMSC at tumor implantation sites. Left, representative images of HE stained brain sections; Right, representative fluorescence confocal microscope images showing implanted red fluorescent cells RL-R-tTK-hAMSC (arrow), and PL-G-U87 cells (green). (A) Control mouse (1:4+PBS) at T = 0, (B) control mouse (1:4+PBS) at T = 49, (C) treated mouse (1:4+GCV) at day 49. Blue, Hoescht stained nuclei. Scale bar = 10 µm.

In well developed tumors (T= 49) from control group 1:4 +PBS, red fluorescent RL-R-tTK-hAMSCs could also be detected in clusters within the green fluorescent mass of the well developed tumor (Figure 27 B). However, brains from mice in the 1:4 + GCV group had few detectable tumor cells and no detectable RL-R-tTK-hAMSCs, in accordance with the BLI analysis (Figure 27 C).

1.3.1 Post-engraftment survival of therapeutic hAMSCs

Previously it has been observed that a large proportion of hAMSCs disappears when injected in immunosupressed mice[163]. We monitored the fate of injected RL-R-tTK-hAMSCs by BLI at the implantation day (T= -6) and 6 days later (T= 0), at the beginning of GCV treatment (Figure 28). The number of detected PHCs at T= 0 corresponded with that produced by $1.5x10^4$ RL-R-tTK-hAMSCs in standard plots (Figure 23 B), near to a 10 fold decrease relative to T= -6. However, due to their rapid proliferation the amount of light produced by PL-G-U87 tumor cells in the 1:4 + GCV and 1:4 + PBS groups, at T= 0 corresponded to approximately $2x10^5$ cells. Therefore, during the 6 days previous to GCV treatment, the ratio of PL-G-U87: RL-R-tTK-hAMSCs changed by 52 fold, from 1:4 to 13:1. Thus, the later is the actual ratio at which therapeutic effect is exerted.

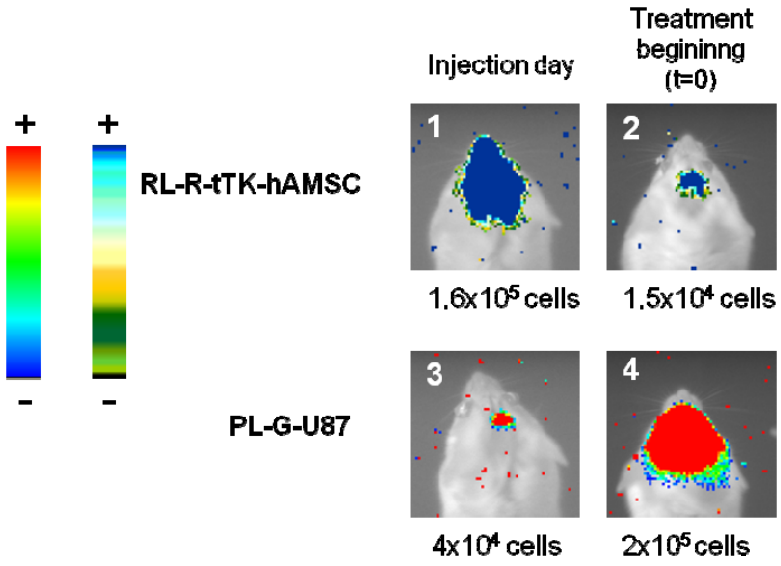

Figure 28 Representative pseudo-color images from RL-R-tTK-hAMSC and PL-G-U87 at day of implantation, T= -6 (1 and 3) and at initiation of GCV treatment, T= 0 (2 and 4). Luciferase images are superimposed on black and white images of the same mouse. The included numerical values indicate the cell numbers extrapolated from the "light vs cells" standard curve. Arbitrary color bars illustrate relative light intensities from PLuc and Rluc luciferases, lowest: blue and black; highest: red and blue, respectively.

1.4 Bystander glioblastoma therapy mediated by direct implantation of RL-R-tTK-hAMSC on established tumors

After evaluating the efficiency of the glioblastoma cytotoxic therapy we wanted to verify that the RL-R-tTK-hAMSC mediated therapeutic approach is also effective under more clinical like conditions. To mimic a postsurgical inoculation of therapeutic cells we first established gliomas in mice brain. 6 week old SCID mice were stereotactically inoculated at the previously indicated coordinates (see page 71) only with $4x10^4$ PL-G-U87 cells. Six days post implantation (T= 0) one halve of the mice randomly chosen (n=4) received an intracranial intratumoral injection of $1.6x10^5$ RL-R-tTK-hAMSCs. On day 3 mice were imaged by BLI to monitor PL-G-U87 tumor development, following which GCV treatment was initiated consistent of a daily dose of GCV during a four week periods, followed by 3 day rest periods. Weekly BLI was used to monitor tumor development during the experiment. On days 33 and 68, when the drop in Renilla

luciferase emission indicated the disappearance of implanted RL-R-tTK-hAMSCs, additional intratumoral inoculations of $1.6x10^5$ RL-R-tTK-hAMSCs were performed (Figure 29).

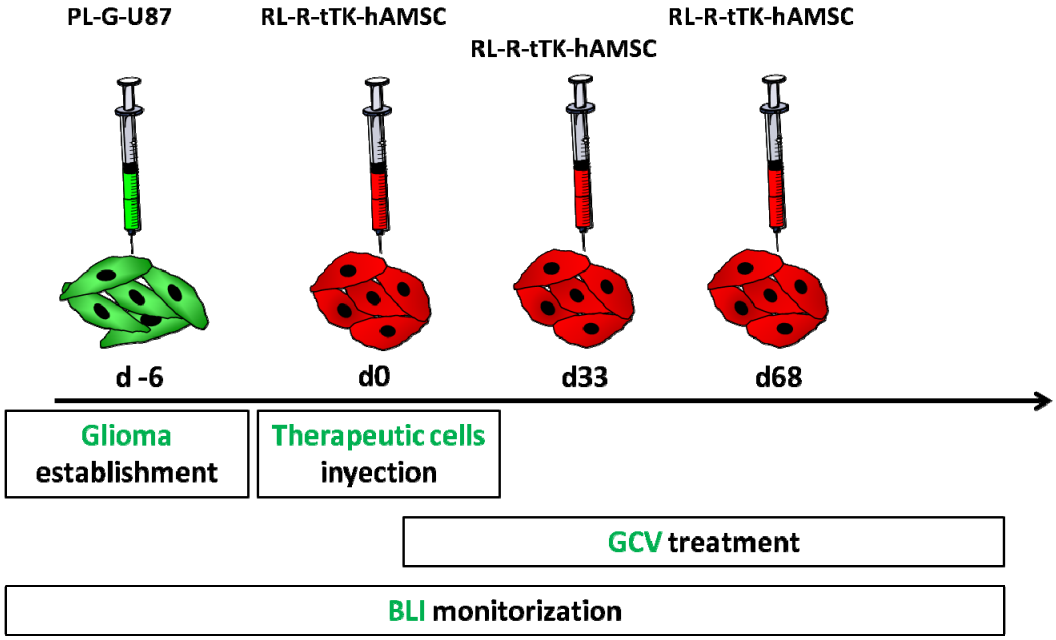

Figure 29 Diagram illustrating experimental procedure.

The administration of RL-R-tTK-hAMSCs in combination with GCV resulted in the inhibition of tumor growth. Moreover, as shown on Figure 30A the tendency of treated tumors to regain growth when implanted therapeutic cells disappear is effectively counteracted by repeated inoculations of additional RL-R-tTK-hAMSC and GCV treatment. By day 53 right before all the control mice were sacrificed in accordance to animal care protocols, light produced by tumors treated with therapeutic cells plus GCV was only 0,12 % of that produced by the control tumors. Monitorization of mice survival was performed. Kaplan-Meier survival graph (Figure 30 B) showed that the treatment protocol resulted in significant ($p<0.05$) increase in animal survival. Median survival was 88,5d (treated animals) and 51d (control animals).

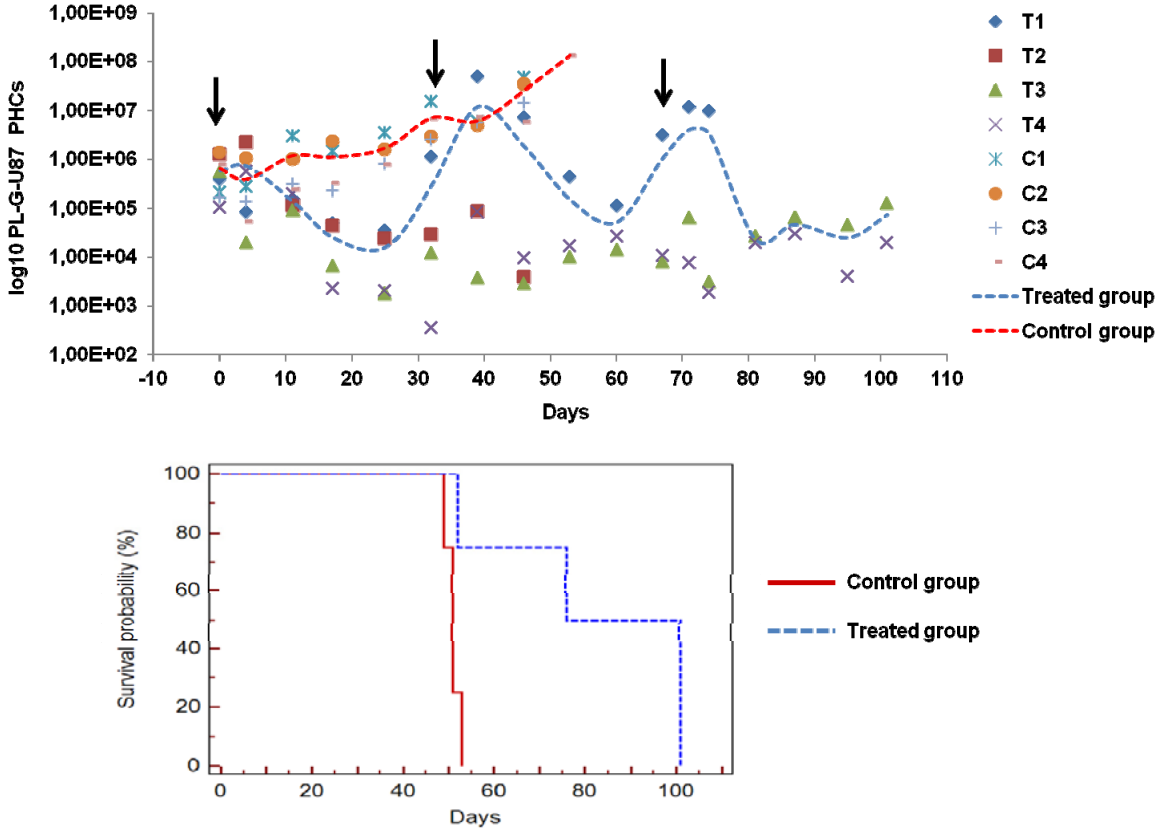

Figure 30 Response of U87 tumors to direct implantation of therapeutic cells and GCV treatment. (A) *In vivo* changes in light production by U87 tumors expressing Pluc, resulting from inoculation of RL-R-tTK-hAMSCs and GCV treatment. Dots represent PHCs values from individual animals (T: Treated mice; C: Control mice). The bars represent the average values from each group. Arrows indicate the inoculation of RL-R-tTK-hAMSCs. Light values, calculated from the recorded images, are represented as log10 of the mean ± SEM; n=4; * p< 0.05, compared to the control group. (B) Kaplan-Meyer graph summarizing mice survival following the above treatment. Median survival, treated mice, 88,5d; control mice, 51 d, p<0.05.

2 STUDY OF HAMSC INTERACTION WITH TUMOR VASCULATURE

As described in the previous section cytotoxic therapy mediated by hAMSCs had a very strong bystander effect on tumoral cells, although only a small number of therapeutic cells survived after injection. We hypothesized that injected hAMSCs entered in close association with tumoral vasculature and GCV/tTK mediated bystander effect induced its destruction. To confirm this hypothesis we pursued the following objective:

V. Analyze the differentiation behavior of therapeutic cells in the tumor microenvironment.

2.1 Intracerebral differentiation of RL-R-tTK-hAMSCs therapeutic cells

In an attempt to understand the mechanism by which the RL-R-tTK-hAMSCs + GCV treatment achieves the observed high degree of therapeutic effect, the differentiation behavior of therapeutic cells was analyzed. To do this, we used hAMSCs with a double bioluminescent labeling.

2.1.1 hAMSC double labeling

We used, previously described, RL-R-tTK-hAMSCs that expressed Rluc under constitutive CMV promoter. These cells were selected by FACS and then labeled with a second Pluc-eGFP reporter under transcriptional control by the PECAM/CD31 promoter. This luciferase serves as a reporter of differentiation to the endothelial lineage. As a result we obtained PECAM-PLuc-G:RL-R-tTK-hAMSC. With this strategy, changes in PECAM-regulated luciferase expression could be quantitatively related to those of the constitutively expressed Rluc, now an internal standard in the same cell that allows the elimination of potential artifacts related to changes in hAMSC number.

2.1.2 Fate of tumor implanted RL-R-tTK-hAMSCs therapeutic cells

The doubly labeled hAMSCs were mixed with unlabelled U87 tumor cells and implanted at the standard brain location. BLI analysis of Pluc and Rluc expression at days 0 and 7 post-implantation showed (Figure 31 A) that while the bulk of implanted

hAMSCs disappears from the tumor during the 7 day period, cells expressing PECAM-promoter regulated Pluc remained associated to the tumor. Moreover, the ratio of PECAM/CD31 promoter-regulated Pluc activity to constitutively-expressed Rluc increased considerably by 92 fold, indicating that a subpopulation of the implanted hAMSCs had differentiated to the endothelial lineage and remained at the tumor site (Figure 31 B).

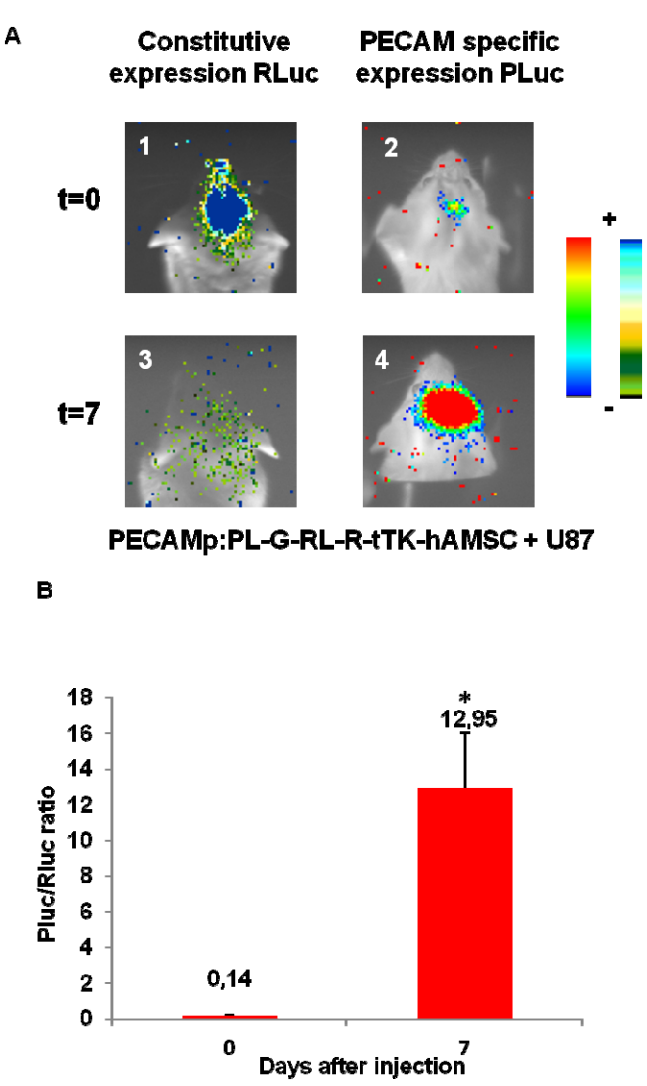

Figure 31 Endothelial differentiation of hAMSCs in U87 tumors. Double transduced hAMSCs expressing PECAM-promoter regulated PLuc-GFP and CMV-promoter regulated Rluc-R-tTK were mixed 4:1 with unlabelled U87 glioma cells, implanted in the brain of mice and imaged at the indicated times. Mice were then inoculated with a 2,000,000 MW FITC-conjugated dextran and the brains harvested, fixed in formalin and prepared for microscopy. (A) Representative BLI images showing Rluc (left) and Pluc (right) activities at T = 0 (1 and 2) and T = 7 (3 and 4), respectively. Pseudo color images are superimposed on black and white dorsal images of recipient mice. Color bars illustrate relative light intensities of Pluc (right) and Rluc (left); low: blue and black; high: red and blue, respectively. (B) Histograms showing the change in the ratio of Pluc/Rluc activities during the indicated time period. Bars represent mean ± SEM of photon counts recorded in BLI images. * $p < 0.05$, n=4.

2.1.3 Microscopic analysis of hAMSC endothelial marker expression and association with vasculature

One week after implantation mice were sacrificed and analysis by laser confocal microscopy was performed on the brains. Confocal microscope analysis of tumor sections showed the presence of therapeutic cells expressing the RFP under constitutive promoter and the eGFP regulated by the PECAM/CD31 promoter that also positively stained with an anti-human endothelial specific PECAM/CD31 antibody but not with an anti-human pericyte specific αSm22 antibody (Figure 32 A,B). Control immunohistochemistry was performed on human miocardium tissue confirming the specificity of both antibodies (Figure 32 C,D).

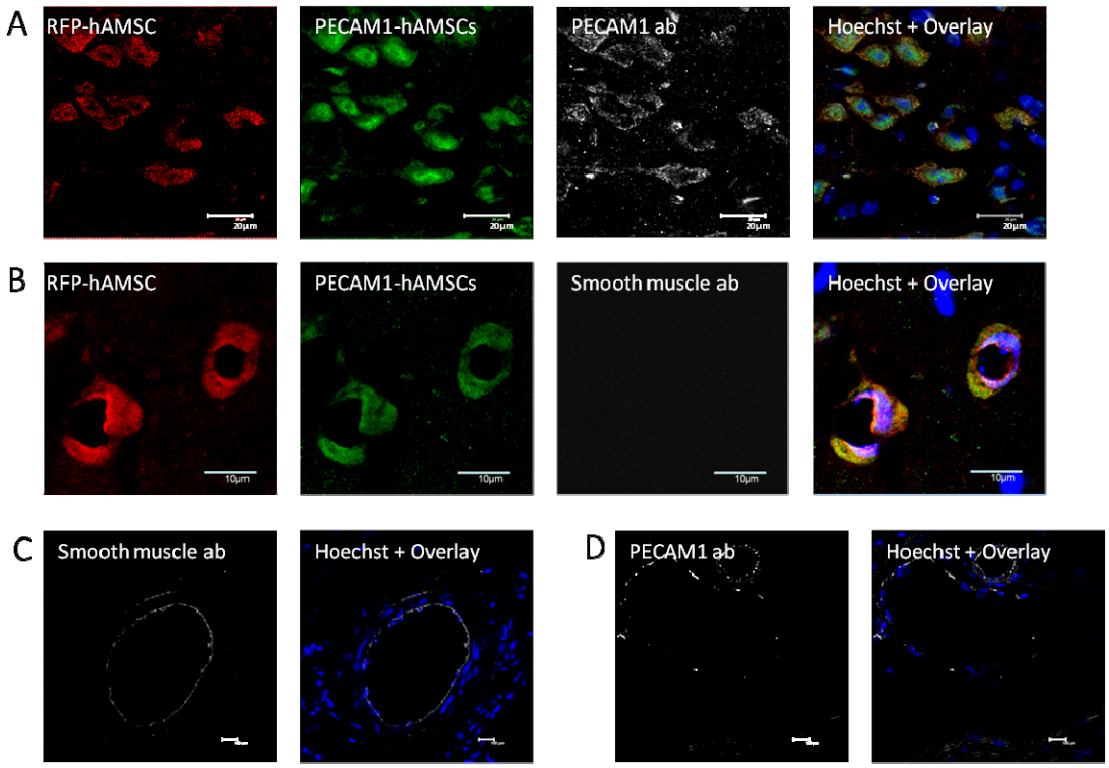

Figure 32 Endothelial differentiation of hAMSCs in U87 tumors. Confocal microscopy analysis was performed on slices from brain tumors implanted with PECAM:PL-G-RL-R-tTK-hAMSCs to determine co-expression of grafted cells with endothelial PECAM1 and pericytic αSM22 markers. hAMSCs expressing CMV-promoter regulated RFP (red) and PECAM-promoter regulated eGFP (green) also labeled by an anti-human PECAM antibody (gray) (A) but did not express αSM22 antibody (B). Scale bar= 25µm (A), 10µm (B). Control immunohistochemistry was performed on human miocardium tissue confirming both antibodies specificity (C,D). Scale bar=100µm. 00

The endothelial lineage of therapeutic cells associated to vascular structures in the tumor was further verified by perfusing some of the mice with a fluorescein-conjugated high MW dextran (FITC), not diffusible past the vascular endothelium, followed by immunohistochemistry of fixed tissue sections to detect endothelial specific markers. Confocal microscope analysis of sections of the perfused tumors showed the presence of RFP expressing therapeutic cells that positively stained with an anti-human PECAM/CD31 antibody and were closely associated to FITC-dextran labeled vascular structures (Figure 33).

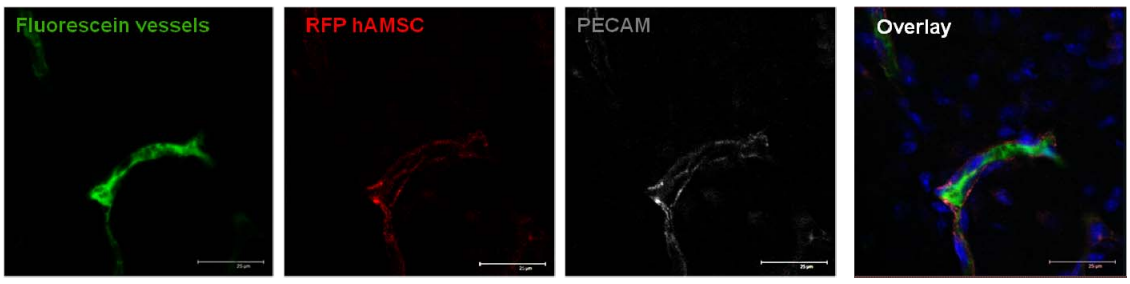

Figure 33 Association of hAMSCs to tumor vasculature. Representative laser confocal microscope images of a FITC-stained microvessel (green), associated with red fluorescent hAMSCs (red), also labeled by an anti human PECAM antibody (gray) Scale bar= 25 µm.

2.2 Stability of the CMV promoter activity

In this experiment all the implanted therapeutic cells express RFP but only a fraction of them is induced to express the endothelial lineage reporters. This double label strategy offered the possibility of determining if the decrease in RLuc expressing therapeutic cells previously observed in tumors could be due to silencing of the CMV promoter that regulates RLuc, RFP and tTK expression. To do this, tumor sections were analyzed to determine the proportion of eGFP expressing therapeutic cells that did not express RFP. Our assessment showed that most of eGFP expressing cells also expressed RFP and only 10% or less of the eGFP expressing cells did not express RFP, ruling out CMV promoter silencing as the cause for the decrease in production RLuc photons within tumors.

2.3 Silencing of αNotch1 in hAMSCs

Notch1 signaling is involved in a number of processes including vascular/endothelial differentiation. Previous studies showed that inhibition of Notch signaling by a γ-secretase inhibitor abolishes endothelial differentiation of bone marrow derived MSC [164]. To explore if αNotch is required in our tumor therapy model, we inhibited the Notch signaling pathway in RL-R-tTK-hAMSCs and PECAM-PL-G:RL-R-tTK-hAMSC by transduction with αNotch1 ShRNA (see pages 83 and 100); to generate αNotch1-RL-R-tTK-hAMSCs and αNotch1-PECAM:PL-G-RL-R-tTK-hAMSCs, respectively. Two additional sets of control cells were generated by transducing RL-R-tTK-hAMSCs and PECAM-PL-G:RL-R-tTK-hAMSC with an empty pLKO.1-puro vector: sh-RL-R-tTK-hAMSC and sh-PECAM:PL-G-RL-R-tTK-hAMSC. This controls served as controls of transduction.

2.3.1 *In vitro* validation of vascular differentiation impairment by αNotch1 ShRNA

To assess the effect of αNotch ShRNA on the tube formation capacity of hAMSCs we used a Matrigel assay. This assay is based on the endothelial differentiation of cells and the formation of tube-like structures on an extracellular matrix. As shown on Figure 34, while positive control PECAM:PL-G-RL-R-tTK-hAMSCs and mock transduced sh-PECAM:PL-G-RL-R-tTK-hAMSCs are capable of forming tubes in Matrigel, αNotch1-PECAM:PL-G-RL-R-tTK-hAMSC completely lack tube formation capacity (3 different αNotch1 clones were tested with similar results, data not shown). The clone with the highest level of tube formation inhibition was selected for further experiments.

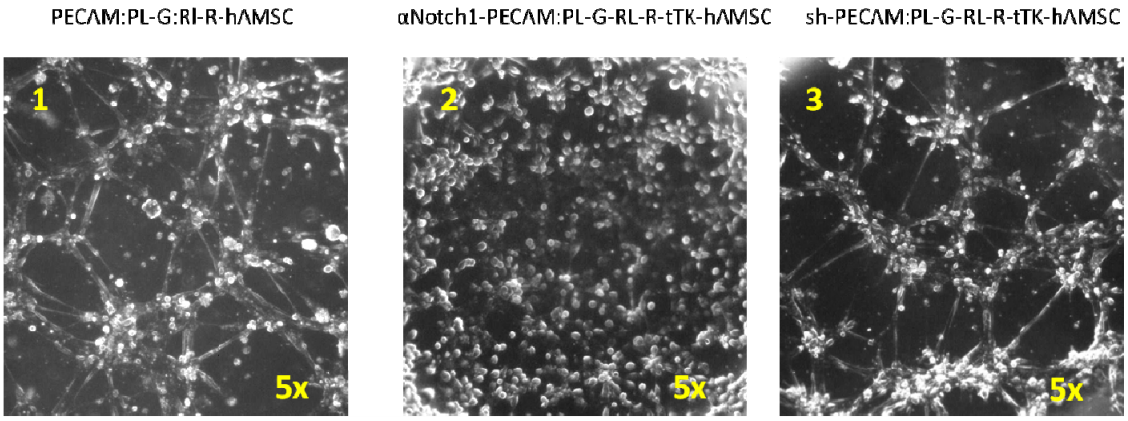

Figure 34 Tube formation by hAMSC *in vitro* requires Notch1 expression. Phase contrast photomicrographs of untransduced (1), αNotch1 ShRNA transduced (2) and moch shRNA transduced (3) PECAM:PL-G-RL-R-tTK-hAMSCs incubated in Matrigel for 4 h to evaluate their tubulogenic capacity.

We performed a Real-Time PCR quantification of mRNA from the same cells following the Matrigel tube formation assay to study expression of endothelial markers in these cells. The level of mRNA expression for Notch1 and other endothelial specific markers (ILK, SDF1, EGR3, PECAM1) was significantly reduced in αNotch1-PECAM:PL-G-RL-R-tTK-hAMSC relative to positive control PECAM:PL-G-RL-R-tTK-hAMSCs and to mock transduced sh-PECAM:PL-G-RL-R-tTK-hAMSC (Figure 35).

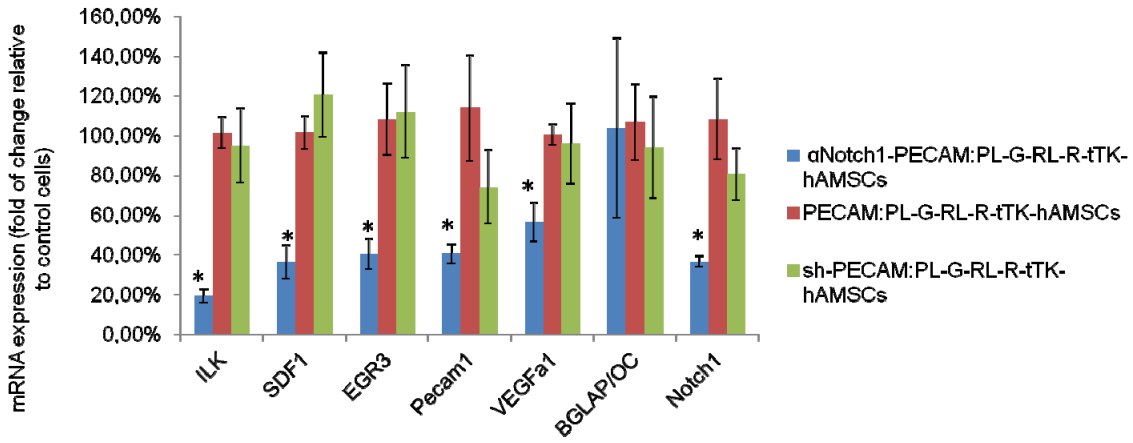

Figure 35 Endothelial marker expression in different hAMSCs cell lines. RNA extracted from cells in matrigel was assayed by qRT-PCR to determine transcription levels of the indicated endothelial (ILK, SDF1, EGR3,PECAM-1, VEGFA-1, Notch-1) and bone BGLAP/Octeocalcin differentiation markers. The histogram shows % change in fold change relative to control PECAM:PL-G-RL-R-tTK-hAMSCs. n = 3; *p<0,05 relative to control.

However no significant reduction in the expression level of the Notch1 independent BGLAP/Osteocalcin gen was observed in either of the 3 cell types. These results validate, the Matrigel assay results confirming the capacity of αNotch1 ShRNA to inhibit vascular lineage gene expression in these cells.

2.3.2 *In vivo* imaging of vascular lineage differentiation inhibition by Notch1 silencing

To assay vascular differentiation capacity of previously described cells *in vivo* un-labelled U87 glioma tumor cells were implanted in the brain of SCID mice together with either αNotch1-PECAM:PL-G-RL-R-tTK-hAMSCs or sh-PECAM:PL-G-RL-R-tTK-hAMSCs and monitored by BLI. Again we used the double labelling strategy that allowed us to evaluate changes in the expression of the differentiation reporter relative to that for cell number, minimizing potential artefacts due to cell death or proliferation (see page 100).

After 7 days post-implantation, imaging of cell distribution and number showed that a large proportion of both types of implanted cells have disappeared or dispersed from the implantation sites (Figure 36 A 1,3 and B 1,3), although a subpopulation of the implanted cells appears to remain within the tumor implantation site. For these tumor associated cells, imaging of the endothelial differentiation reporter PECAM-PLuc shows (Figure 36 A 2,4 and B 2,4) little activity from αNotch1-PECAM:PL-G-RL-R-tTK-hAMSCs but a considerable increase from sh-PECAM:PL-G-RL-R-tTK-hAMSC mock treated cells.

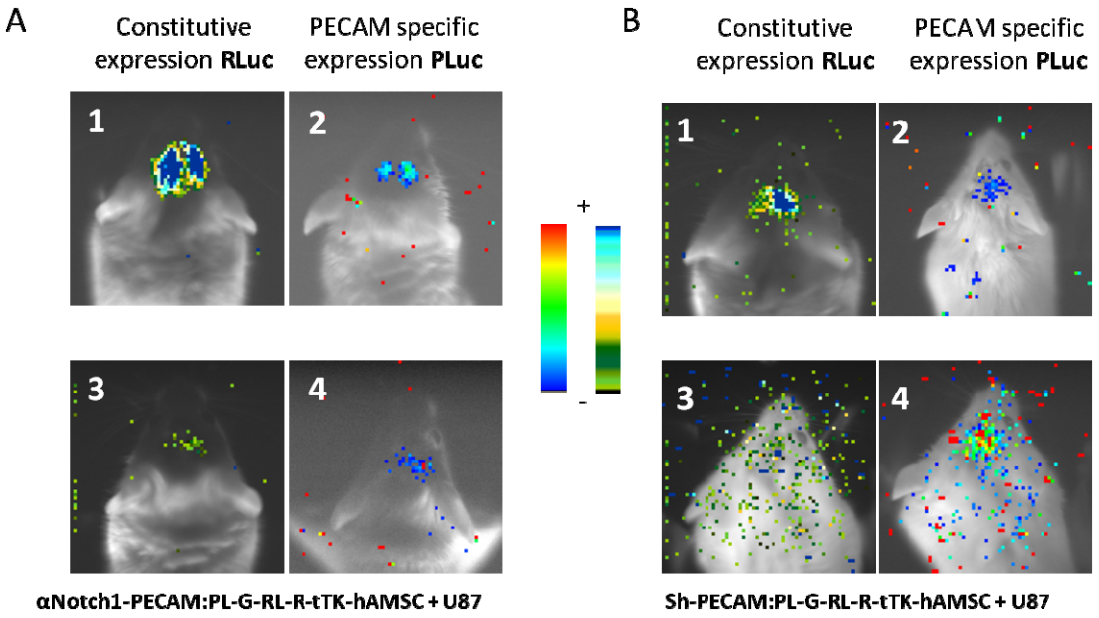

Figure 36 Endothelial differentiation of hAMSCs in U87 glioma tumors requires Notch1 expression Independent mixtures comprising unlabelled U87 glioma cells and either αNotch1-PECAM:PL-G-RL-R-tTK-hAMSCs (A) or sh-PECAM:PL-G-RL-R-tTK-hAMSCs (B) in a ratio of 1:4 were implanted at specific brain coordinates. Implanted cells were monitored to determine cell fate (A1,3; B1,3) and differentiation to the endothelial lineage (A2,4 and B2,4) by BLI of Renilla and Photinus luciferases, respectively. Pseudo color images are superimposed on black and white dorsal images of recipient mice. Color bars illustrate relative light intensities of PLuc (left) and RLuc (right); low: blue and black; high: red and blue, respectively.

For each of the two cell types, the level of differentiation was quantified by calculating the ratio of light photons produced by the differentiation reporter (PECAM-PLuc) divided by those generated by the constitutively expressed reporter (CMV-RLuc) representing cell number. As shown in the histogram (Figure 37) αNotch inhibited cells increased their endothelial differentiation level by a 4x factor in the 7 day post implantation, while mock inhibited cells increased by a 57 fold factor in the same time period. These results indicate that while differentiation to the endothelial lineage was active in control, mock treated, sh-PECAM:PL-G-RL-R-tTK-hAMSC, it was effectively reduced in cells transduced with αNotch1 ShRNA.

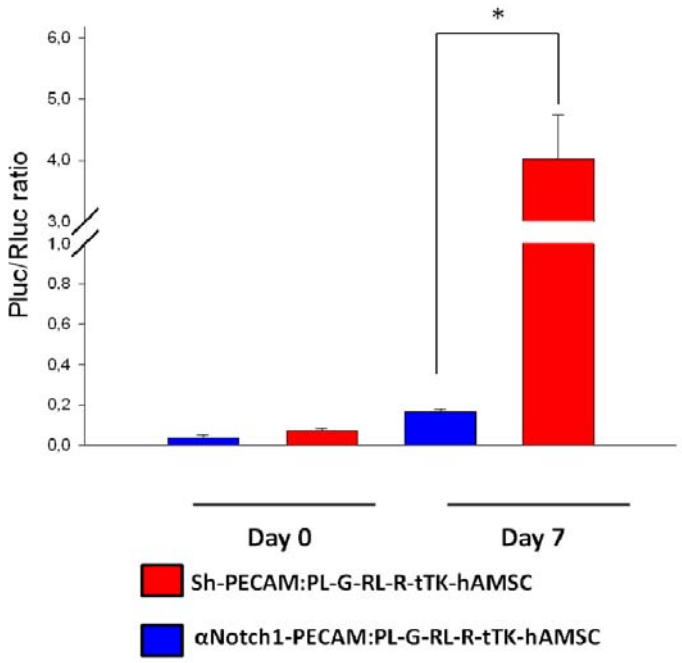

Figure 37 The ratio between photons acquired from Photinus luciferase and Renilla luciferase generated images (PLuc/RLuc) at day 0 and 7 was used to evaluate differentiation of implanted cells to the endothelial lineage * $p < 0.05$, n=4.

2.3.3 Microscopy study of hAMSC association to vascular structures

Following BLI analysis, mice from the previous experiment were perfused using a high (2,000,000 MW) fluorescein conjugated dextran, sacrificed and brains extracted and fixed in formaldehyde.

Analysis by fluorescence laser confocal microscopy of tumor slices revealed frequent RFP expressing sh-PECAM:PL-G-RL-R-tTK-hAMSCs with endothelial morphology and in close association with tumor vascular structures labelled with fluorescein (41,9±7,8%)(Figure 38 A). However RFP expressing αNotch1-PECAM:PL-G-RL-R-tTK-hAMSCs were not so frequently associated with vascular structures (17,8±6,7%). Quantification of hAMSC association with fluorescein labelled vessels showed that αNotch1-PECAM:PL-G-RL-R-tTK-hAMSCs associated significatively less than mock inhibited cells with vascular structures (Figure 38 B). These results indicate that

inhibition of endothelial lineage differentiation by αNotch ShRNA also interferes with the participation of hAMSCs in the formation of tumor vascular structures as expected.

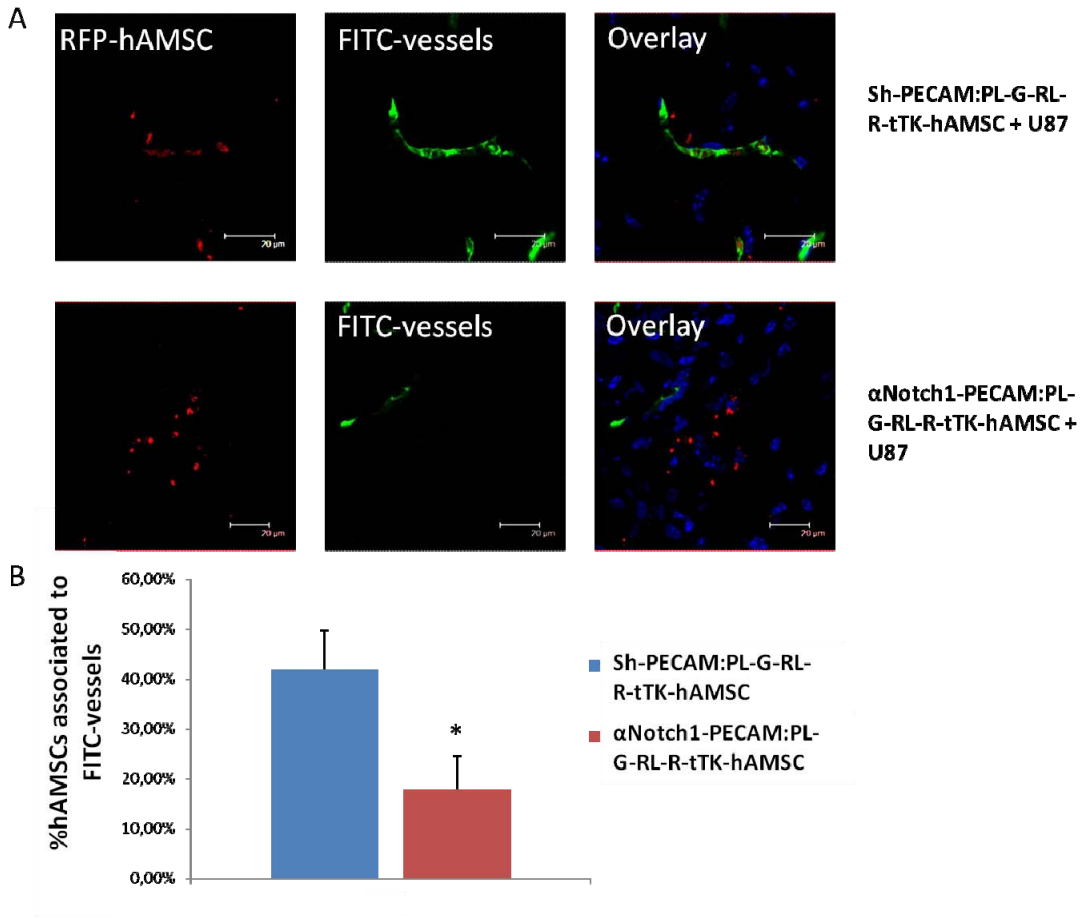

Figure 38 hAMSCs association to tumor microvessels. Representative laser confocal microscope images of the corresponding brain tumor slices showing RFP expressing sh-PECAM:PL-G-RL-R-tTK-hAMSCs (top) and αNotch1-PECAM:PL-G-RL-R-tTK-hAMSCs (bottom) location respect FITC-labelled microvessel (A). Histogram representing percentage of red hAMSC associated to FITC-labelled microvessel in the case of sh-PECAM:PL-G-RL-R-tTK-hAMSCs and αNotch1-PECAM:PL-G-RL-R-tTK-hAMSCs. Bars represent mean ± SEM of percent. * $p < 0.05$, n=25.

2.4 Evaluation of the therapeutic effectiveness of hAMSCs with inhibited endothelial differentiation capacity

Once we had verified that endothelial differentiation capacity of αNotch1-PECAM:PL-G-RL-R-tTK-hAMSCs was inhibited we proceeded to evaluate their therapeutic effectiveness in vitro and in vivo.

2.4.1 *In vitro* determination of bystander cytotoxic effect of human αNotch1 inhibited AMSCs expressing the HSV tTK gene

Human glioma PL-G-U87 cells expressing *Photinus Luciferase* and GFP were mixed in a 1:5 proportion with either sh-RL-R-tTK-hAMSCs or αNotch1-RL-R-tTK-hAMSCs, cultivated during 8 days and treated with prodrug GCV at 4 µg/ml or PBS. To monitor the effect of GCV on cell number, cocultures were subject to bioluminescence imaging of PLuc activity following luciferin administration. As is shown in Figure 39, un-treated mixtures of sh-RL-R-tTK-hAMSCs or αNotch1-RL-R-tTK-hAMSCs plus PL-G-U87 cells grow well in the absence of GCV. However, GCV treatment had a clear cytotoxic effect and resulted in a nearly complete abolition of PL-G-U87 cell growth (*P<0,01), regardless of the accompanying hAMSC type.

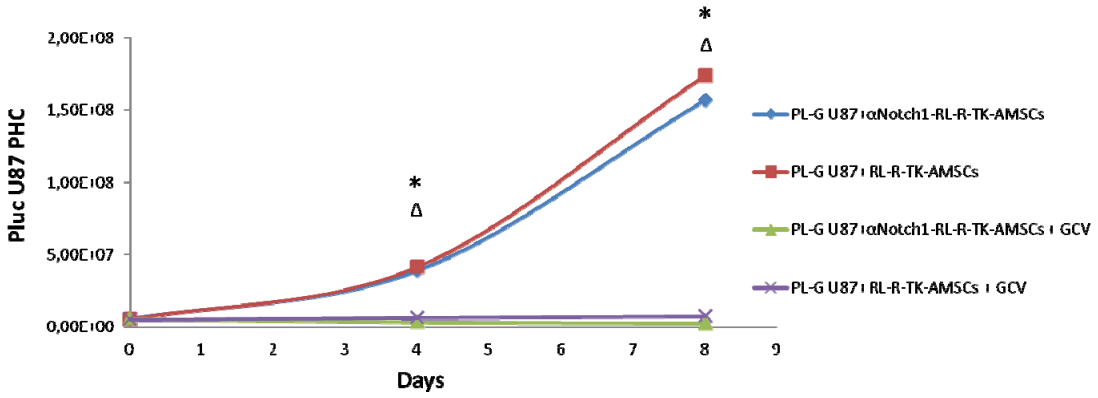

Figure 39 BLI of tumor therapy mediated by αNotch1-expressing hAMSCs *in vitro*. PL-G-U87 were grown during the indicated times in combination with sh-RL-R-tTK-hAMSCs or αNotch1-RL-R-tTK-hAMSCs and treated with GCV (4 µg/ml), as indicated. Number of viable cells was evaluated by BLI, and expressed as PL-G-U87 PHCs. Dots show mean ± SEM, *p<0.01 sh-RL-R-tTK-hAMSCs+GCV treated group vs sh-RL-tTK-hAMSC control group, Δp<0.01 αNotch1-RL-R-tTK-hAMSCs+GCV treated group vs αNotch1-RL-R-tTK-hAMSC control group, n=3 for each group.

This result indicates that both sh-RL-R-tTK-hAMSCs and αNotch1-RL-R-tTK-hAMSCs are equivalently effective at converting GCV to its toxic form and at delivering a bystander effect to U87 cells, independently of their vascular differentiation capacity.

2.4.2 *In vivo* tumor killing capacity of tTK expressing hAMSCs requires differentiation to the endothelial lineage

Next we explored the relation between vascular differentiation of hAMSCs and their capacity to deliver cytotoxic therapy to U87 tumors. For this purpose we compared the therapeutic effectiveness of sh-RL-R-tTK-hAMSC and αNotch1-RL-R-tTK-hAMSC in a model of glioblastoma described previously (see page 92). A group of 12, 6 week old SCID mice was stereotactically inoculated in the brain with a mixture of $4x10^4$ PL-G-U87 and either $1.6x10^5$ sh-RL-R-tTK-hAMSCs or the same number of αNotch1-RL-R-tTK-hAMSCs. An additional control group received $4x10^4$ PL-G-U87 tumor cells only. Light emission by PL-G-U87 cells was monitored by BLI beginning on the implantation day, and every week thereafter. Seven days post implantation the treatment with the GCV prodrug was initiated. Representative BLI results (Figure 40 A) and their quantitative evaluation (Figure 40 B) based on image captured photons show that growth of U87 tumors with either sh-RL-R-tTK-hAMSC or αNotch1-RL-R-tTK-hAMSC cells was similar up to the initiation of GCV treatment on day 6 and considerably faster (75 fold) than that of tumors without hAMSCs. However, by day 14, only 7 days after initiation of GCV treatment, the number of cells in tumors with sh-RL-R-tTK-hAMSCs had droped considerably and by day 21 the number of tumor cells had been reduced by 94% relative to that at day 6. Tumors with αNotch1-RL-R-tTK-hAMSCs responded with only a 36% drop to GCV treatment, and showed a slight growth reinitiation trend within the same time period. These results show that the tumor growth promoting capacity of hAMSCs and their capacity to deliver bystander therapy are based on independent mechanisms. More importantly these results support the hypothesis that vascular differentiation of hAMSCs is required for the delivery of bystander therapy.

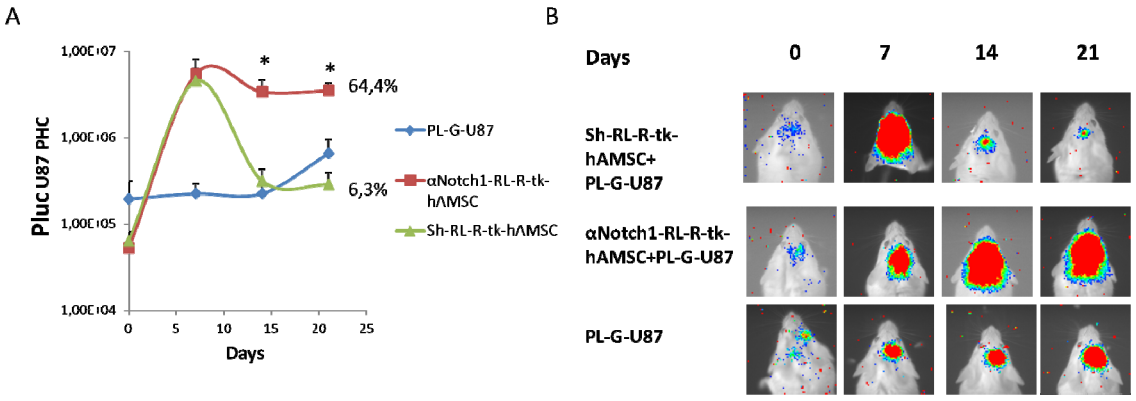

Figure 40 BLI of tumor therapy mediated by αNotch1-expressing hAMSCs *in vivo*. (A) *In vivo* changes in light production by U87 tumors expressing PLuc, resulting from GCV treatment and tumor cell death. Light values, calculated from the recorded images, are represented as log10 mean ± SEM; n=8; * p< 0.05. (B) Composite pseudo-color BLI images from mice implanted with $4x10^4$ PL-G-U87 plus 1.6x105 sh-RL-R-tTK-hAMSCs or αNotch1-RL-R-tTK-hAMSCs, or only $4x10^4$ PL-G-U87, treated with GCV. Images were acquired once per week.

To confirm our initial hypothesis we proceeded to the next objective:

VI. Study the interaction of therapeutic hAMSCs with tumor cells.

2.5 Glioma hAMSC interactions

In an attempt to understand the mechanism by which the sh-RL-R-tTK-hAMSCs + GCV treatment achieves the observed high degree of therapeutic effect, we studied the association of therapeutic cells and GSC in tumors. SCID mice 6 week old, were stereotactically inoculated at the previously indicated coordinates with a mixture of $4x10^4$ PL-G-U87 cells and $1.6x10^5$ sh-RL-R-tTK-hAMSCs or αNotch1-RL-R-tTK-hAMSCs. One week later mice were sacrificed and brains were harvested, fixed and subject to fluorescence confocal microscope analysis to detect associations between red fluorescent hAMSCs and green fluorescent tumor cells also stained with an anti-human CD133 monoclonal antibody, a frequently used marker of GSCs. Our results showed frequent GFP expressing tumor cells that positively stained with the GSC marker (Figure 41 A top), and were also in close association with RFP expressing sh-RL-R-tTK-hAMSCs (42,6 + 5,5%) (Figure 41 B). Although such associations were also detected in the tumors inoculated with αNotch1-RL-R-tTK-hAMSCs (Figure 41 A bottom), in the

latter case they were significantly less frequent (18,68 ± 5,53%) p< 0,05 (Figure 41 B). There was no difference in the total number of GSC and hAMSCs in either case. This result suggests that the interaction between hAMSCs and tumor stem cells is dependent on the vascular differentiation capacity of the former.

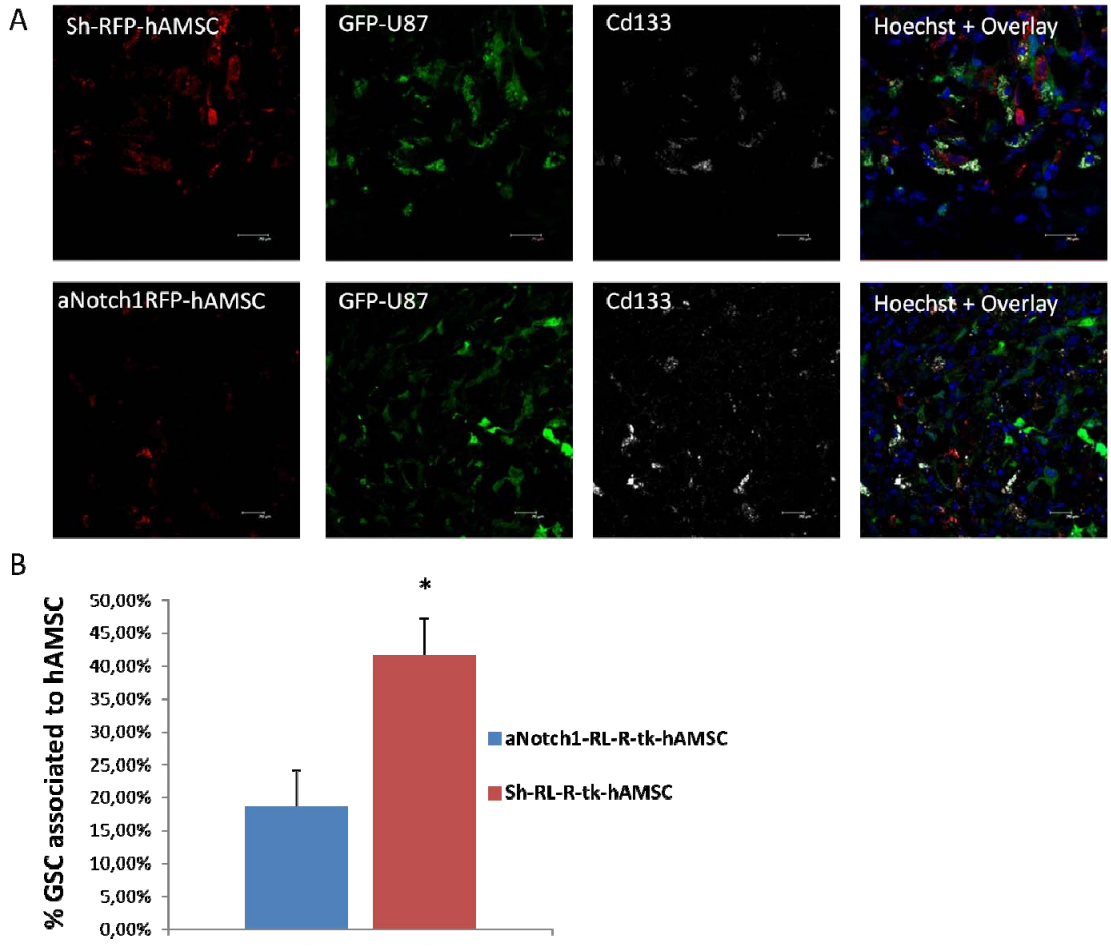

Figure 41 Colocalization of hAMSCs and U87 cancer stem cells. (A) Representative laser confocal microscope images of the corresponding brain tumor slices showing sh-RL-R-tTK-hAMSCs or αNotch1-RL-R-tTK-hAMSCs expressing RFP (red), PL-G-U87 expressing eGFP (green) also labeled by an anti human CD133 antibody (gray), Hoechst nuclear stain (blue); Scale bar= 20 µm. (B) Histogram representing percentage of PL-G-U87 GSC associated to hAMSC in the case of sh-RL-R-tTK-hAMSCs and αNotch1-RL-R-tTK-hAMSCs. Bars represent mean ± SEM of percent. * p< 0.05, n=15.

3 STUDY OF ATRACTION BETWEEN HAMSCS AND GLIOMA CELLS

To further evaluate the potential of hAMSCs for glioblastoma therapy we considered the following objective:

VII. Evaluate the homing capacity of tumor and therapeutic cells.

3.1 BLI determination of homing capacity between tumor and therapeutic cells

To evaluate homing capacity between hAMSCs and U87 cells *in vivo*, intracranial xerographs of the human glioma cell line expressing Pluc and eGFP (PL-G-U87) were inoculated in the previously described brain coordinates in SCID mice. Seven days after tumor inoculation when xerographs were established, $1.6x10^5$ hAMSCs expressing Rluc and RFP (RL-R-tTK-hAMSC) were injected into the opposite brain lobe at the symmetrical coordinates (0,6 mm posterior, -2 mm lateral and 2,75 mm depth respect Bregma) (n=4). As a control, a group of tumor-bearing animals received intracranial injection of PBS, to create a brain injury similar to that of mice implanted with cells (n=2). Animals were imaged by BLI for expression of both luciferases on day 0 of hAMSC injection and seven days later. Figure 42 shows representative images of mice with Rluc expression and Pluc expression of hAMSCs and U87, respectively, at day 0 (hAMSCs injection) and 7 days later. Images show RL-R-tTK-hAMSCs clearly in the left hemisphere and PL-G-U87 in the right side of the brain at day 0. By day 7 light emitted by PL-G-U87 is still located on the right side of the brain, but also appears to expand to the left side. Light emitted by RL-R-tTK-hAMSC decreases 7 days post implantation due to cell death as described previously, but seems to be spreading through the brain towards the tumor. In control mice injected with PBS in the left hemisphere, the light signal emmited by PL-G-U87 is fixed at the original location on the right hemisphere. Since BLI had not enough resolution to precisely detect migration of small populations of cells, mice were sacrificed and frozen sections of brains were analyzed by confocal microscopy.

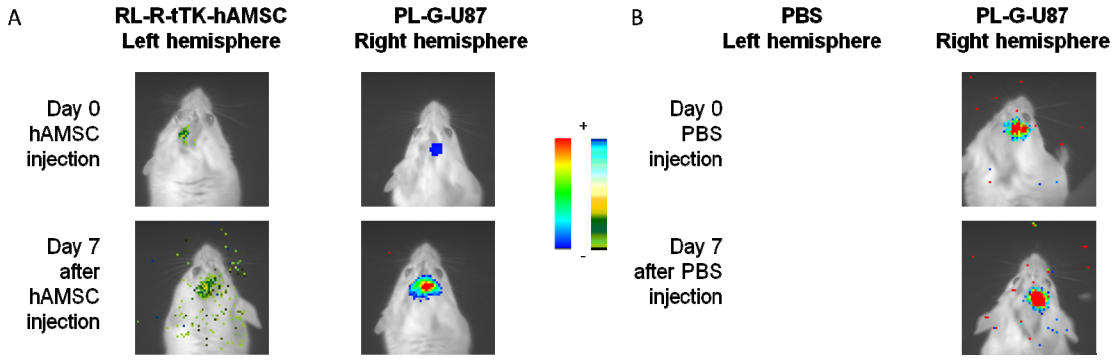

Figure 42 *In vivo* imaging of cell migration. Mice were inoculated with PL-G-U87 in the right hemisphere and one week later with RL-R-hAMSCs (A) or PBS (B) in the symmetric coordinates in the left hemisphere. Implanted cells were monitored to determine cell position by BLI of Renilla and Photinus luciferases. Pseudo color images are superimposed on black and white dorsal images of recipient mice. Color bars illustrate relative light intensities of PLuc (left) and RLuc (right); low: blue and black; high: red and blue, respectively.

3.2 Confocal microscopy study of tumor and therapeutic cell homing capacity

Brain sections from the previous experiment were immuno stained for expression of GFP (PL-G-U87) and RFP (RL-R-hAMSCs) to enhance cell signal and analyzed by confocal microscopy (Figure 43). In mice injected with RL-R-hAMSCs when tumors were well established, hAMSCs where found mixed with green fluorescent tumor cells, thus confirming previously described tumor homing capacity of MSCs[63,91,165]. Surprisingly, in the left hemisphere site of RL-R-tTK-hAMSCs implantation, eGFP expressing U87 cells were also detected, evenly distributed through the hAMSCs cell mass (Figure 43 A left).

In control mice, that received an injection of PBS instead of hAMSCs in the left hemisphere, no eGFP expressing U87 were detected at the site of PBS injection, by either confocal microscopy or by BLI (Figure 43B).

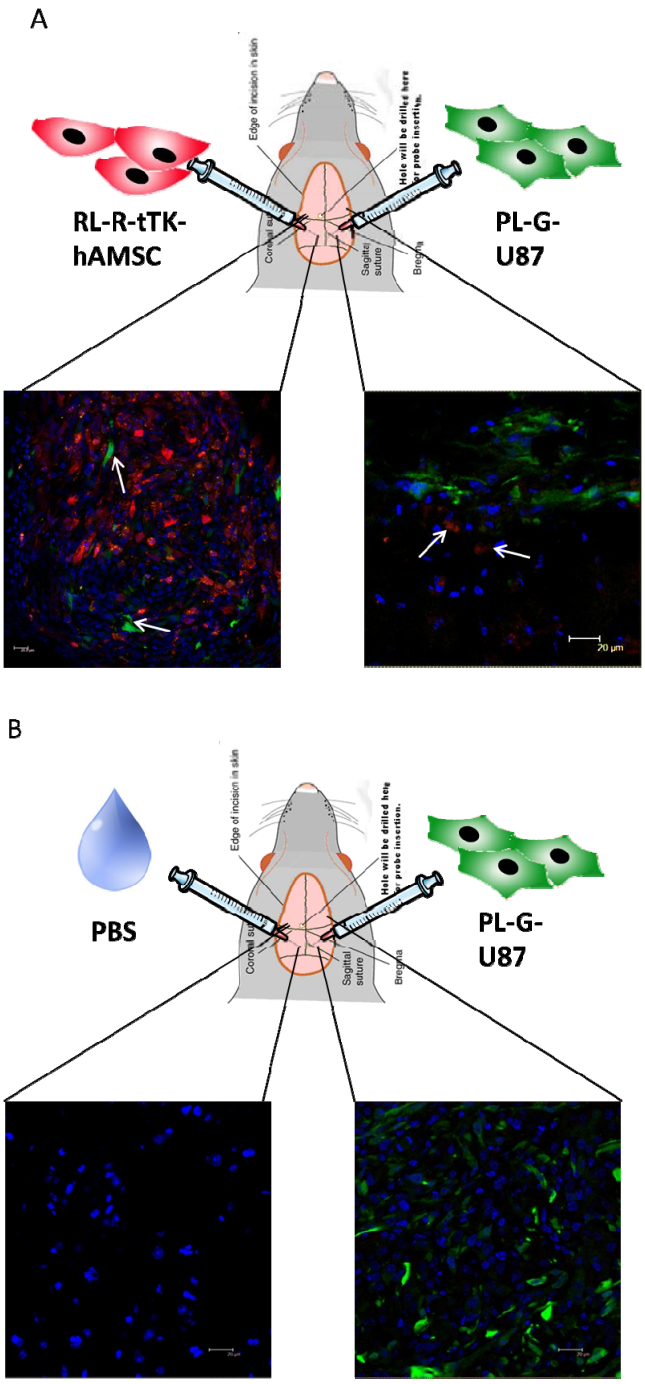

Figure 43 Distribution of hAMSCs and tumor cells after contralateral injection. (A) Representative laser confocal microscope images of the corresponding brain tumor slices showing PL-G-U87 (green) that migrate to the left hemisphere and integrate hAMSCs mass (left). At the right RL-R-hAMSCs locate in the right hemisphere and surrounding tumor cell mass. Hoechst nuclear stain (blue); Scale bar= 20 µm, n=4. (B) Representative laser confocal microscope images of the corresponding brain tumor slices showing PL-G-U87 (green) that are found only in the right hemisphere. No cells were detected in the left hemisphere at PBS injection site. Hoechst nuclear stain (blue); Scale bar= 20 µm, n=2.

To confirm that bilateral attraction happened independently of hAMSCs location the experiment was repeated injecting hAMSCs in the brain frontal lobe (n=2). Briefly, $4x10^4$ PL-G-U87 were inoculated in standard coordinates in SCID mice in the right hemisphere. Seven days after tumor inoculation when xerographs were established, $1.6x10^5$ RL-R-tTK-hAMSC were injected into the opposite frontal lobe (1 mm anterior, -

2 mm lateral and 2,75 mm depth respect Bregma) (n=2). Seven days later mice were sacrificed, their brains were removed, and frozen sections were analyzed by confocal microscopy.

Confocal microscopy analysis of mouse brain sections showed that bilateral attraction between tumoral and therapeutic cells also occurred in the frontal direction (

Figure **44**). The right hemisphere shows the presence of red fluorescent RL-R-tTK-hAMSCs mixed with green fluorescent tumor cells (right), as in the previous experiment. In the left hemisphere, eGFP expressing U87 were also detected among hAMSCs cell mass (left).

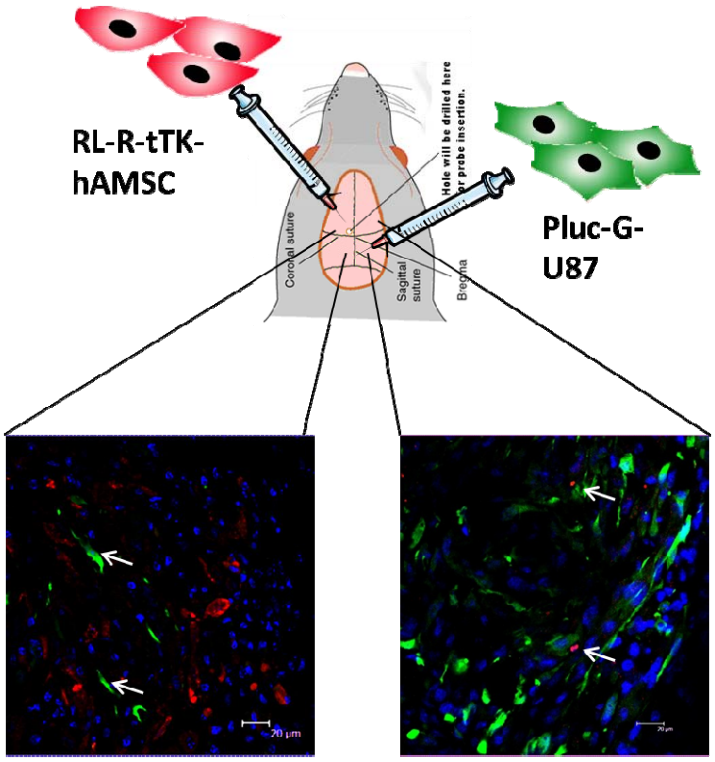

Figure 44 Frontal cell migration. Left, representative laser confocal microscope images of the corresponding brain tumor slices showing PL-G-U87 (green) that migrate to the frontal left hemisphere and integrate hAMSCs mass. At the right, RL-R-hAMSCs locate in the dorsal right hemisphere and integrate tumor cell mass. Hoechst nuclear stain (blue); Scale bar= 20 µm, n=2.

To further investigate the role of hAMSCs endothelial differentiation in the attraction mechanism the homing experiment was repeated. However, this time injecting hAMSCs impaired for endothelial differentiation in the contralateral lobe of the brain (n=2). Briefly, $4x10^4$ PL-G-U87 were inoculated in standard coordinates in SCID mice in the right hemisphere. Seven days after tumor inoculation when xerographs were established, $1.6x10^5$ αNotch1-RL-R-tTK-hAMSCs were injected into the opposite lobe

(n=2). Seven days later mice were sacrificed, their brains were removed, and frozen sections were analyzed by confocal microscopy.

Analysis of mouse brain sections showed the presence of red fluorescent αNotch1-RL-R-tTK-hAMSCs surrounding green fluorescent tumor cells, in the right hemisphere (Figure 45 right). However in the left hemisphere, no eGFP expressing U87 could be detected. Thus, U87 showed no homing towards hAMSC that were impaired for differentiation to endothelial lineage.

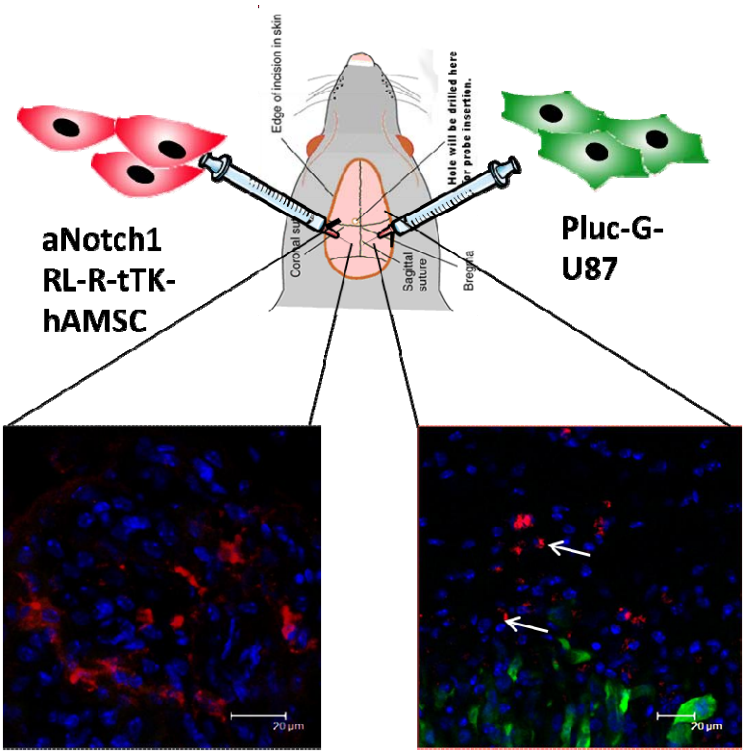

Figure 45 Attraction between αNotch1-RL-R-tTK-hAMSCs and U87. Representative laser confocal microscope images of the corresponding brain tumor slices showing no PL-G-U87 in the left hemisphere (left). At the right, αNotch1-RL-R-tTK-hAMSCs locate in the right hemisphere and integrate tumor cell mass. Hoechst nuclear stain (blue); Scale bar= 20 µm, n=2.

3.2.1 *In vitro* homing capacity

The homing capacity analysis was also performed *in vitro* to further study the mechanism of attraction between therapeutic and tumoral cells. In these experiments, either αNotch1-RL-R-tTK-hAMSCs or sh-RL-R-tTK-hAMSCs were seeded in one of the wells of a well pair separated by culture-inserts and PL-G-U87 were seeded in the opposite well. Following the removal of the insert separating the wells the progression of cell invasion of the insert generated gap was monitored by contrast microscopy. As shown on Figure 46, U87 exert a stronger attraction for normal hAMSCs, than for

hAMSCs impaired for endothelial differentiation; in concordance with results obtained *in vivo.* A mutual attraction exists between normal hAMSCs and U87, and 24 hours after the culture-insert is removed the total invasion of the wound can be observed (Figure 46 B). Conversely, Notch1 inhibited hAMSCs expand slowly and while there also appear to be cell attraction, 24 hours after beginning the experiment the wound between wells still remains unfilled (Figure 46 A).

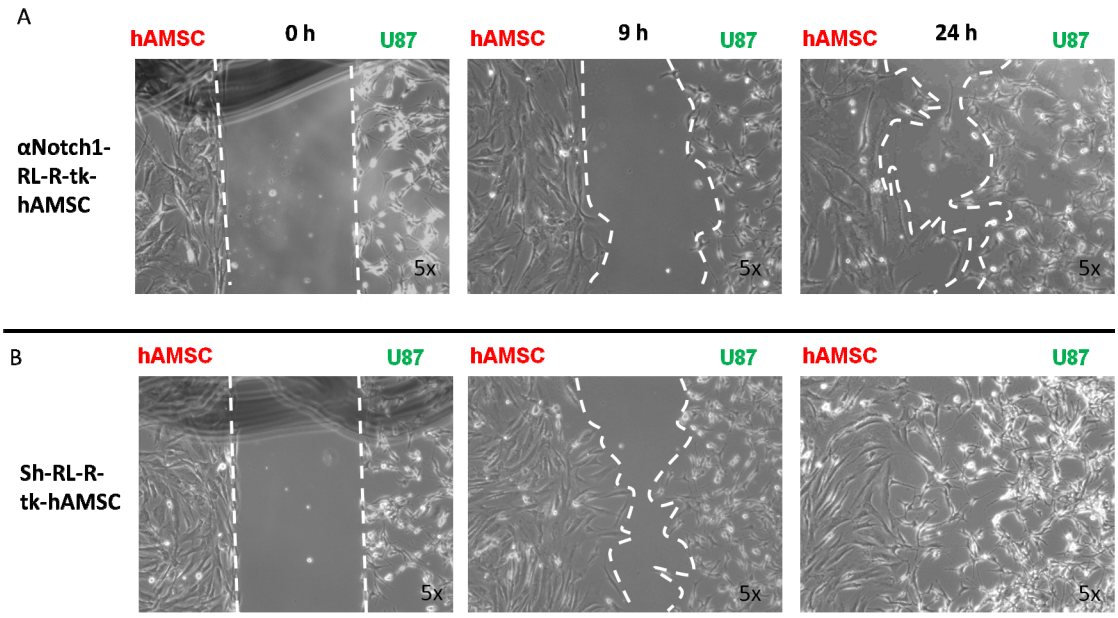

Figure 46 Sequence of events during *in vitro* invasion assay. In each image monolayers of hAMSCs (left) and PL-G-U87 (right) were created as described in methods and materials. A: representative images of αNotch1-RL-R-tk-hAMSC vs PL-G-U87 invasion. B: representative images of Sh-RL-R-tk-hAMSC vs PL-G-U87 invasion.

DISCUSSION

GBM is a primary brain tumor with high morbidity and mortality and is the first cause of death from brain tumors. Current treatment protocols for GBM are ineffective due to its invasiveness, which makes complete surgical removal almost impossible, and to survival of radiation and chemotherapy resistant cells after therapy. A promising approach based on the use of cellular vehicles to deliver localized treatment targeting the primary tumor mass has been proposed [57]. Targeted suicide gene strategies, are based on the activation of a systemically delivered low toxicity prodrug to a cytotoxic agent in the vicinity of tumors, mediated by the action of a specific activating enzyme expressed by the therapy vehicle [166]. The delivery of cytotoxicity in the vicinity of a tumor has the advantage of avoiding systemic toxicity.

Strong anti-tumor effects have been reported following intracranial administration of gene modified NSC expressing IL-12[66], BMSCs expressing TRAIL[167] and others. However from ethical points of view, and due to ease of isolation and manipulation autologous hAMSC are more attractive cell vehicles for clinical use.

In the current thesis we demonstrate a procedure to develop a therapeutic strategy against a human U87 glioblastomas and an effective therapy model in SCID mice. The procedure is based on the use of hAMSCs genetically modified to express the herpes Simplex tTK as vehicles to deliver bystander toxicity to tumors. The HSV-TK was used in the first cell suicide gene therapy proof of principle and still is one of the most widely used systems in clinical and experimental applications [168,169]. This cytotoxic system has been applied to the treatment of gliomas with significant increases in survival[170]. tTK is the truncated version of HSV-TK with 30 fold higher activity than wild type HSV-TK [133,152].

To analyze the behavior of tumor and therapeutic cells *in vitro* and *in vivo*, we labeled the former with a CMV promoter regulated Pluc-eGFP chimerical reporter, and the latter with a different trifunctional chimerical reporter comprising Rluc-RFP and tTK activities [133]. This approach allowed us to monitor the location and number of tumor and therapeutic cells in live mice during treatment with GCV, and optimize cell and prodrug treatment.

We established that both, tTK activity in genetically modified hAMSCs, and administration of GCV were required for bystander killing of tumor cells co-cultivated with hAMSCs.

In vivo BLI of predetermined numbers of hAMSC and U87 cells, stereotactically implanted at a specific site of the mouse brain, allowed us to correlate the number of photon events recorded by BLI with that of implanted cells, for their quantification during therapy.

An optimum therapeutic ratio of 4 hAMSCs to 1 U87 cell was empirically determined by implanting predetermined proportions of both cell types in mouse brains and administering GCV i.p. after a 6 day period, allowed for tumor establishment. Analysis of hAMSC behavior during the 6 day pre-treatment period indicated that a large proportion of the therapeutic cells disappeared, while tumor cells proliferated. This lead to a 50 fold, reduction in the proportion of therapeutic to tumor cells, that was 1:13 by the time the GCV treatment began. This result not only emphasizes the effectiveness of hAMSCs as therapeutic vehicles, but also suggests that procedures or scaffold materials for their protection would likely improve even more the therapeutic outcome. Thought the scaffold for this aim have to be cautiously selected, since it should provide an environment that enhances transplanted stem cell survival, and controls the delivery of therapeutic cells to the tumors, but should not enhance tumor cell proliferation. Options include some of the biocompatible scaffolds that have been used in regenerative therapies to support transplanted stem cells[171,172].

The disappearance of a large proportion of hAMSCs when injected in immunosupressed mice has been previously observed[163]. However, the reduction in hAMSC number should not be attributed to CMV promoter silencing. In a previous study by Vilalta et al. [173], hAMSCs expressing Pluc regulated by the constitutively active SV40 promoter also lost between 75-90% of cells within the first 10 days post inoculation in SCID mice. Moreover, since in our cell differentiation experiment all the therapeutic cells are initially red fluorescent and become also green fluorescent upon differentiation to the endothelial lineage, silencing of the CMV promoter should result in the appearance of green fluorescent cells that show no red fluorescence. Thus CMV

silencing can be evaluated by determining the proportion of therapeutic cells expressing GFP (regulated by the inducible PECAM/CD31 promoter) that do not express RFP (regulated by the CMV promoter) in histological sections of tumors. While extensive silencing of the CMV promoter would be required to produce the 92 fold increase in PECAM/CD31-PLuc expression observed in the BLI experiments, our assessment found less than 10% of GFP positive cells that were not RFP positive. This result excludes CMV promoter silencing, and points to cell death or diffusion from the tumor sites as the likely causes for the drop in Rluc activity production following cell implantation.

The therapeutic effectiveness of hAMSCs was evaluated by comparing their capacity to inhibit U87 tumor growth by implanting the optimal 4:1 (hAMSC to U87) proportion in mice brains, and treating with GCV or PBS. Such experiments showed that treatment with GCV of tumors containing hAMSCs reduced the number of tumor cells by a factor of 10^4, relative to tumors without hAMSCs, also treated with GCV, or tumors with hAMSCs treated with PBS. For the same tumor, by the end of the experiment, treatment with hAMSCs plus GCV had reduced tumor cell number to 0,12% of that at T=0. However, in tumors without hAMSCs but also treated with GCV tumor cell number increased by 319 fold in the same period.

Macroscopic and laser confocal microscope examination of brain slices at the end of experiments corroborated BLI imaging results. While brains from mice with untreated mixed-cell tumors had large tumor masses containing green and red fluorescent cells, no macroscopic tumors and few green fluorescent cells were found in the brains of mice implanted with tumors plus therapeutic cells and treated with GCV.

In experiments better modeling a clinical situation, we showed that implantation of therapeutic hAMSCs on preestablished glioblastoma U87 tumors and treatment with GCV also results in tumor growth inhibition that lasts as long as there were surviving therapeutic hAMSCs. Moreover, repeated inoculations of therapeutic hAMSCs resulted in a progressive reduction of tumor size and a significant extension of mice survival, relative to untreated controls.

Insight on the therapeutic mechanism mediated by tTK expressing hAMSCs was gained using a double label strategy that allows monitoring of changes in gene expression on a "per cell" basis. This was achieved by labeling of the same therapeutic cell that already expressed Rluc-RFP reporter constitutively, with a different Pluc-eGFP reporter regulated by the inducible human PECAM promoter. By co-implanting these cells with unlabelled U87 tumors and monitoring cell behavior by BLI we could observe that within the first 7 days post implantation, a large proportion of the hAMSCs disappeared from the tumor site, either by death or dispersion. However, a subpopulation of the cells that expressed PECAM-promoter regulated luciferase remained in close association with the tumor site. Moreover, in the tumor associated cell population, the ratio of PECAM-regulated to CMV-regulated luciferase activity increased with time reaching by day 7 a value 92 fold higher than that at implantation time. This results indicated that tumor associated hAMSCs were actively differentiating to the endothelial lineage. Independent analysis by fluorescence laser confocal microscopy of tumor slices revealed RFP and eGFP expressing hAMSCs with endothelial morphology in close association with tumor vascular structures. This latter result was further corroborated by positive staining of microvessel associated red fluorescent hAMSCs with an anti human PECAM antibody.

Association of bone marrow derived MSCs with vascular structures in tumors has been reported previously[165,174]. However, the vascular associated cells were shown to express pericyte specific antigens but not endothelial specific markers. Contrary to this our results showed that hAMSC expressed PECAM/CD31 that is considered an endothelial specific marker and did not express perycite SM22 marker. Both findings are not mutually exclusive, and in the absence of additional data, could be reconciled by considering that differentiation of mesenchymal stromal cells may depend on their tissue of origin as well as on the specific tumor environment in which they are implanted [175]. Our results suggested that GCV induced suicide of hAMSCs not only kills neighboring tumor cells by bystander effect but also by eliminating the associated vascular system that supplies oxygen and nutrients to the tumor.

We further explored the interaction between hAMSCs and U87 glioma in a SCID mouse model, to understand the basis of hAMSC effectiveness to deliver cytotoxic tumor therapy and the importance of hAMSCs differentiation to the endothelial lineage.

Deletion of the DII4 receptor or Notch1 during embryogenesis results in vascular anomalies and lethality[176,177]. Notch1 signaling is required for endothelial cell differentiation, and inhibition of this pathway in bone marrow derived MSC has been shown to block their differentiation into functional endothelial cells, and the expression of endothelial-specific markers[164,178].

We first showed that, by using αNotch1 shRNA to interfere with Notch1 signaling, we were able to abolish the network formation capacity of hAMSCs in an *in vitro* matrigel assay, a good indicator of vasculogenic potential[179,180]. Loss of network formation capacity was accompanied by a significant reduction in the expression of endothelial markers ILK, SDF1, EGR3, PECAM and Notch1 itself, in the same cells, but not of osteocalcin, an independent bone differentiation marker.

We then used hAMSCs with double bioluminescence reporter systems, one (CD31-PLuc-eGFP) regulated by the CD31 promoter and the other (CMV-Rluc-RFP) regulated by CMV promoter, to report on endothelial differentiation and cell number, respectively. Luciferase tagged cells were also transduced with lentiviral vectors for the expression of either αNotch shRNA to generate hAMSCs that were impaired to differentiate to the endothelial lineage. Another group of cells were transduced with an empty lentiviral vector to generate corresponding control cells.

By monitoring the activity of luciferase reporters in control hAMSCs or αNotch hAMSCs independently implanted with U87 cells in the brain of SCID mice, we were able to observe that a large proportion of the hAMSCs implanted with tumors die or disappear. However, while control hAMSCs that remained associated with the tumor suffered a pronounced increase in the activity of the CD31 regulated luciferase, this was not the case when Notch1 signaling was inhibited in αNotch hAMSCs. This result was further supported by fluorescence confocal microscope analysis of tissue slices from the same tumors showing that while control hAMSCs associated with tumor

vascular structures, the vascular association of αNotch inhibited hAMSCs was significatively reduced.

These results show that inhibition of Notch1 signaling also precludes differentiation of hAMSCs to the endothelial lineage *in vivo* and suggested the analysis of the relation between endothelial differentiation and therapeutic capacity of hAMSCs.

We showed that in the presence of GCV both control and αNotch shRNA inhibited hAMSCs are equally effective at killing U87 tumor cells *in vitro*, demonstrating that Notch1 inhibition does not affect HSV thymidin kinase activity, essential for cytotoxic bystander effect.

Then, Photinus luciferase expressing U87 tumors (Pluc-U87) were implanted together with mock transduced hAMSC, αNotch inhibited hAMSCs, or without hAMSCs, and allowed to grow during 7 days. Following this tumor establishment period, GCV treatment was initiated and continued during 2 additional weeks. The results from BLI of tumors clearly showed that both mock-transduced and αNotch inhibited hAMSCS had an effective tumor growth promoting capacity during the first week without GCV, in comparison with tumors without hAMSCs. The acceleration of tumor growth in animals co-injected with MSCs was previously observed[181]. MSCs may support tumor growth by several mechanisms, such as growth factor production, immunosuppression, and by collaborating in the generation of a favorable microenvironment for cancer cells[182].

Although treatment with GCV had a clearly inhibitory effect on tumor growth, this was significantly more pronounced (96%) in tumors containing mock-transduced hAMSCs, than in those containing Notch inhibited hAMSCs (36%) $p<0,05$, clearly showing that Notch1 signaling is required for an effective delivery of cytotoxicity by hAMSCs. The residual tumor killing effect of αNotch inhibited hAMSCs is likely the result of a lower than 100% efficiency on Notch signaling inhibition by αNotch ShRNA.

These results show that hAMSCs exert a powerful tumor promoting effect of orthotopically implanted U87 tumors, and that such effect is independent of the Notch signaling pathway. However, the capacity of hAMSCs to deliver bystander therapy to

the tumors is strongly dependent of Notch1 activity suggesting that vasculogenic differentiation is essential for the delivery of therapy.

Confocal microscopy analysis of tissue slices from control and Notch1 inhibited hAMSCs in U87 tumors that had been perfused *in vivo* with a high MW fluorescein-tagged dextran showed that Notch1-expressing control hAMSCs, but not Notch-inhibited hAMSCs, were found in association with tumor vascular structures and show endothelial phenotype, adding supplementary clues towards explaining the basis for the therapeutic effectiveness of these cells.

Recent studies have shown that a subpopulation of tumor cells with stem cell characteristics (GSCs) including self-renewal capacity is responsible for tumor initiation, progression and infiltration of adjacent normal parenchyma, and for tumor recurrences after surgery, radio- or chemo-resistance of gliomas[183]. It has been described that GSC locate next to capillaries in brain tumors constituting a niche that is critical for their maintenance[33,34].

CD133 is a widely accepted marker for glioma-derived cancer stem cells. In our study, by using a monoclonal antibody against the CD133 antigen, we were able to observe frequent (42,6%) association of control Notch1 expressing hAMSCs with CD133+ tumor cells. However, in the case of Notch inhibited-hAMSCs the frequency of such associations was significantly lower (18,62%) $p<0,05$. Differentiation of hAMSCs to endothelial lineage and association to GSC and vascular structures suggests that when implanted in the brain these cells migrate to the vascular niche of GSCs.

Tumor tropism of MSCs is of great advantage especially in treatment of high-grade brain tumors with inherent neovascularization capability and ability to infiltrate deeply into the brain[62-64]. In this study we corroborate previous evidence that hAMSC migrate toward human gliomas after local contraletral or frontal intracranial injection. This observation is in accordance with the hypothesis suggesting that, endogenous hMSC are recruited during the process of tumor stroma formation[184,185]. Most importantly, we show, for the first time to our knowledge, that tumor U87 cells also migrate towards hAMSCs injection site and integrate into the cell mass. The prospect of tumor cell migration towards an injury site led us to perform a “fake operation”, injecting PBS

in the left hemisphere to mimic an inflammatory response. However no tumor cells were detected at the injury site; suggesting that the presence of hAMSC promotes tumor cell migration.

Glioma cells have a remarkable capacity to infiltrate the brain and migrate long distances from the tumor. Previous studies have shown that glioma cells extensively infiltrated the brain by migrating along the abluminal surface of blood vessels[186,187]. Considering, previously described capacity of hAMSC to differentiate to endothelial lineage we hypothesized that it was formation of new microvasculature at the hAMSCs injection site that induced gliomas migratory behavior. Using contralateral injection experiments we showed that U87 tumor cells did not migrate towards the injection site of αNotch inhibited hAMSCs. However αNotch inhibited hAMSCs did retain their tumor homing capacity; proving evidence that bidirectional attraction between tumor and therapeutic cells occurs by different mechanisms. *In vitro* migration assays showed that impairment of Notch1 also inhibits attraction between hAMSCs and U87, supporting the involvement of paracrine mechanisms and suggested a practical assay for their further study. Previous experiments with hemizygous deletion of Notch1 had shown that mobilization and migration of bone marrow-derived cells may be mediated by CSF3R and CXCR4[188]. Furthermore, glioma cell infiltration in living brain tissue is directed by interactions with host brain vasculature[186] further supporting our observation that tropism of U87 cells towards hAMSC is motivated by factors released by hAMSC differentiating to the endothelial lineage.

Our results strongly suggest that hAMSCs interact with glioma tumors through multiple mechanisms, some of which act at a distance and are likely of paracrine nature.

The therapeutic safety of these cells has been recently demonstrated[112]. Moreover, the potential to use autologous cells is a further guaranty for their safe application. Although we have used a single enzymatic system to deliver cytotoxicity, additional and very promising prodrug converting systems are currently being developed that may further improve treatment of inoperable gliomas[113,165].

In future work we will focus on evaluating procedures for therapeutic cell delivery, including the use of a biomaterial to protect and control the delivery of therapeutic

cells implanted in tumors. We will also evaluate the relevance of the immune environment on the therapeutic effectiveness, we will use immune-competent mice implanted with singeneic glioma tumor model that will be treated with autologous therapeutic hAMSCs. Finally, we will seek to validate the generality of the therapeutic procedure using glioma tumors from human biopsies implanted in immunedefficient mice.

CONCLUSIONS

- A bioluminescence imaging system was developed to monitor behavior of tumor and therapeutic cells in live animals.

- The system allowed the development of an effective model of glioblastoma therapy using adipose tissue stromal cells genetically modified to generate a cytotoxic bystander effect.

- In combination with standard procedures it has been possible to study the interaction of tumor and hAMSCs mediating the therapeutic mechanism:

  - Tumor implanted hAMSCs do not proliferate and most of them die rapidly.
  - hAMSCs surviving tumor implantation tend to differentiate to the endothelial lineage.

- Endothelial lineage differentiated hAMSCs:

  - are capable of delivering a very effective cytotoxic bystander effect to U87 tumors.
  - associate with the tumor vascular system and GSCs.
  - are attracted to U87 tumors.
  - are capable of attracting U87 tumor cells.

- The cytotoxic capacity of endothelial lineage differentiated hAMSCs results from their proximity to the tumor vascular system and to GSCs.

- hAMSCs impaired to differentiate to the endothelial lineage:

  - have a potent U87 growth promoting capacity; possibly mediated by paracrine factors, although no evidence is provided.
  - do not associate with the tumor vascular system or GSCs.

- are unable to deliver bystander cytotoxic effect to U87 tumors; possibly the result of not being able to associate with the tumor vascular system and GSCs.
- are unable to attract U87 tumor cells; possibly the result of not producing chemokines for which U87 have receptors.
- are attracted by U87 tumors; likely the result of expressing receptors for U87 produced chemokines.

- At this point we cannot evaluate whether the therapeutic effect of hAMSCs is exerted by destruction of the tumor vascular system, the tumor stem cells or both. However, the surprising therapeutic effectiveness of the few hAMSCs that survive implantation in tumors suggests that GSCs may be the primary targets.

REFERENCES

1. Ferlay J, Parkin DM, Steliarova-Foucher E. Estimates of cancer incidence and mortality in Europe in 2008. Eur J Cancer 2010;46:765-81.
2. Schneider T, Mawrin C, Scherlach C, Skalej M, Firsching R. Gliomas in adults. Dtsch Arztebl Int 2010;107:799-807; quiz 8.
3. Figarella-Branger D, Colin C, Coulibaly B, et al. [Histological and molecular classification of gliomas]. Rev Neurol (Paris) 2008;164:505-15.
4. Hickey MJ, Malone CC, Erickson KL, et al. Cellular and vaccine therapeutic approaches for gliomas. J Transl Med 2010;8:100.
5. Grossman SA, Ye X, Piantadosi S, et al. Survival of patients with newly diagnosed glioblastoma treated with radiation and temozolomide in research studies in the United States. Clin Cancer Res 2010;16:2443-9.
6. Wrensch M, Minn Y, Chew T, Bondy M, Berger MS. Epidemiology of primary brain tumors: current concepts and review of the literature. Neuro Oncol 2002;4:278-99.
7. Phillips HS, Kharbanda S, Chen R, et al. Molecular subclasses of high-grade glioma predict prognosis, delineate a pattern of disease progression, and resemble stages in neurogenesis. Cancer Cell 2006;9:157-73.
8. Shete S, Hosking FJ, Robertson LB, et al. Genome-wide association study identifies five susceptibility loci for glioma. Nat Genet 2009;41:899-904.
9. Hodges LC, Smith JL, Garrett A, Tate S. Prevalence of glioblastoma multiforme in subjects with prior therapeutic radiation. J Neurosci Nurs 1992;24:79-83.
10. Salvati M, Artico M, Caruso R, Rocchi G, Orlando ER, Nucci F. A report on radiation-induced gliomas. Cancer 1991;67:392-7.
11. Shintani T, Hayakawa N, Hoshi M, et al. High incidence of meningioma among Hiroshima atomic bomb survivors. J Radiat Res (Tokyo) 1999;40:49-57.
12. Bondy M, Wiencke J, Wrensch M, Kyritsis AP. Genetics of primary brain tumors: a review. J Neurooncol 1994;18:69-81.
13. Liu Y, Shete S, Hosking FJ, Robertson LB, Bondy ML, Houlston RS. New insights into susceptibility to glioma. Arch Neurol 2010;67:275-8.
14. Efird JT. Season of birth and risk for adult onset glioma. Int J Environ Res Public Health 2010;7:1913-36.
15. Zheng T, Cantor KP, Zhang Y, Keim S, Lynch CF. Occupational risk factors for brain cancer: a population-based case-control study in Iowa. J Occup Environ Med 2001;43:317-24.
16. Buckner JC, Brown PD, O'Neill BP, Meyer FB, Wetmore CJ, Uhm JH. Central nervous system tumors. Mayo Clin Proc 2007;82:1271-86.
17. Chandana SR, Movva S, Arora M, Singh T. Primary brain tumors in adults. Am Fam Physician 2008;77:1423-30.
18. Weller M. Novel diagnostic and therapeutic approaches to malignant glioma. Swiss medical weekly 2011;141:w13210.
19. Fueyo J, Gomez-Manzano C, Yung WK. Advances in translational research in neuro-oncology. Arch Neurol 2011;68:303-8.
20. Stupp R, Mason WP, van den Bent MJ, et al. Radiotherapy plus concomitant and adjuvant temozolomide for glioblastoma. N Engl J Med 2005;352:987-96.
21. Stupp R, Hegi ME, van den Bent MJ, et al. Changing paradigms--an update on the multidisciplinary management of malignant glioma. Oncologist 2006;11:165-80.
22. Rich JN, Bigner DD. Development of novel targeted therapies in the treatment of malignant glioma. Nature reviews Drug discovery 2004;3:430-46.
23. Van Meir EG, Hadjipanayis CG, Norden AD, Shu HK, Wen PY, Olson JJ. Exciting new advances in neuro-oncology: the avenue to a cure for malignant glioma. CA Cancer J Clin 2010;60:166-93.
24. Chang SM, Wen P, Cloughesy T, et al. Phase II study of CCI-779 in patients with recurrent glioblastoma multiforme. Invest New Drugs 2005;23:357-61.

25. Paez-Ribes M, Allen E, Hudock J, et al. Antiangiogenic therapy elicits malignant progression of tumors to increased local invasion and distant metastasis. Cancer Cell 2009;15:220-31.
26. Furnari FB, Fenton T, Bachoo RM, et al. Malignant astrocytic glioma: genetics, biology, and paths to treatment. Genes Dev 2007;21:2683-710.
27. Al-Hajj M, Wicha MS, Benito-Hernandez A, Morrison SJ, Clarke MF. Prospective identification of tumorigenic breast cancer cells. Proc Natl Acad Sci U S A 2003;100:3983-8.
28. Lathia JD, Venere M, Rao MS, Rich JN. Seeing is believing: are cancer stem cells the Loch Ness monster of tumor biology? Stem Cell Rev 2011;7:227-37.
29. Li Z, Wang H, Eyler CE, Hjelmeland AB, Rich JN. Turning cancer stem cells inside out: an exploration of glioma stem cell signaling pathways. J Biol Chem 2009;284:16705-9.
30. Cheng L, Bao S, Rich JN. Potential therapeutic implications of cancer stem cells in glioblastoma. Biochem Pharmacol 2010;80:654-65.
31. Heddleston JM, Li Z, McLendon RE, Hjelmeland AB, Rich JN. The hypoxic microenvironment maintains glioblastoma stem cells and promotes reprogramming towards a cancer stem cell phenotype. Cell Cycle 2009;8:3274-84.
32. Wang J, Sakariassen PO, Tsinkalovsky O, et al. CD133 negative glioma cells form tumors in nude rats and give rise to CD133 positive cells. Int J Cancer 2008;122:761-8.
33. Calabrese C, Poppleton H, Kocak M, et al. A perivascular niche for brain tumor stem cells. Cancer Cell 2007;11:69-82.
34. Christensen K, Schroder HD, Kristensen BW. CD133 identifies perivascular niches in grade II-IV astrocytomas. J Neurooncol 2008;90:157-70.
35. Bao S, Wu Q, Sathornsumetee S, et al. Stem cell-like glioma cells promote tumor angiogenesis through vascular endothelial growth factor. Cancer Res 2006;66:7843-8.
36. Vauleon E, Avril T, Collet B, Mosser J, Quillien V. Overview of cellular immunotherapy for patients with glioblastoma. Clin Dev Immunol 2010;2010.
37. Kuan CT, Wakiya K, Herndon JE, 2nd, et al. MRP3: a molecular target for human glioblastoma multiforme immunotherapy. BMC Cancer 2010;10:468.
38. Huszthy PC, Giroglou T, Tsinkalovsky O, et al. Remission of invasive, cancer stem-like glioblastoma xenografts using lentiviral vector-mediated suicide gene therapy. PLoS One 2009;4:e6314.
39. Niranjan A, Wolfe D, Tamura M, et al. Treatment of rat gliosarcoma brain tumors by HSV-based multigene therapy combined with radiosurgery. Mol Ther 2003;8:530-42.
40. Nguyen LT, Atobe K, Barichello JM, Ishida T, Kiwada H. Complex formation with plasmid DNA increases the cytotoxicity of cationic liposomes. Biol Pharm Bull 2007;30:751-7.
41. Yoshida J, Mizuno M. Clinical gene therapy for brain tumors. Liposomal delivery of anticancer molecule to glioma. J Neurooncol 2003;65:261-7.
42. Perez-Cruet MJ, Trask TW, Chen SH, et al. Adenovirus-mediated gene therapy of experimental gliomas. J Neurosci Res 1994;39:506-11.
43. Fu YJ, Du J, Yang RJ, Yin LT, Liang AH. Potential adenovirus-mediated gene therapy of glioma cancer. Biotechnol Lett 2010;32:11-8.
44. Ito H, Kanzawa T, Miyoshi T, et al. Therapeutic efficacy of PUMA for malignant glioma cells regardless of p53 status. Hum Gene Ther 2005;16:685-98.
45. Lang FF, Bruner JM, Fuller GN, et al. Phase I trial of adenovirus-mediated p53 gene therapy for recurrent glioma: biological and clinical results. J Clin Oncol 2003;21:2508-18.
46. Fukazawa T, Matsuoka J, Yamatsuji T, Maeda Y, Durbin ML, Naomoto Y. Adenovirus-mediated cancer gene therapy and virotherapy (Review). Int J Mol Med 2010;25:3-10.
47. Dey M, Ulasov IV, Lesniak MS. Virotherapy against malignant glioma stem cells. Cancer Lett 2010;289:1-10.
48. Markert JM, Medlock MD, Rabkin SD, et al. Conditionally replicating herpes simplex virus mutant, G207 for the treatment of malignant glioma: results of a phase I trial. Gene Ther 2000;7:867-74.

49. Csatary LK, Gosztonyi G, Szeberenyi J, et al. MTH-68/H oncolytic viral treatment in human high-grade gliomas. J Neurooncol 2004;67:83-93.
50. Chiocca EA, Abbed KM, Tatter S, et al. A phase I open-label, dose-escalation, multi-institutional trial of injection with an E1B-Attenuated adenovirus, ONYX-015, into the peritumoral region of recurrent malignant gliomas, in the adjuvant setting. Mol Ther 2004;10:958-66.
51. Forsyth P, Roldan G, George D, et al. A phase I trial of intratumoral administration of reovirus in patients with histologically confirmed recurrent malignant gliomas. Mol Ther 2008;16:627-32.
52. Zemp FJ, Corredor JC, Lun X, Muruve DA, Forsyth PA. Oncolytic viruses as experimental treatments for malignant gliomas: using a scourge to treat a devil. Cytokine Growth Factor Rev 2010;21:103-17.
53. Fueyo J, Gomez-Manzano C, Alemany R, et al. A mutant oncolytic adenovirus targeting the Rb pathway produces anti-glioma effect in vivo. Oncogene 2000;19:2-12.
54. Alonso MM, Jiang H, Gomez-Manzano C, Fueyo J. Targeting brain tumor stem cells with oncolytic adenoviruses. Methods Mol Biol 2012;797:111-25.
55. Abate-Daga D, Andreu N, Camacho-Sanchez J, et al. Oncolytic adenoviruses armed with thymidine kinase can be traced by PET imaging and show potent antitumoural effects by ganciclovir dosing. PLoS One 2011;6:e26142.
56. Alavi JB, Eck SL. Gene therapy for high grade gliomas. Expert Opin Biol Ther 2001;1:239-52.
57. Aboody KS, Najbauer J, Danks MK. Stem and progenitor cell-mediated tumor selective gene therapy. Gene Ther 2008;15:739-52.
58. Tabatabai G, Wick W, Weller M. Stem cell-mediated gene therapies for malignant gliomas: a promising targeted therapeutic approach? Discov Med 2011;11:529-36.
59. Glick RP, Lichtor T, Kim TS, Ilangovan S, Cohen EP. Fibroblasts genetically engineered to secrete cytokines suppress tumor growth and induce antitumor immunity to a murine glioma in vivo. Neurosurgery 1995;36:548-55.
60. Bjerkvig R, Read TA, Vajkoczy P, et al. Cell therapy using encapsulated cells producing endostatin. Acta Neurochir Suppl 2003;88:137-41.
61. Ahmed AU, Alexiades NG, Lesniak MS. The use of neural stem cells in cancer gene therapy: predicting the path to the clinic. Curr Opin Mol Ther 2010;12:546-52.
62. Kucerova L, Altanerova V, Matuskova M, Tyciakova S, Altaner C. Adipose tissue-derived human mesenchymal stem cells mediated prodrug cancer gene therapy. Cancer Res 2007;67:6304-13.
63. Nakamizo A, Marini F, Amano T, et al. Human bone marrow-derived mesenchymal stem cells in the treatment of gliomas. Cancer Res 2005;65:3307-18.
64. Hamada H, Kobune M, Nakamura K, et al. Mesenchymal stem cells (MSC) as therapeutic cytoreagents for gene therapy. Cancer Sci 2005;96:149-56.
65. Benedetti S, Pirola B, Pollo B, et al. Gene therapy of experimental brain tumors using neural progenitor cells. Nat Med 2000;6:447-50.
66. Ehtesham M, Kabos P, Kabosova A, Neuman T, Black KL, Yu JS. The use of interleukin 12-secreting neural stem cells for the treatment of intracranial glioma. Cancer Res 2002;62:5657-63.
67. De Palma M, Mazzieri R, Politi LS, et al. Tumor-targeted interferon-alpha delivery by Tie2-expressing monocytes inhibits tumor growth and metastasis. Cancer Cell 2008;14:299-311.
68. Menon LG, Kelly K, Yang HW, Kim SK, Black PM, Carroll RS. Human bone marrow-derived mesenchymal stromal cells expressing S-TRAIL as a cellular delivery vehicle for human glioma therapy. Stem Cells 2009;27:2320-30.

69. Vajkoczy P, Blum S, Lamparter M, et al. Multistep nature of microvascular recruitment of ex vivo-expanded embryonic endothelial progenitor cells during tumor angiogenesis. J Exp Med 2003;197:1755-65.
70. Li S, Tokuyama T, Yamamoto J, Koide M, Yokota N, Namba H. Bystander effect-mediated gene therapy of gliomas using genetically engineered neural stem cells. Cancer Gene Ther 2005;12:600-7.
71. van Eekelen M, Sasportas LS, Kasmieh R, et al. Human stem cells expressing novel TSP-1 variant have anti-angiogenic effect on brain tumors. Oncogene 2010;29:3185-95.
72. Tyler MA, Ulasov IV, Sonabend AM, et al. Neural stem cells target intracranial glioma to deliver an oncolytic adenovirus in vivo. Gene Ther 2009;16:262-78.
73. Li S, Gao Y, Tokuyama T, et al. Genetically engineered neural stem cells migrate and suppress glioma cell growth at distant intracranial sites. Cancer Lett 2007;251:220-7.
74. De Palma M, Naldini L. Role of haematopoietic cells and endothelial progenitors in tumour angiogenesis. Biochim Biophys Acta 2006;1766:159-66.
75. Ljungman P, Bregni M, Brune M, et al. Allogeneic and autologous transplantation for haematological diseases, solid tumours and immune disorders: current practice in Europe 2009. Bone Marrow Transplant 2010;45:219-34.
76. Wei J, Wahl J, Nakamura T, et al. Targeted release of oncolytic measles virus by blood outgrowth endothelial cells in situ inhibits orthotopic gliomas. Gene Ther 2007;14:1573-86.
77. Takahashi K, Yamanaka S. Induction of pluripotent stem cells from mouse embryonic and adult fibroblast cultures by defined factors. Cell 2006;126:663-76.
78. Cai W, Zhang Y, Kamp TJ. Imaging of Induced Pluripotent Stem Cells: From Cellular Reprogramming to Transplantation. Am J Nucl Med Mol Imaging 2011;1:18-28.
79. Li HY, Chien Y, Chen YJ, et al. Reprogramming induced pluripotent stem cells in the absence of c-Myc for differentiation into hepatocyte-like cells. Biomaterials 2011;32:5994-6005.
80. Herberts CA, Kwa MS, Hermsen HP. Risk factors in the development of stem cell therapy. J Transl Med 2011;9:29.
81. Vaananen HK. Mesenchymal stem cells. Ann Med 2005;37:469-79.
82. Pittenger MF, Mackay AM, Beck SC, et al. Multilineage potential of adult human mesenchymal stem cells. Science 1999;284:143-7.
83. Jiang Y, Jahagirdar BN, Reinhardt RL, et al. Pluripotency of mesenchymal stem cells derived from adult marrow. Nature 2002;418:41-9.
84. Nauta AJ, Fibbe WE. Immunomodulatory properties of mesenchymal stromal cells. Blood 2007;110:3499-506.
85. Myers TJ, Granero-Molto F, Longobardi L, Li T, Yan Y, Spagnoli A. Mesenchymal stem cells at the intersection of cell and gene therapy. Expert Opin Biol Ther 2010;10:1663-79.
86. Dominici M, Le Blanc K, Mueller I, et al. Minimal criteria for defining multipotent mesenchymal stromal cells. The International Society for Cellular Therapy position statement. Cytotherapy 2006;8:315-7.
87. Maria OM, Khosravi R, Mezey E, Tran SD. Cells from bone marrow that evolve into oral tissues and their clinical applications. Oral Dis 2007;13:11-6.
88. Salem HK, Thiemermann C. Mesenchymal stromal cells: current understanding and clinical status. Stem Cells 2010;28:585-96.
89. Song L, Tuan RS. Transdifferentiation potential of human mesenchymal stem cells derived from bone marrow. FASEB J 2004;18:980-2.
90. Nakamura K, Ito Y, Kawano Y, et al. Antitumor effect of genetically engineered mesenchymal stem cells in a rat glioma model. Gene Ther 2004;11:1155-64.
91. Lee DH, Ahn Y, Kim SU, et al. Targeting rat brainstem glioma using human neural stem cells and human mesenchymal stem cells. Clin Cancer Res 2009;15:4925-34.

92. Yong RL, Shinojima N, Fueyo J, et al. Human bone marrow-derived mesenchymal stem cells for intravascular delivery of oncolytic adenovirus Delta24-RGD to human gliomas. Cancer Res 2009;69:8932-40.
93. Amano S, Li S, Gu C, et al. Use of genetically engineered bone marrow-derived mesenchymal stem cells for glioma gene therapy. Int J Oncol 2009;35:1265-70.
94. Zuk PA, Zhu M, Mizuno H, et al. Multilineage cells from human adipose tissue: implications for cell-based therapies. Tissue Eng 2001;7:211-28.
95. Izadpanah R, Trygg C, Patel B, et al. Biologic properties of mesenchymal stem cells derived from bone marrow and adipose tissue. J Cell Biochem 2006;99:1285-97.
96. Kern S, Eichler H, Stoeve J, Kluter H, Bieback K. Comparative analysis of mesenchymal stem cells from bone marrow, umbilical cord blood, or adipose tissue. Stem Cells 2006;24:1294-301.
97. Zuk PA. The adipose-derived stem cell: looking back and looking ahead. Mol Biol Cell 2010;21:1783-7.
98. Gimble JM, Katz AJ, Bunnell BA. Adipose-derived stem cells for regenerative medicine. Circ Res 2007;100:1249-60.
99. McIntosh K, Zvonic S, Garrett S, et al. The immunogenicity of human adipose-derived cells: temporal changes in vitro. Stem Cells 2006;24:1246-53.
100. Zimmerlin L, Donnenberg VS, Pfeifer ME, et al. Stromal vascular progenitors in adult human adipose tissue. Cytometry A 2010;77:22-30.
101. Traktuev DO, Merfeld-Clauss S, Li J, et al. A population of multipotent CD34-positive adipose stromal cells share pericyte and mesenchymal surface markers, reside in a periendothelial location, and stabilize endothelial networks. Circ Res 2008;102:77-85.
102. Gronthos S, Franklin DM, Leddy HA, Robey PG, Storms RW, Gimble JM. Surface protein characterization of human adipose tissue-derived stromal cells. J Cell Physiol 2001;189:54-63.
103. Chen CW, Montelatici E, Crisan M, et al. Perivascular multi-lineage progenitor cells in human organs: regenerative units, cytokine sources or both? Cytokine Growth Factor Rev 2009;20:429-34.
104. Tobita M, Orbay H, Mizuno H. Adipose-derived stem cells: current findings and future perspectives. Discov Med 2011;11:160-70.
105. Bertolini F, Shaked Y, Mancuso P, Kerbel RS. The multifaceted circulating endothelial cell in cancer: towards marker and target identification. Nat Rev Cancer 2006;6:835-45.
106. Hall B, Dembinski J, Sasser AK, Studeny M, Andreeff M, Marini F. Mesenchymal stem cells in cancer: tumor-associated fibroblasts and cell-based delivery vehicles. Int J Hematol 2007;86:8-16.
107. Zhang Y, Daquinag A, Traktuev DO, et al. White adipose tissue cells are recruited by experimental tumors and promote cancer progression in mouse models. Cancer Res 2009;69:5259-66.
108. Cavarretta IT, Altanerova V, Matuskova M, Kucerova L, Culig Z, Altaner C. Adipose tissue-derived mesenchymal stem cells expressing prodrug-converting enzyme inhibit human prostate tumor growth. Mol Ther 2010;18:223-31.
109. Lamfers M, Idema S, van Milligen F, et al. Homing properties of adipose-derived stem cells to intracerebral glioma and the effects of adenovirus infection. Cancer Lett 2009;274:78-87.
110. Zhang Y, Bellows CF, Kolonin MG. Adipose tissue-derived progenitor cells and cancer. World J Stem Cells 2010;2:103-13.
111. Choi SA, Lee JY, Wang KC, et al. Human adipose tissue-derived mesenchymal stem cells: characteristics and therapeutic potential as cellular vehicles for prodrug gene therapy against brainstem gliomas. Eur J Cancer 2012;48:129-37.
112. Choi SA, Hwang SK, Wang KC, et al. Therapeutic efficacy and safety of TRAIL-producing human adipose tissue-derived mesenchymal stem cells against experimental brainstem glioma. Neuro Oncol 2011;13:61-9.

113. Altanerova V, Cihova M, Babic M, et al. Human adipose tissue-derived mesenchymal stem cells expressing yeast cytosinedeaminase::uracil phosphoribosyltransferase inhibit intracerebral rat glioblastoma. Int J Cancer 2011.
114. Seth P. Vector-mediated cancer gene therapy: an overview. Cancer Biol Ther 2005;4:512-7.
115. Portsmouth D, Hlavaty J, Renner M. Suicide genes for cancer therapy. Mol Aspects Med 2007;28:4-41.
116. Saukkonen K, Hemminki A. Tissue-specific promoters for cancer gene therapy. Expert Opin Biol Ther 2004;4:683-96.
117. Yakkundi A, McErlane V, Murray M, et al. Tumor-selective drug activation: a GDEPT approach utilizing cytochrome P450 1A1 and AQ4N. Cancer Gene Ther 2006;13:598-605.
118. Dachs GU, Hunt MA, Syddall S, Singleton DC, Patterson AV. Bystander or no bystander for gene directed enzyme prodrug therapy. Molecules 2009;14:4517-45.
119. Dilber MS, Abedi MR, Christensson B, et al. Gap junctions promote the bystander effect of herpes simplex virus thymidine kinase in vivo. Cancer Res 1997;57:1523-8.
120. Fick J, Barker FG, 2nd, Dazin P, Westphale EM, Beyer EC, Israel MA. The extent of heterocellular communication mediated by gap junctions is predictive of bystander tumor cytotoxicity in vitro. Proc Natl Acad Sci U S A 1995;92:11071-5.
121. Yamasaki H, Enomoto K, Fitzgerald DJ, Mesnil M, Katoh F, Hollstein M. Role of intercellular communication in the control of critical gene expression during multistage carcinogenesis. IARC Sci Publ 1988:57-75.
122. Kianmanesh AR, Perrin H, Panis Y, et al. A "distant" bystander effect of suicide gene therapy: regression of nontransduced tumors together with a distant transduced tumor. Hum Gene Ther 1997;8:1807-14.
123. Pierrefite-Carle V, Baque P, Gavelli A, et al. Cytosine deaminase/5-fluorocytosine-based vaccination against liver tumors: evidence of distant bystander effect. J Natl Cancer Inst 1999;91:2014-9.
124. Freeman SM, Abboud CN, Whartenby KA, et al. The "bystander effect": tumor regression when a fraction of the tumor mass is genetically modified. Cancer Res 1993;53:5274-83.
125. Moolten FL. Tumor chemosensitivity conferred by inserted herpes thymidine kinase genes: paradigm for a prospective cancer control strategy. Cancer Res 1986;46:5276-81.
126. Chen SH, Pearson A, Coen DM. Failure of thymidine kinase-negative herpes simplex virus to reactivate from latency following efficient establishment. J Virol 2004;78:520-3.
127. Fillat C, Carrio M, Cascante A, Sangro B. Suicide gene therapy mediated by the Herpes Simplex virus thymidine kinase gene/Ganciclovir system: fifteen years of application. Curr Gene Ther 2003;3:13-26.
128. Balzarini J, Bohman C, De Clercq E. Differential mechanism of cytostatic effect of (E)-5-(2-bromovinyl)-2'-deoxyuridine, 9-(1,3-dihydroxy-2-propoxymethyl)guanine, and other antiherpetic drugs on tumor cells transfected by the thymidine kinase gene of herpes simplex virus type 1 or type 2. J Biol Chem 1993;268:6332-7.
129. Asklund T, Appelskog IB, Ammerpohl O, et al. Gap junction-mediated bystander effect in primary cultures of human malignant gliomas with recombinant expression of the HSVtk gene. Exp Cell Res 2003;284:185-95.
130. Black ME, Newcomb TG, Wilson HM, Loeb LA. Creation of drug-specific herpes simplex virus type 1 thymidine kinase mutants for gene therapy. Proc Natl Acad Sci U S A 1996;93:3525-9.
131. Gambhir SS, Bauer E, Black ME, et al. A mutant herpes simplex virus type 1 thymidine kinase reporter gene shows improved sensitivity for imaging reporter gene expression with positron emission tomography. Proc Natl Acad Sci U S A 2000;97:2785-90.

132. Black ME, Kokoris MS, Sabo P. Herpes simplex virus-1 thymidine kinase mutants created by semi-random sequence mutagenesis improve prodrug-mediated tumor cell killing. Cancer Res 2001;61:3022-6.
133. Ray P, De A, Min JJ, Tsien RY, Gambhir SS. Imaging tri-fusion multimodality reporter gene expression in living subjects. Cancer Res 2004;64:1323-30.
134. Cao F, Lin S, Xie X, et al. In vivo visualization of embryonic stem cell survival, proliferation, and migration after cardiac delivery. Circulation 2006;113:1005-14.
135. Condeelis J, Weissleder R. In vivo imaging in cancer. Cold Spring Harbor perspectives in biology 2010;2:a003848.
136. Weissleder R, Pittet MJ. Imaging in the era of molecular oncology. Nature 2008;452:580-9.
137. Blasberg RG. In vivo molecular-genetic imaging: multi-modality nuclear and optical combinations. Nucl Med Biol 2003;30:879-88.
138. Bowie LJ, Irwin R, Loken M, De Luca M, Brand L. Excited-state proton transfer and the mechanism of action of firefly luciferase. Biochemistry 1973;12:1852-7.
139. Rice BW, Cable MD, Nelson MB. In vivo imaging of light-emitting probes. J Biomed Opt 2001;6:432-40.
140. Contag CH, Spilman SD, Contag PR, et al. Visualizing gene expression in living mammals using a bioluminescent reporter. Photochem Photobiol 1997;66:523-31.
141. Costa GL, Sandora MR, Nakajima A, et al. Adoptive immunotherapy of experimental autoimmune encephalomyelitis via T cell delivery of the IL-12 p40 subunit. J Immunol 2001;167:2379-87.
142. Contag CH, Contag PR, Mullins JI, Spilman SD, Stevenson DK, Benaron DA. Photonic detection of bacterial pathogens in living hosts. Mol Microbiol 1995;18:593-603.
143. Greer LF, 3rd, Szalay AA. Imaging of light emission from the expression of luciferases in living cells and organisms: a review. Luminescence 2002;17:43-74.
144. de Wet JR, Wood KV, Helinski DR, DeLuca M. Cloning of firefly luciferase cDNA and the expression of active luciferase in Escherichia coli. Proc Natl Acad Sci U S A 1985;82:7870-3.
145. Wu JC, Sundaresan G, Iyer M, Gambhir SS. Noninvasive optical imaging of firefly luciferase reporter gene expression in skeletal muscles of living mice. Mol Ther 2001;4:297-306.
146. Hastings JW. Chemistries and colors of bioluminescent reactions: a review. Gene 1996;173:5-11.
147. Lorenz WW, McCann RO, Longiaru M, Cormier MJ. Isolation and expression of a cDNA encoding Renilla reniformis luciferase. Proc Natl Acad Sci U S A 1991;88:4438-42.
148. Bhaumik S, Gambhir SS. Optical imaging of Renilla luciferase reporter gene expression in living mice. Proc Natl Acad Sci U S A 2002;99:377-82.
149. Loening AM, Wu AM, Gambhir SS. Red-shifted Renilla reniformis luciferase variants for imaging in living subjects. Nat Methods 2007;4:641-3.
150. Celia-Terrassa T, Meca-Cortes O, Mateo F, et al. Epithelial-mesenchymal transition can suppress major attributes of human epithelial tumor-initiating cells. The Journal of clinical investigation 2012;122:1849-68.
151. Hosseinkhani S. Molecular enigma of multicolor bioluminescence of firefly luciferase. Cell Mol Life Sci 2011;68:1167-82.
152. Vilalta M, Degano IR, Bago J, et al. Human adipose tissue-derived mesenchymal stromal cells as vehicles for tumor bystander effect: a model based on bioluminescence imaging. Gene therapy 2009;16:547-57.
153. El Hilali N, Rubio N, Blanco J. Noninvasive in vivo whole body luminescent analysis of luciferase labelled orthotopic prostate tumours. Eur J Cancer 2004;40:2851-8.
154. Vilalta M, Jorgensen C, Degano IR, et al. Dual luciferase labelling for non-invasive bioluminescence imaging of mesenchymal stromal cell chondrogenic differentiation in demineralized bone matrix scaffolds. Biomaterials 2009;30:4986-95.

155. Bago JR, Aguilar E, Alieva M, et al. In vivo bioluminescence imaging of cell differentiation in biomaterials: a platform for scaffold development. Tissue engineering Part A 2012.
156. Benaron DA, Cheong WF, Stevenson DK. Tissue optics. Science 1997;276:2002-3.
157. Dothager RS, Flentie K, Moss B, Pan MH, Kesarwala A, Piwnica-Worms D. Advances in bioluminescence imaging of live animal models. Curr Opin Biotechnol 2009;20:45-53.
158. Abdelwahab MG, Sankar T, Preul MC, Scheck AC. Intracranial implantation with subsequent 3D in vivo bioluminescent imaging of murine gliomas. Journal of visualized experiments : JoVE 2011:e3403.
159. Rome C, Couillaud F, Moonen CT. Gene expression and gene therapy imaging. Eur Radiol 2007;17:305-19.
160. Sanz L, Santos-Valle P, Alonso-Camino V, et al. Long-term in vivo imaging of human angiogenesis: critical role of bone marrow-derived mesenchymal stem cells for the generation of durable blood vessels. Microvascular research 2008;75:308-14.
161. Livak KJ, Schmittgen TD. Analysis of relative gene expression data using real-time quantitative PCR and the 2(-Delta Delta C(T)) Method. Methods 2001;25:402-8.
162. Pfeifer A, Ikawa M, Dayn Y, Verma IM. Transgenesis by lentiviral vectors: lack of gene silencing in mammalian embryonic stem cells and preimplantation embryos. Proc Natl Acad Sci U S A 2002;99:2140-5.
163. van der Bogt KE, Schrepfer S, Yu J, et al. Comparison of transplantation of adipose tissue- and bone marrow-derived mesenchymal stem cells in the infarcted heart. Transplantation 2009;87:642-52.
164. Xu J, Liu X, Chen J, et al. Simvastatin enhances bone marrow stromal cell differentiation into endothelial cells via notch signaling pathway. Am J Physiol Cell Physiol 2009;296:C535-43.
165. Bexell D, Gunnarsson S, Tormin A, et al. Bone marrow multipotent mesenchymal stroma cells act as pericyte-like migratory vehicles in experimental gliomas. Mol Ther 2009;17:183-90.
166. Altaner C. Prodrug cancer gene therapy. Cancer Lett 2008;270:191-201.
167. Menon LG, Kelly K, Wei Yang H, Kim SK, Black PM, Carroll RS. Human Bone Marrow Derived Mesenchymal Stromal Cells Expressing S-TRAIL as a Cellular Delivery Vehicle for Human Glioma Therapy. Stem cells (Dayton, Ohio) 2009.
168. Caruso M, Panis Y, Gagandeep S, Houssin D, Salzmann JL, Klatzmann D. Regression of established macroscopic liver metastases after in situ transduction of a suicide gene. Proceedings of the National Academy of Sciences of the United States of America 1993;90:7024-8.
169. Sangro B, Mazzolini G, Ruiz M, et al. A phase I clinical trial of thymidine kinase-based gene therapy in advanced hepatocellular carcinoma. Cancer Gene Ther 2010;17:837-43.
170. Huang Q, Pu P, Xia Z, You Y. Exogenous wt-p53 enhances the antitumor effect of HSV-TK/GCV on C6 glioma cells. J Neurooncol 2007;82:239-48.
171. Hwang do W, Jang SJ, Kim YH, et al. Real-time in vivo monitoring of viable stem cells implanted on biocompatible scaffolds. Eur J Nucl Med Mol Imaging 2008;35:1887-98.
172. Ziane S, Schlaubitz S, Miraux S, et al. A thermosensitive low molecular weight hydrogel as scaffold for tissue engineering. Eur Cell Mater 2012;23:147-60; discussion 60.
173. Vilalta M, Degano IR, Bago J, et al. Biodistribution, long-term survival, and safety of human adipose tissue-derived mesenchymal stem cells transplanted in nude mice by high sensitivity non-invasive bioluminescence imaging. Stem Cells Dev 2008;17:993-1003.
174. Bexell D, Scheding S, Bengzon J. Toward brain tumor gene therapy using multipotent mesenchymal stromal cell vectors. Mol Ther 2010;18:1067-75.
175. Nakanishi C, Nagaya N, Ohnishi S, et al. Gene and Protein Expression Analysis of Mesenchymal Stem Cells Derived From Rat Adipose Tissue and Bone Marrow. Circ J 2011.
176. Krebs LT, Xue Y, Norton CR, et al. Notch signaling is essential for vascular morphogenesis in mice. Genes Dev 2000;14:1343-52.

177. Limbourg FP, Takeshita K, Radtke F, Bronson RT, Chin MT, Liao JK. Essential role of endothelial Notch1 in angiogenesis. Circulation 2005;111:1826-32.
178. Yurugi-Kobayashi T, Itoh H, Schroeder T, et al. Adrenomedullin/cyclic AMP pathway induces Notch activation and differentiation of arterial endothelial cells from vascular progenitors. Arterioscler Thromb Vasc Biol 2006;26:1977-84.
179. Ribeiro MJ, Phillips DJ, Benson JM, Evatt BL, Ades EW, Hooper WC. Hemostatic properties of the SV-40 transfected human microvascular endothelial cell line (HMEC-1). A representative in vitro model for microvascular endothelium. Thromb Res 1995;79:153-61.
180. Shao R, Bao S, Bai X, et al. Acquired expression of periostin by human breast cancers promotes tumor angiogenesis through up-regulation of vascular endothelial growth factor receptor 2 expression. Mol Cell Biol 2004;24:3992-4003.
181. Zhu W, Xu W, Jiang R, et al. Mesenchymal stem cells derived from bone marrow favor tumor cell growth in vivo. Exp Mol Pathol 2006;80:267-74.
182. Kucerova L, Matuskova M, Hlubinova K, Altanerova V, Altaner C. Tumor cell behaviour modulation by mesenchymal stromal cells. Mol Cancer 2010;9:129.
183. Dong J, Huang Q. Targeting glioma stem cells: enough to terminate gliomagenesis? Chin Med J (Engl) 2011;124:2756-63.
184. Studeny M, Marini FC, Champlin RE, Zompetta C, Fidler IJ, Andreeff M. Bone marrow-derived mesenchymal stem cells as vehicles for interferon-beta delivery into tumors. Cancer Res 2002;62:3603-8.
185. Korbling M, Estrov Z. Adult stem cells for tissue repair - a new therapeutic concept? N Engl J Med 2003;349:570-82.
186. Farin A, Suzuki SO, Weiker M, Goldman JE, Bruce JN, Canoll P. Transplanted glioma cells migrate and proliferate on host brain vasculature: a dynamic analysis. Glia 2006;53:799-808.
187. Liu D, Martin V, Fueyo J, et al. Tie2/TEK modulates the interaction of glioma and brain tumor stem cells with endothelial cells and promotes an invasive phenotype. Oncotarget 2010;1:700-9.
188. Li Y, Hiroi Y, Ngoy S, et al. Notch1 in bone marrow-derived cells mediates cardiac repair after myocardial infarction. Circulation 2011;123:866-76.

ANNEX

1 RESUMEN DE LA TESIS EN CASTELLANO

INTRODUCCION

Los tumores primarios cerebrales más comunes, como glioblastomas y astrocitomas anaplasticos, representan el 2 % de todos los cánceres, pero presentan una tasa desproporcionada de morbilidad y mortalidad. La supervivencia media de un paciente diagnosticado con un tumor cerebral es de 3 años, y sólo el 2 % de los pacientes sobrevive hasta los 5 años. Los protocolos de tratamiento actuales incluyen la resección quirúrgica del tumor sólido, evitando el daño neurológico. Después de la cirugía, normalmente se usan la quimioterapia local o sistémica y la radioterapia. Sin embargo debido al comportamiento infiltrativo de los gliomas y la capacidad de difusión limitada de los agentes quimioterapéuticos estos pasos no son suficientes para frenar la proliferación de las células malignas.

En los últimos años se ha sugerido una nueva estrategia basada en la trasmisión génica mediante células estromales. Se ha descrito que debido a la capacidad de migración hacia los tumores de las células estromales, estas podrían ser usadas para transportar agentes citotóxicos a la zona tumoral produciendo un potente efecto adyacente. Las células estromales mesenquimales humanas del tejido adiposo (hAMSCs) presentan varias ventajas para esta clase de terapia citadas a continuación: son fáciles de obtener y expandir, forman parte del estroma de diferentes tumores, su capacidad de migración hacia tumores ha sido demostrada; las hAMSCs pueden ser modificadas genéticamente con relativa facilidad, tienen la capacidad de inhibir reacciones inmunes e inflamatorias y no generan tumores cuando son implantadas durante largos períodos de tiempo. Por otro lado, también debe considerarse la capacidad de las hAMSCs para la modulación del crecimiento del tumor.

Agentes citotóxicos

Las estrategias citotóxicas dirigidas, desarrolladas durante los últimos 20 años, se basan en la conversión de un profármaco de baja toxicidad, administrado sistémicamente, en una sustancia citotóxica que se libera en la proximidad del tumor Esta conversión es resultado de la acción de un enzima activador específico, que se ha

introducido en las células terapéuticas. La difusión del agente citotóxico a través del medio extracelular o directamente a las células contiguas, mediante uniones GAP y/u otros mecanismos, provoca la muerte de las células vecinas, estimulando el sistema inmune y produciendo una amplificación del fenómeno denominado: efecto adyacente. Se han estudiado y desarrollado diversos pares enzima activadora-profármaco, entre ellos la Timidina quinasa del virus Herpes simplex (HSV-TK).

Timidina quinasa del virus herpes simplex

La timidina quinasa codificada por el virus del herpes simplex es responsable de la conversión de la deoxitimidina en deoxitimidina monofosfato. El enzima tiene capacidad de fosforilar múltiples derivados de nucleósidos. La activación del análogo 9-([2-hidroxi-1-hidroximetil)epoxi]metil) guanina (GCV) por la HSV-TK fue la primera demostración de principio de terapia génica suicida y sigue siendo uno de los sistemas más ampliamente utilizados en aplicaciones clínicas y experimentales. El efecto terapéutico se basa en la afinidad 1000 veces superior del enzima vírico por el análogo GCV que la de la timidina kinasa de mamífero. Se produce un efecto citotóxico a través de la inhibición de las ADN polimerasas celulares y por la competición con la deoxiguanosina trifosfato, resultando en su incorporación en la cadena de ADN y la generación de rupturas de la cadena y la muerte celular. El GCV es muy difusible, mientras que su fosfato no lo es y depende principalmente de las uniones GAP y vesículas apoptóticas producidas por las células afectadas para su difusión intercelular. La HSV-TK se ha utilizado en el tratamiento de gliomas con incrementos significativos de la supervivencia de los pacientes.

Imagen fotónica no invasiva

Las luciferasas catalizan la oxidación de sus sustratos (luciferinas) en presencia, generalmente, de ATP y oxígeno, generando fotones de luz y oxiluciferina. Los fotones de luciferasa generados en homogeneizados de tejidos, desprovistos de reacciones luminiscentes endógenas, se pueden cuantificar fácilmente con un luminómetro. Propiamente, estos instrumentos tienen una alta sensibilidad, responden linealmente en un rango de seis o más órdenes de magnitud y están idealmente adaptados para la medición de la actividad de luciferasa *in vitro*.

A pesar de la aparente opacidad de los tejidos, la luz se puede utilizar para examinar las funciones fisiológicas y las estructuras a varios milímetros de profundidad en animales vivos. Así, se pueden generar imágenes de tumores utilizando fotones generados por células marcadas para la expresión de luciferasas. La luz producida por estas células ha sido utilizada para monitorizar de forma no invasiva la expresión de genes en los tejidos de diversos animales vivos. En ratones, la luciferasa se ha utilizado para reportar la actividad del promotor del virus de la inmunodeficiencia humana y para estudiar la velocidad de desaparición de tumores durante el tratamiento con fármacos. También se ha utilizado una estrategia videométrica-luminométrica combinada para monitorizar el desarrollo de tumores prostáticos humanos y sus metástasis en ratones inmunodeprimidos, para seguir células progenitoras mesenquimales y neuronales. Nuestro grupo ha puesto a punto una estrategia de marcaje celular con varios tipos de luciferasas que permite seguir simultáneamente varias poblaciones celulares diferentes o seguir, en una sola población celular, el comportamiento proliferativo y la diferenciación celular.

OBJETIVOS

El objetivo principal de esta tesis ha sido desarrollar y monitorizar *in vivo* una terapia citotóxica en un modelo murino para el tratamiento del glioblastoma multiforme. Para cumplir con este objetivo, los siguientes objetivos fueron planteados:

Desarrollo de un sistema que permita evaluar el crecimiento tumoral y la eficacia de la terapia in vivo

I. Generar células tumorales y terapéuticas que expresen marcadores bioluminiscentes y fluorescentes para monitorizar de forma no invasiva la respuesta de estas células.
II. Desarrollo de un modelo de terapia contra gliomas basado en la implantación intracerebral de las células tumorales y terapéuticas en ratones SCID.

Optimizacion del modelo de terapia

III. Optimización del sistema de imagen bioluminiscente para monitorizar la respuesta celular de forma no invasiva.
IV. Optimización de la distribución del agente citotóxico.

Estudio del mecanismo terapéutico

V. Análisis de la diferenciación de las células terapéuticas en el microentorno tumoral.
VI. Estudio de la interacción de las células terapéuticas y tumorales.
VII. Evaluación de la capacidad migratoria de las células tumorales y terapéuticas.

RESULTADOS

Expresión de fotoproteínas por las hAMSC y las U87

Para seguir de forma no invasiva el comportamiento de las células tumorales y terapéuticas durante la terapia, las hAMSCs fueron modificadas genéticamente mediante la transducción con vectores lentivíricos para la expresión estable de un reportero tri-funcional quimérico que incluía la *Renilla luciferasa* (Rluc), la RFP y la tTK, para dar lugar a RL-R-tTK-HAMSC o “vehículos terapéuticos". Las células U87 de glioblastoma humano también fueron modificadas genéticamente mediante la transducción con un vector lentivírico para la expresión estable de un reportero quimérico con *Photynus pyralis* (Pluc) y la eGFP, dando lugar a células tumorales "PL-G-U87". Esta estrategia permitió un seguimiento independiente de las células terapéuticas y tumorales debido al uso de sustratos de luciferasa que no tenían actividad cruzada, coelenterazina y luciferina, respectivamente. Además, la inclusión de dos reporteros fluorescentes diferentes, permite la selección de las células marcadas por FACS, y la detección de las células terapéuticas y tumorales en secciones de tejido por microscopía confocal de fluorescencia. La transducción lentiviral no cambió el tiempo de duplicación ni el immunofenotipo de las RL-R-tTK-hAMSCS, como ha sido determinado por citometría de flujo y análisis de marcadores de las hAMSC.

Muerte de las células de glioblastoma PL-G-U87 mediada por RL-R-TTK-HAMSC in vitro

Para demostrar que el gen tTK era funcional en los vehículos terapéuticos genéticamente modificados, se sembraron triplicados de PL-G-U87, hAMSCs y RL-R-tTK-hAMSCS en placas de cultivo y fueron tratados con ganciclovir (GCV) o PBS y la supervivencia de las células fue evaluada usando el *CellTiter 96 Aqueous One Solution Cell Proliferation Assay*. El tratamiento con GCV no tenía ningún efecto sobre la supervivencia de las PL-G-U87 solas o sobre las hAMSCs que carecían del gen tTK. Además, en ausencia de GCV el patrón de crecimiento de las hAMSCs era similar independientemente de si expresaban o no el gen tTK, indicando que el gen tTK no tenía ningún efecto negativo sobre la proliferación de las células. Sin embargo, como era de esperar, el tratamiento con GCV realmente ejerció un efecto citotóxico fuerte sobre las RL-R-tTK-hAMSCS, proporcional a la concentración de GCV.

En un experimento diferente quisimos evaluar el efecto adyacente, para ello se sembraron cocultivos de células terapéuticos y tumorales que expresan luciferasas en diferentes proporciones (1:20, 2:20, 4:20) RL-R-tTK-hAMSC:PL-G-U87 y se trataron con GCV (4 µg/ml) o PBS. En estos experimentos, donde el tumor y células terapéuticas expresan reporteros de luciferasa, la supervivencia de las células PL-G-U87 fue evaluada por bioluminiscencia (BLI).

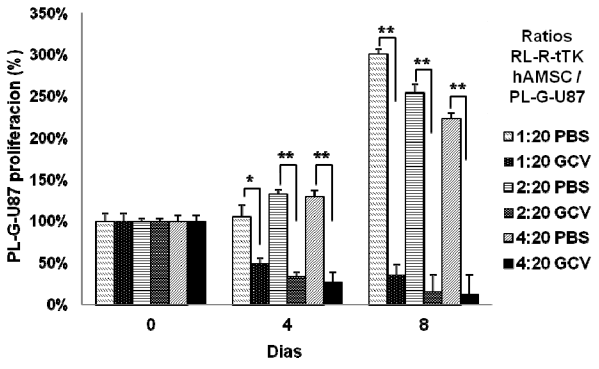

Figura 1. RL-R-TK-AMSC muestran un efecto adyacente citotoxico sobre PL-G-U87. Los cocultivos de RL-R-tTK-hAMSC:PL-G-U87 en las proporciones 1:20; 2:20; 4:20 se trataron con GCV o PBS. La viabilidad de las PL-G-U87 está afectada de forma proporcional a la cantidad de RL-R-tTK-hAMSC. Los datos se muestran como media± SEM.

Como se muestra en la Fig 1, la viabilidad de las células PL-G-U87 en presencia de GCV era inversamente proporcional a la proporción de células terapéuticas respecto a tumorales (88%, 93%, 94% de muerte celular para 1:20, 2:20, 4:20 RL-R-tTK-hAMSC:PL-G-U87), pero no fue afectada por el tratamiento con PBS (*p <0,05; ** p> 0,01).

Sensibilidad de detección de PL-G-U87 y RL-R-TK-AMSC in vivo

En animales vivos el hueso del cráneo y el tejido cerebral reducen la eficacia con la cual los fotones de luz alcanzan el detector de la cámara de vídeo usada para BLI. Para establecer una correlación entre medidas de luz y el número de células, un número predeterminado de PL-G-U87 y RL-R-TK-AMSC fue implantado en el cerebro de ratones vivos en coordenadas específicas (0,6 mm posterior, 2 mm lateral y 2,75 mm de profundidad respeto a Bregma). Inmediatamente después de la implantación se tomaron imágenes por BLI, después de la administración del sustrato de luciferasa correspondiente, luciferina o coelenterazina. El número de fotones registrados (PHCs) fue extraído de las imágenes registradas y representado, después de la substracción de fondo, respecto al número de células inoculadas. La sensibilidad de detección (la curva de correlación) era similar para ambos tipos celulares y también había una buena correlación lineal entre la cantidad de luz producida y el número de células implantadas, 34,2 PHCs /célula, R2 = 0,994 y 20,64 PHCs /célula, R2 = 0,974 para PL-G-U87 y RL-R-TK-AMSC, respectivamente.

Dosis optima de RL-R-TK-AMSC para un efecto adyacente eficiente

Mezclas de poblaciones celulares que comprendían células PL-G-U87 ($4x10^4$) con diferentes proporciones de RL-R-TK-AMSC (1:1, 1:2, 1:4) respectivamente fueron usadas para generar tumores cerebrales mediante la inyección en el cerebro de ratones SCID, en las coordenadas indicadas previamente (n=15). Dos grupos control (n=10), también fueron incluidos: en uno de ellos solo se inyectó $4x10^4$ PL-G-U87; y en el otro se inyectó el mismo número de células PL-G-U87 en una proporción 1:1 con RL-R-TK-AMSC. Seis días después de la implantación, y durante un período de un 35 día, los ratones inoculados fueron tratados diariamente por inyección intraperitoneal (ip) de GCV o PBS. La emisión de luz por la luciferasa Pluc fue evaluada por BLI desde el primer dia de tratamiento con GCV (T=0) y cada semana a partir de entonces. El análisis cuantitativo de los fotones detectados en las imágenes mostró (Fig 2) que el tratamiento con GCV de tumores que llevan células terapéuticas inhibe el crecimiento del tumor.

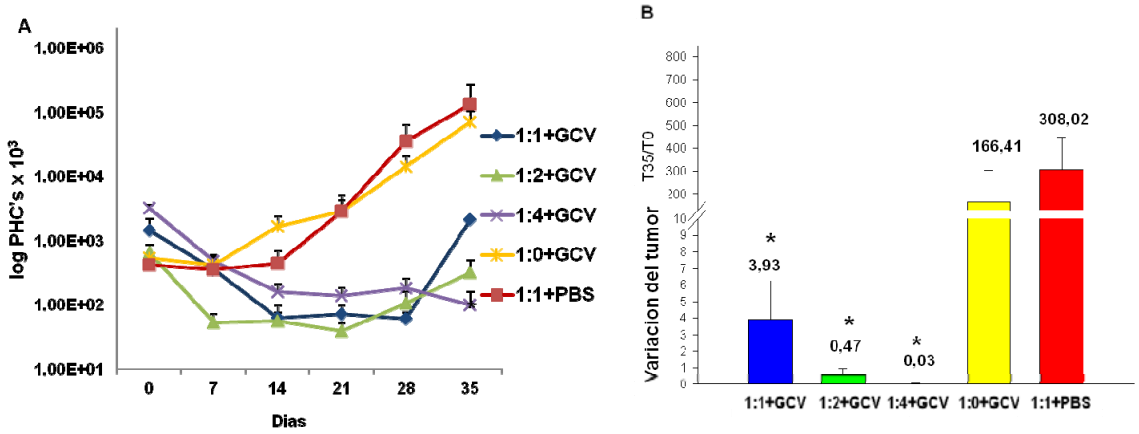

Figura 2. Optimización in vivo de la proporción de PL-G-U87 tumorales respecto a RL-R-TK-AMSC terapéuticas para un efecto adyacente eficaz. (a) Cambio de la producción de luz *in vivo* por las células tumorales que expresan Pluc como resultado del tratamiento con GCV. (b) Valores de PHC al final del experimento (T=35) fueron normalizados en relación con aquellos en T=0 según la fórmula [(T5/T0) x 100 = variación de tumor (el %)]. Los datos se muestran como media±SEM, *P <0.05, comparados al grupo 1:0+GCV , n=5 para cada grupo.

Se detectó una inhibición del crecimiento del tumor desde el inicio del tratamiento Además, el efecto terapéutico estaba directamente correlacionado con la proporción de células terapéuticas, siendo 1:4 la dosis más eficaz (Fig 2b). En este grupo de ratones, hacia el final del experimento (T=35) la cantidad de luz producida por los tumores era 10^4 veces más baja que la producida por el grupo control (PL-G-U87 sólo) (p <0,05), y sólo el 3 % de luz producida por la células de tumor detectadas a T=0 permaneció en el sitio de inoculación.

Terapia contra el glioblastoma mediada in vivo por el efecto adyacente de las RL-R-TK-AMSC

A un grupo de 24 ratones SCID ratones de 6 semanas se les inoculó estéreotácticamente en las coordenadas antes indicadas con una mezcla de $4x10^4$ PL-G-U87 y $1.6x10^5$ RL-R-tTK-hAMSCs (n=16) o solo con $4x10^4$ PL-G-U87 (n=8). Se inició un régimen de tratamiento con GCV y se siguió la evolución celular mediante BLI como está descrito en el diagrama de la Fig 3A. La mitad de los ratones implantados con PL-

G-U87 y células RL-R-tTK-hAMSCs recibió GCV, mientras la otra mitad recibió el mismo volumen de PBS. Los ratones implantados sólo con PL-G-U87 también recibieron GCV.

Como está indicado en la Fig 3B, que muestra imágenes representativas tomadas por BLI de animales de cada uno de los grupos experimentales, el tratamiento con PBS de tumores mezclados con células terapéuticas, o de los tumores control (sin células terapéuticas) con GCV, no tuvo ningún efecto inhibitorio sobre el crecimiento de tumor, y la producción de luz por las PL-G-U87 se fue incrementando hasta el final del experimento. Sin embargo, el tratamiento de los tumores mezclados con RL-R-tTK-hAMSCs con GCV produjo la reducción progresiva de luz producida por PL-G-U87 hasta el final del experimento, cuando la luz de PL-G-U87 alcanzó el nivel del ruido de fondo. La Fig 3C muestra la evolución cuantitativa del efecto terapéutico mediante la sustracción de PHCs totales de luz registrados en las imágenes del tumor en el área del tumor respecto al tiempo. Este análisis muestra como la cantidad de luz producida por los tumores que contienen células terapéuticas y que fueron tratadas con GCV era 10^4 veces más bajo que el producido por los tumores control tratados con GCV o por tumores con células terapéuticas tratados con PBS al final del experimento ($p < 0,05$). Además, la luz producida por los tumores tratados con células terapéuticas y GCV era sólo el 0,12 % de la cantidad de luz producida por los mismos tumores a T=0 (6 días después de la implantación celular). El análisis mediante microscopia de fluorescencia confocal también corroboró los resultados obtenidos por BLI. A T=0 antes del comienzo del tratamiento, los cortes de cerebro de ratón mostraron la presencia de RL-R-tTK-hAMSCs con fluorescencia roja uniformemente distribuidas en todo el sitio de implantación junto a células de tumor con fluorescencia verde. En los tumores desarrollados (a T = 49) del grupo control 1:4+PBS, las RL-R-tTK-tAMSCS rojas también se encontraban agrupadas dentro de la masa tumoral verde. Sin embargo, en los cortes de cerebro de ratones del grupo 1:4 + GCV tenían pocas células tumorales perceptibles y ninguna RL-R-tTK-hAMSC pudo ser detectada.

Este experimento se repitió implantando primero las células tumorales y luego varias dosis de células terapéuticas a 6 días (cuando el tumor ya estaba establecido), 30 días y 60 días después. Se obtuvieron resultados similares de inhibición de crecimiento

tumoral y además se vio una prolongación de la supervivencia en los ratones del grupo tratado.

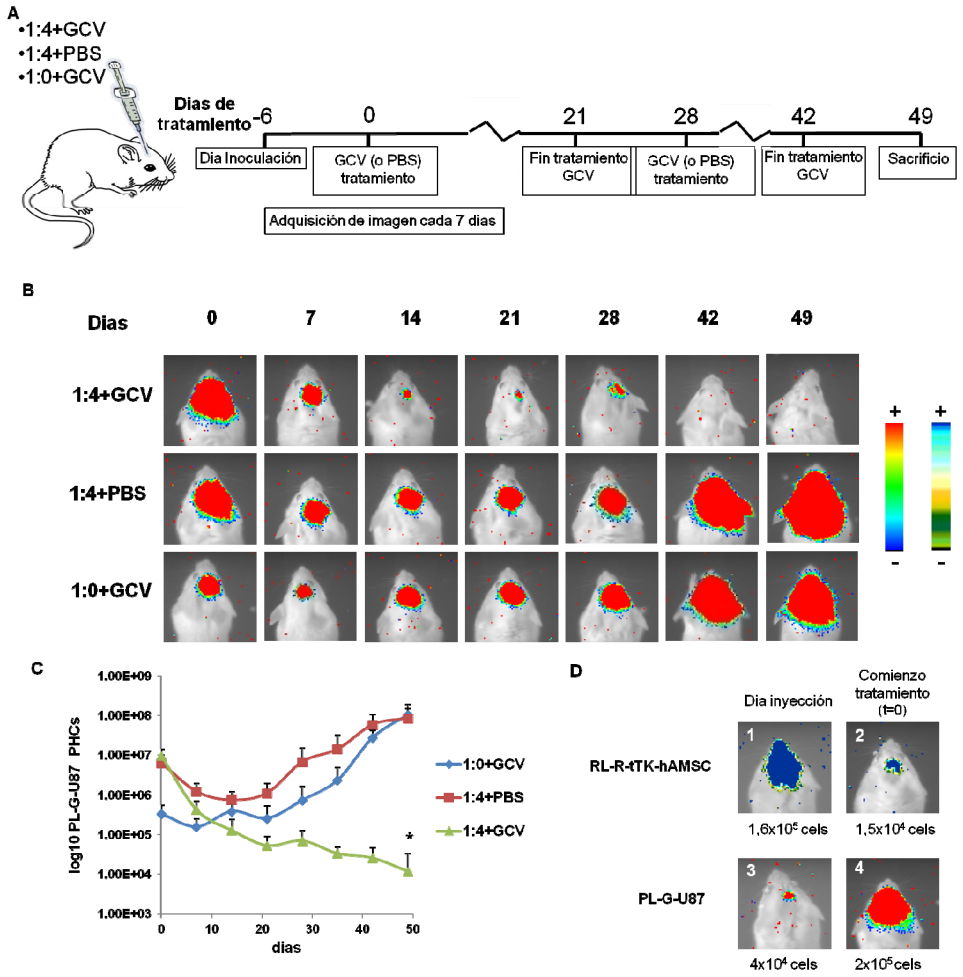

Figura 3. Terapia tumoral *in vivo* mediada por hAMSC. (A) Diagrama del procedimiento experimental. (B) Pseudoimágenes en color de ratones implantados con PL-G-U87 y RL-R-TK-AMSCS y tratados con GCV (1:4+GCV); PL-G-U87 y RL-R-TK-AMSC y tratados con PBS (1:4 +PBS), y con PL-G-U87 sólo y tratados con GCV (1:0+GCV). Las imágenes fueron adquiridas una vez por semana. (C) Cambios de la producción de luz de los tumores U87 que expresan Pluc *in vivo* como resultado del tratamiento con GCV y la muerte de las células tumorales. Los valores de luz, obtenidos de las imágenes tomadas, son representados como log10 de la media ± SEM; n=8; * p <0.05, respecto 1:0+GCV. (D) Pseudoimágenes representativas de RL-R-TK-AMSC y PL-G-U87 al día de implantación, T =-6 (1,3) y al inicio del tratamiento con GCV, T = 0 (2,4). Las imágenes de luciferasa estan sobrepuestas sobre las imágenes en blanco y negro del mismo ratón. Los valores numéricos indican el número celular extrapolado de la curva estándar obtenida en la Fig 2.

Se tomaron imágenes de las RL-R-TK-AMSC en el día de implantación (T =-6) y 6 días más tarde (T = 0), justo antes de empezar el tratamiento con GCV (Fig 3D). El número

de PHCs en T = 0, a día 6 tras la implantación, correspondía a $1,5x10^4$ RL-R-TK-AMSCs. Sin embargo, debido a la proliferación de células tumorales, a T = 0 la cantidad de luz producida por los tumores PL-G-U87 de los grupos 1:4 GCV y 1:4 PBS correspondía a aproximadamente $2x10^5$ células. Por consiguiente, al inicio del tratamiento con GCV había una proporción 13 veces mayor de células tumorales respecto a células terapéuticas.

Estudio de las células terapéuticas RL-R-tTK-hAMSCs implantadas junto al tumor

Para entender el mecanismo por el cual el tratamiento RL-R-tTK-hAMSCs + GCV alcanza el alto grado de efecto terapéutico observado, analizamos la diferenciación de las células terapéuticas. Con este fin, las RL-R-tTK-hAMSCs seleccionadas por FACS se marcaron con un segundo vector reportero Pluc-eGFP bajo control transcriptional del promotor PECAM/CD31. Este segundo vector nos sirve como reportero de la diferenciación al linaje endotelial mediante el análisis de su expresión y utilizando la expresión constitutiva del vector RL-R-TK como control interno, eliminando así los artefactos potenciales relacionados con cambios en el número de hAMSCs.

HAMSCs doblemente marcadas mezcladas con U87 sin marcar se implantaron en la posición estándar en el cerebro. El análisis por BLI de la expresión Pluc y Rluc a los días 0 y 7 postimplantación mostró (Fig 4A) que mientras la mayor parte de hAMSCs implantadas desaparece del tumor durante los 7 días, las células que expresan Pluc regulado por el promotor PECAM permanecen asociadas al tumor.

Además, la proporción de la actividad Pluc regulada por PECAM/CD31 respecto a la actividad Rluc expresada constitutivamente aumentó 92 veces, indicando que una subpoblación de hAMSCs implantadas se había diferenciado al linaje endotelial y había permanecido en el sitio del tumor (Fig 4B). Además, el análisis mediante microscopia confocal de los cortes de tumores mostró la presencia de células terapéuticas que expresaban RFP y que mostraban marcaje positivo con un anticuerpo PECAM/CD31 antihumano y se encontraban asociadas a estructuras vasculares funcionales marcadas con FITC-dextrano (Fig 4C).

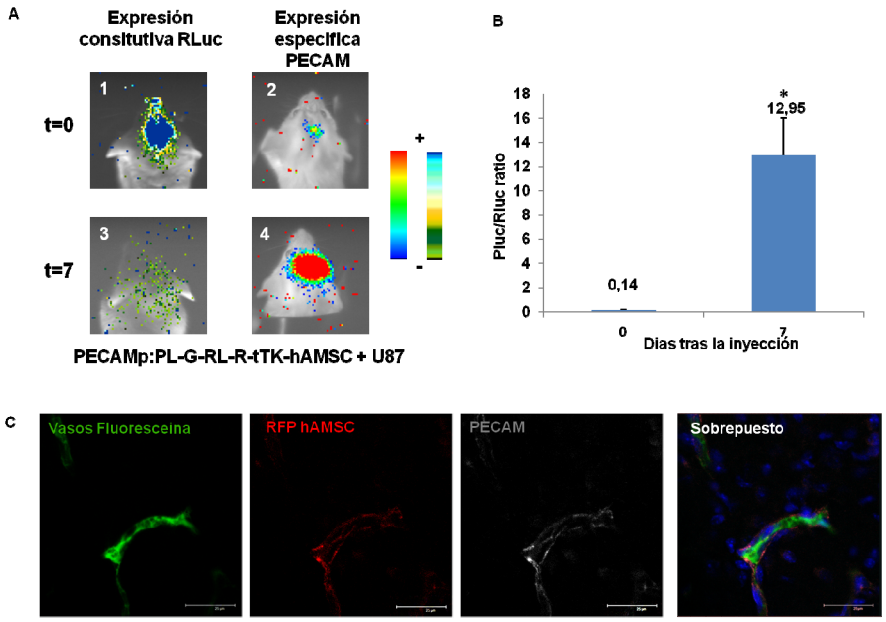

Figura 4. Diferenciación endotelial de las hAMSCs en los tumores U87. (A) Imágenes representativas de BLI mostrando las actividades Rluc (izquierda) y Pluc (derecha) a T = 0 (1 y 2) y T = 7 (3 y 4), respectivamente. Pseudoimágenes en color sobrepuestas sobre las imágenes en blanco y negro en posición dorsal de los ratones. Las barras de color ilustran las intensidades relativas de luz de Pluc (izquierda) y Rluc (derecha); bajo: azul y negro; alto: rojo y azul, respectivamente. (B) Histogramas mostrando el cambio de la proporción de actividades Pluc/Rluc durante el período de tiempo indicado. Las barras representan media±SEM de fotónes registrados en imágenes de BLI. * P <0.05, n=4. (C) Imágenes representativas mediante microscopia confocal de cortes de tumor mostrando hAMSCs bajo el control del promotor CMV (rojo) asociados a la microvasculatura marcada con FITC (verde), y marcadas con el anticuerpo contra la proteina PECAM humana (gris), la escala = 25 µm.

Silenciamiento de Notch1 para inhibir la diferenciación al linaje endotelial in vitro e in vivo

La señalización Notch1 está implicada en varias funciones celulares como la diferenciación endotelial. Estudios anteriores mostraron que la inhibición de la vía Notch1, una γ-secretasa, suprime la diferenciación de MSC de médula ósea. Para determinar si la diferenciación de las hAMSCs a linaje endotelial y la formación de la microvasculatura aumenta el efecto terapéutico, inhibimos la diferenciación endotelial de RL-R-tTK-hAMSCS y PECAM:PL-G-RL-R-tTK-hAMSCs mediante la incorporación estable de shRNA de α-Notch1, dando lugar a αNotch1- RL-R-tTK-hAMSCs y αNotch1-PECAM:PL-G-RL-R-tTK-hAMSCs, respectivamente. Un vector vacio con puromicina fue

usado como control para examinar el efecto de la transfección sobre la expresión génica, dando lugar a sh-RL-R-tTK-hAMSCs y sh-PECAM:PL-G-RL-R-tTK-hAMSCs.

La capacidad de diferenciación a linaje endotelial de las αNotch1-PECAM:PL-G-RL-R-tTK-hAMSCs fue evaluada *in vitro* e *in vivo* mediante un ensayo de formación de tubo en Matrigel. αNotch1-PECAM:PL-G-RL-R-tTK-hAMSCs carecen de la capacidad de formación de tubo, respeto a sh-PECAM:PL-G-RL-R-tTK-hAMSCs normales.

Además, el efecto de la inhibición de la diferenciación endotelial de las hAMSCs se comprobó *in vivo*. αNotch1-PECAM:PL-G-RL-R-tTK-hAMSCs y sh-PECAM:PL-G-RL-R-tTK-hAMSCs fueron implantadas en el cerebro de ratones SCID en combinación con U87 sin marcar. 7 días tras la implantación la proporción de la actividad Pluc regulada por PECAM/CD31 respecto a la actividad Rluc expresada constitutivamente aumentó 57 veces en sh-PECAM:PL-G-RL-R-tTK-hAMSCs, indicando que una subpoblación de hAMSCs implantada se había diferenciado al linaje endotelial (Fig 5A). Sin embargo en ratones implantados con αNotch1-PECAM:PL-G-RL-R-tTK-hAMSCs, la proporción Pluc/Rluc aumentó sólo 4 veces en el mismo tiempo. La falta de expresión Pluc en las αNotch1-PECAM:PL-G-RL-R-tTK-hAMSCs implantadas indica que la inhibición del mRNA Notch1 inhabilita la diferenciación endotelial de hAMSCs *in vivo*.

Finalmente se evaluó el efecto terapéutico de las RL-R-tTK-hAMSCs que expresan αNotch1. Un grupo de 12 de ratones SCID de 6 semanas fueron inoculados estereotácticamente en las coordenadas antes indicadas con una mezcla de $4x10^4$ PL-G-U87 y $1.6x10^5$ sh-RL-R-tTK-hAMSCs o αNotch1-RL-R-tTK-hAMSCs. La emisión de luz por la luciferasa Pluc fue evaluada a partir del día de implantación y cada semana a partir de entonces. Seis días tras la implantación se inició un tratamiento con GCV. El análisis cuantitativo de fotones capturados en las imágenes mostró (Fig 5B) que el tratamiento con GCV de los tumores que llevaban sh-RL-R-tTK-hAMSCs y αNotch1-RL-R-tTK-hAMSCs inhibió el crecimiento tumoral de manera diferencial.

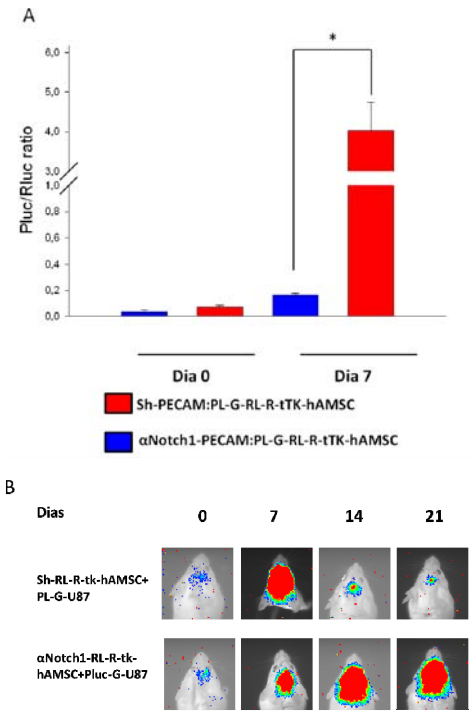

Figura 5. Inhibición de la diferenciación de las hAMSC mediante sh ARN αNotch1. (A) Histograma muestra la proporción PLuc/RLuc (PHCs) de sh-PECAM:PL-G-RL-R-tTK-hAMSCs y aNotch1-PECAM:PL-G-RL-R-tTK-hAMSCs implantados en el cerebro de ratones en combinación con U87 sin marcar, a día 0 y día 7. Histogramas muestran media ± SEM, *p <0.05, n=3 para cada grupo. (B) Pseudoimágenes compuestas de ratones implantados con PL-G-U87 más sh-RL-R-tTK-hAMSCs (arriba) o aNotch1-RL-R-tTK-hAMSCs (abajo) y tratados con GCV. Las imágenes fueron adquiridas una vez por semana.

A día 14 fue evidente una disparidad de la inhibición del crecimiento tumoral, y esta fue aun más clara a día 21, cuando solo el 6,3 % de la luz producida por las células tumorales al principio del tratamiento con GCV persistió en el sitio de inoculación en el caso de tumores tratados con sh-RL-R-tTK-hAMSCs, respecto al 64,4 % en el caso de los tumores inoculados con αNotch1-RL-R-tTK-hAMSCs.

Adicionalmente, se ha realizado una tinción contra CD133 (un marcador de células madre de glioma (GSC)) en cerebros de ratón U87 inyectados con sh-RL-R-tTK-hAMSCs o αNotch1-RL-R-tTK-hAMSCs. Se ha detectado que la asociación de sh-RL-R-tTK-hAMSCs normales con GSC era significativamente más frecuente que en el caso de hAMSC inhibidas para la diferenciación a linaje endotelial.

Atracción bilateral entre hAMSCs y U87

Para evaluar la capacidad de atracción entre las hAMSC y las U87 *in vivo*, se inocularon primero U87 que expresaban Pluc y eGFP en las coordenadas previamente descritas en el lóbulo derecho de ratones SCID. Siete días más tarde se implantaron hAMSC que expresaban RLuc y RFP en las coordenadas simétricas en el lóbulo izquierdo. Tras otros siete días los ratones se sacrificaron y los cortes de cerebros fueron analizados mediante microscopia confocal. Se observo una atracción bilateral entre las hAMSC y las U87 que se localizaban en ambos hemisferios cerebrales. Mediante experimentos adicionales se rechazó la posibilidad de migración inespecífica debido a la herida

causada por la operación. Finalmente, se comprobó que al implantar αNotch1-RL-R-tTK-hAMSCs, estas no son capaces de atraer U87 al sitio de implantación. Sin embargo, las αNotch1-RL-R-tTK-hAMSCs si se localizan alrededor del tumor U87 en el hemisferio derecho.

DISCUSIÓN Y CONCLUSIONES

En este estudio, describimos un modelo para la terapia contra el glioma que permite a un seguimiento no invasivo mediante bioluminiscencia del tumor y de las células terapéuticas. Mostramos que las hAMSCs de tejido adiposo modificadas genéticamente reducen considerablemente la proliferación del glioma primario *in vivo*. Recientemente, se ha aplicado una estrategia antitumoral basada en el uso de vehículos celulares para llevar genes y agentes terapéuticos a tumores. Aunque muchos estudios se han realizado usando células madre de diferentes orígenes como vehículos celulares hay pocos que hayan monitorizado *in vivo* la eficacia de dicha terapia.

En este estudio mostramos que tanto *in vitro* como *in vivo* el efecto adyacente de la timidina quinasa expresada por hAMSCs es directamente proporcional a la cantidad de células implantadas. Determinamos que la dosis óptima de hAMSCs para una terapia eficaz es 4 veces más que de células tumorales. Mostramos una reducción de luz de tumor del 0,12 % en el día 49 respecto al día 0 para la dosis más alta de hAMSCs. Sin embargo considerando que las células mueren cuando son inyectadas en el cerebro, la cantidad de hAMSCs que persiste en el momento del inicio de tratamiento es 13 veces menor que la cantidad de células tumorales. Por lo tanto, este modelo de terapia es conveniente para usos clínicos, ya que un número reducido de hAMSCs sería suficiente. Sin embargo una de las incógnitas que quedan por resolver es como se produce esta inhibición del crecimiento. Una explicación posible podría ser el fenómeno llamado "efecto adyacente", que consiste en la transferencia en metabolítos tóxicos de las hAMSCs que expresan la HSV-TK a las células tumorales que las rodean. La transferencia de metabolítos tóxicos es mediada por comunicación intercelular mediada por uniones GAP (GJIC). Sin embargo deben haber otros

mecanismos a parte de las GJIC, ya que ha sido descrito que las hAMSCs promueven la proliferación tumoral y mejoran el entorno tumoral. La capacidad de diferenciación a endotelio de las hAMSC, nos llevó a evaluar si este aumento tumoral es debido a la formación de vasos por las hAMSCs. Nuestros experimentos de BLI mostraron que una población hAMSCs permanece asociada al tumor. La proporción de la actividad Pluc regulada por PECAM/CD31 respecto a la actividad Rluc expresada constitutivamente aumentó alcanzando a día 7 un valor 92 veces más alto que al día de implantación. Esto fue corroborado por los resultados obtenidos mediante microscopía confocal que no sólo indicaron que las hAMSCs asociadas al tumor se diferenciaban activamente al linaje endotelial, sino que también se encontraban estrechamente asociadas a estructuras vasculares marcadas con FITC-dextrano. La localización de las hAMSCs en estructuras vasculares intensificaría su función citotóxica, destruyendo la vasculatura tumoral e inhibiendo el suministro de nutrientes y oxigeno a las células tumorales.

La terapia antitumoral con hAMSCs genéticamente modificados para la expresión de HSV-tk, ejerce una inhibición potente sobre el crecimiento del glioma. Repetidas inoculaciones de células terapéuticas limitaron el crecimiento tumoral y prolongaron la supervivencia en ratones.

Se inhibió la diferenciación endotelial de las hAMSCs mediante la incorporación estable de shRNA αNotch1 y evaluamos la capacidad terapéutica de estas células. La inhibición de crecimiento de tumor fue menor en el caso de las αNotch1 hAMSCs respeto a las hAMSCs normales, indicando que la diferenciación de las hAMSC al linaje endotelial y la incorporación a la vasculatura tumoral es esencial para un efecto terapéutico eficiente.

Finalmente se mostró que existe una atracción bilateral entre las U87 y las hAMSC, que se da por mecanismos paracrinos diferentes para cada tipo celular.

APPENDIX

- Cytoreduction: is the surgical removal of part of a malignant tumor which cannot be completely excised, so as to enhance the effectiveness of radiation or chemotherapy.
- Hydrocephalus: is a medical condition in which there is an abnormal accumulation of cerebrospinal fluid in the ventricles, or cavities, of the brain.
- Low-penetrance genes: these genes only sometimes produce the symptom or trait with which it has been associated at a detectable level. In cases of low penetrance, it is difficult to distinguish environmental from genetic factors.
- EGR3: early growth factor

This gene encodes a transcriptional regulator that belongs to the EGR family of C2H2-type zinc-finger proteins. It is an immediate-early growth response gene which is induced by mitogenic stimulation and may play a role in a wide variety of processes including muscle development, lymphocyte development, endothelial cell growth and migration, and neuronal development.

- CD31: platelet/endothelial cell adhesion molecule 1

The protein encoded by this gene is found on the surface of platelets, monocytes, neutrophils, and some types of T-cells, forms a large portion of endothelial cell intercellular junctions and is involved in migration, angiogenesis, and integrin activation.

- ILK: integrin-linked kinase

The protein encoded by this gene is a phosphoinositide 3-kinase-dependent serine/threonine kinase, that plays a critical structural role in the formation of integrin adhesion complexes and is an important regulator of endothelial cell function and survival.

- SDF-1 (stromal cell-derived factor-1) or CXCL12 (chemokine (C-X-C motif) ligand 12)

This gene encodes a stromal cell-derived alpha chemokine member of the integrine family that plays an important role in angiogenesis by recruiting endothelial progenitor cells from the bone marrow through a CXCR4 dependent mechanism.

- VEGFA1: vascular endothelial growth factor A

This gene is a member of the PDGF/VEGF growth factor family that encodes a glycosylated mitogen that specifically acts on endothelial cells and has various effects, such as mediating increased vascular permeability, inducing angiogenesis, vasculogenesis and endothelial cell growth, promoting cell migration, and inhibiting apoptosis.

- Notch1

This gene encodes a type 1 member of the Notch family that plays a role in a variety of developmental processes by controlling cell fate decisions and is involved in vascular/endothelial differentiation. The Notch signaling network is an evolutionarily conserved intercellular signaling pathway that regulates interactions between physically adjacent cells. Previous studies showed that inhibition of Notch signaling by a γ-secretase inhibitor abolishes endothelial differentiation of BMSCs.

- Osteocalcin BGLAP: bone gamma-carboxyglutamate (gla) protein

This gene encodes a highly conserved protein associated with mineralized bone matrix that is secreted by calcified tissues and is regulated by vitamin D3. Osteocalcin is secreted only by osteoblasts and is implicated in the body's metabolic regulation, bone mineralization and calcium ion homeostasis.

- GAPDH:. glyceraldehyde-3-phosphate dehydrogenase

The product of this gene catalyzes the reversible oxidative phosphorylation of glyceraldehyde-3-phosphate in the presence of inorganic phosphate and nicotinamide adenine dinucleotide (NAD). GAPDH gene is often stably and constitutively expressed at high levels in most tissues and cells and is considered a housekeeping gene. For this reason, GAPDH is commonly used by biological researchers as a loading control for western blot and as a control for RT-PCR.

- CD133: prominin 1

This gene encodes a pentaspan transmembrane glycoprotein that localizes to membrane protrusions and is often expressed on adult stem cells, where it is thought to function in maintaining stem cell properties by suppressing differentiation. Expression of this gene is also associated with several types of cancer. Recent studies in brain tumors have identified a CD133+ cell population thought to be a cancer stem cell population that undergoes self-renewal and differentiation, and can induce tumors when injected into immune-compromised mice.

AGRADECIMIENTOS

El wikipedia define una reacción química de la siguiente manera:

Una reacción química, cambio químico o fenómeno químico, es todo proceso termodinámico en el cual una o más sustancias (llamadas reactantes), por efecto de un factor energético, se transforman en otras sustancias llamadas productos.

Pues bien estos 4 años de doctorado han sido una reacción química muuuuuuy lenta como resultado de la cual se ha obtenido un producto llamado Tesis. El proceso ha sido termo- por el frio que he pasado en el confocal y -dinamico por todos los viajes al estabulario. Y los reactantes que han intervenido en el proceso (aparte de jeringas, pipetas y ratones) sois TODOS VOSOTROS.

El jefinio es un elemento imprescindible para la realización de toda tesis doctoral y se puede encontrar en toda clase de formas, pero a mí me ha tocado el mejor de todos y además en doble formato. Jero y Nuria, muchas gracias por haberme dado la posibilidad de hacer este trabajo, de dirigirme en mis primeros pasos como investigadora y de mostrarme la LUZ! Me habéis enseñado a la vez que me habeis dado suficiente libertad para poder experimentar a mi aire, lo cual intuyo será muy importante en mi próxima etapa científica! Gracias por ser unos jefes tan cercanos, por compartir con nosotros no solo conocimiento científico sino también chistes y entretenernos con historias divertidas durante la comida.

7я! Конечно без своеи семьи у меня не било бы даже возможности до сюда добрατся. Так что Мама и Папа большое вам спасибо за то что меня воспитали, накормили, одели и даже отправили в Университет! За то что постоянно бдили над процессом развития моей диссертации и даже просматривали мои презентации и давали советики (хотя они не всегда и принимались!). Тимуха и Галюхин спасибо вам за то что интересовались моими прогрессами и даже принимали меня дома когда я отлынивала в Мадрид! Тимка очень важный фактор по сколку убедил меня поступит в Посолскую Школу, ведь уначе я бы еще год заканчивала!! И особенно большое вам спасибо за то что будете ухаживать за моим кроликом в моие отсутствие ето мне дало болшое спокойствие в мои последние месяца здесь! Баба Рита, спасибо тебе большое за всю твою помощь в Русской школе, за соченения и диктанты и так же за все твои молитви, которим вот результат. Баба Зина, мне бы очень хотелось чтобы ты была с нами в эти дни, на моей защите, на даче, где

всегда хорошо потому что мы там провели с тобой самое счастливое детство. Большое спасибо всем всем представителям всемирно распространенной семьи Алиевых-Крашенинниковых: дядя Сережа, тетя Люба, Игорь, Наташа, тетя Зюма, дядя Расми, Мирза, Мадина и дедушка Игорь и дедушка Гаджи.

Acaso alguien piensa que es posible realizar una tesis doctoral sin unos cofactores tan importantes como son los compañeros? Quien podría entenderte mejor que aquel que lo sufre en sus propias carnes? Quien te acompañara en tus frustres y compartirá la alegría por un experimento (realmente UNO!) que sale bien? Los compañeros de laboratorio!! Juli-Eli, por separado no somos mas que C-M-P pero juntos formamos: las tres Marias. Sois los mejores compañeros que podría haber tenido, me habéis aguantuado de todo: lagrimas, risas histéricas, ansiedad, bromas malas (*vamos tirando?),* insultos, peleas, maullidos (Miau!),el retraso de los cheques de mis padres... jeje Y habéis estado a mi lado en los momentos más duros de estos años que ahora rememoramos haciendo broma! Me habeis ayudado, apoyado, aconsejado y con tantas As os habeis convertido en *Amigios*! En serio, no me puedo imaginar lo que hubiera hecho sin vosotros, probablemente lo hubiera dejado. Pero gracias a todos nuestros chistes, videos y bromas el dia a dia en el laboratorio se ha convertido en un entretenimiento! Dra. Eli, espero que después de todo lo que has sufrido durante tus dos o más tesis por fin recibas lo merecido y si los vientos económicos son favorables consigas montar tu spin-off o mejor aun el negocio de los espejos! Dr. Juli, para mi eres como un tercer mentor a parte de un segundo padre! Me has enseñado muchísimo y de verdad creo que tienes ideas geniales para este mundo científico (aunque te piques cuando no tienes razón ;P), hacer colaboraciones contigo ha sido estupendo y productivo a la vez que intenso jeje!

Marta y Olaia gracias por crear un buena ambiente laboratoril y compartir esta sauna conmigo en verano! Coja, gracias por corregirme mis documentos, escuchar mis presentaciones y ser tan empollona! Ya sabes que aunque tengas la patita mal te queremos igualmente!!

Y por supuesto a TODOS los compañeros del ICCC a los que he ido conociendo a lo largo de estos años. Gracias por vuestra colaboración, por vuestra ayuda, por vuestras sonrisas!! Siempre es agradable trabajar en un sitio donde estas rodeado de gente amable y dispuesta a prestar ayuda!

Pablo C, gracias por todos los chistes compartidos en el pasillo (de donde los sacas??), por ser tan sincero y abierto! Anna G gracias por ser tan divertida y alegre, por ese viaje tan inolvidable y por todas la tardes de juego!! Quién sabe, quizás organizaremos otras en nuestra buhardilla en Montmartre?? Mar, tendrás que esperar al apartado de *Amigio* para leer tu parte!

Muchas gracias a los queridos habitantes de Can Ruti! Vuestras visitas siempre son una alegría! Carol, gracias por tu paciencia con todas nuestras peticiones de anticuerpos, immunos, etc! Y por supuesto, por ser mi espectadora numero 1!

Tambien quisiera agradecer a mis antiguos compañeros de laboratorio del "Alberto Sols", con los que me inicie en el laboratorio. Ana Guadaño, muchas gracias por dirigirme en mi proyecto fin de carrera, sin el cual no hubiera podido graduarme y llegar hasta aqui!! Gracias, por toda tu ayuda entonces y durante mis años en Barcelona. Ana Montero e Ivan muchas gracias por haber sido unos compañeros estupendos, colaborativos y pacientes!

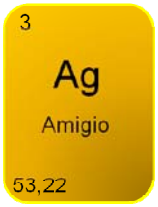

Mis amigios! Todos habeis sido un gran apoyo estos años, tanto los que estabais cerca, como los que estabais lejos, e incluso los que estabais muuuy lejos. Trabajar, experimentar y hacer una tesis todo eso esta muy bien, pero para llegar hasta el final uno necesita también evadirse de ello!! Olvidarse de todo para poder volver al laboratorio con la mente en blanco! Y eso lo he podido hacer gracias a los momentos compartidos con vosotros, las risas, los viajes, las cervezas… jeje

Sois muchos y repartidos por el mundo asi que intentare seguir una organización:

BARCELONA

Mar! Eres mi compañera de piso, de master, de laboratorio y no necesariamente en ese orden! Para mi has sido mi mayor soporte estos años! Te has preocupado por mi, me has sacado de fiesta, me has enseñado lo que es el ukelele, incluso me has cuidado cuando estaba enferma. Me encanta que seas tranquila (en comparación conmigo!), divertida, creativa y justa; y aunque no siempre limpies el lavabo te quiero un monton! Ya se que siempre soy cinica al respecto, pero ojala algún dia montemos ese negocio bohemio con el que soñamos!!

Cris y Marta, mis ratitas atleticas. Gracias por todas las noches de cotilleos, risas y disfrazes! Cris, gracias por estar mi lado incluso cuando el teléfono esta escacharrao! Tu eres la siguiente en hacer la tesis, que eres mi alter-ego!

Irma y Laura, gracias por vuestro soporte en mis primeros momentos por Barcelona, no se que hubiera hecho sin vosotras! Querida Fatimetuuu, muchas gracias por todos nuestros paseos por Gracia, conversas y sobre todo por cuidarme siempre al Pepi!! Jeje

Izaskul! Mi querida Medusoide, has sido muy importante para mi durante estos años en Barcelona, me has dado mucho apoyo y sabiduria! Y me encanta saber que puedo contar contigo y que seamos tan cercanas incluso en la distancia!

Teatro sin hogar!!! Estos últimos tres años con vosotros han sido geniales! Hemos logrado una sinergia que hace que ensayar sea no solo productivo pero también muy divertido. Y me da mucha pena dejaros… Ni se os ocurra sustituirme por una actriz mejor!! Sois todos muy diferentes pero a la vez unos locos como yo y por eso me encantais! Os quiero muchísimo!

Gracias a toda la gente con la que he compartido momentos estupendos en Barcelona: Mariaxo, Adri, Cañi, Suarez, Belen, Victor, Xavi, Carlos, Sandra, David, Paulo, Pablo, Karel, etc. Perdonad, si me olvido a alguien!!

Mariaxo y Adri! Gracias por todos los viajes a Llança, los sanjuanes, los bigotes, los ukelelos!

MADRID

Que hubiera sido de mi sin mis escapadas liberadoras a Madrid!

A mis amigos del colegio-teatro-instituto gracias por vuestro apoyo, vuestro cariño, vuestras risas, vuestros abrazos! Habéis sido algo fundamental para mi, por que aunque desaparezca a veces de vuestras vidas es genial saber que siempre estais allí esperándome con los brazos abiertos!

Dani, Pablo, Luis, Marina, Virginia, Sandra, Aura, Ali, Maria T gracias gracias gracias!

Dani y Pablo, nuestro viaje a Brasil fue genial y liberador! Llego un momento de mi mundo tesil critico y trajo muchos cambios consigo en mi vida! Habeis dejado el liston tan alto que tengo hasta miedo de volver a irme de viaje con vosotros, por que no creo que podamos volver a pasárnoslo tan bien!!

Marina! Gracias por nuestras visitas mutuas! Te quiero un monton!

Biolocos! Los años de la carrera con vosotros han sido muy divertidos, pero encima hemos tenido la suerte de seguir viéndonos después!! Sois todos unos locos y unos apasionados cada uno por lo suyo y por eso me encantais! Me encantan nuestras reuniones anuales (omitiendo la u)! Nuestras cenas de navidad! Nuestras barbacoas hasta reventar! Las patatas en la lavadora! El piano estambotico! Espero seguir con este ritmo muchos años mas!! Ir a esas casas rurales con nuestros hijos… ay que ya me pongo en plan soñador…

Carolina! Mi compi de practicas superproductiva! Mi futura colaboradora-IP-cabrona! Juajuajua Ya se que no nos lo decimos mucho por que somos unas rancias, pero teniendo en cuenta la ocasión de los agradecimientos de mi tesis: muchas gracias por todos estos años! Te quiero mucho!!! (y no estoy embriagada…).

ДАЧА

И наконец мои дачные друзья! Нам очень повезло что хоть наше радостное дачное детство кончилось (почти!) мы все равно продолжем встречатся, даже все чаще и чаще! Спасибо вам за то что не забываете своих дачных друзей, свои костры, свои кражы, свои coolgirl!

Лена ты знаешь что я тебя очень лю, даже если иногда я усчезаю и мы с тобой долго не видемся, когда мы встречаемся (например в Супермаркете в Алпах!) то мы с тобой так же

близки как каждедневие друзья! Вадимчик! Мне очень повезло что у моей подруги такой веселый, жизнерадосный и интересный муж! Хоть у нас с тобой достаточно разные взгляды на жизнь (и ты не можешь расслабится когда я веду машину!) но с тобой всегда весело!! Спасибо вам ребята!

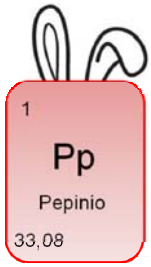

Y por ultimo, pero no por eso menos importante: Gracias al Pepinillo, la bolita, el gordi, el peludillo, el conejillo… Por ser siempre tan tonto y tan mono!